This is to certify that the

dissertation entitled

Experimental Development of a
Microwave Electrothermal Thruster

presented by

Stanley Joseph Whitehair

has been accepted towards fulfillment
of the requirements for

Ph.D. degree in Elect. Engr.

Major professor

Date 10/2/86

EXPERIMENTAL DEVELOPMENT OF A
MICROWAVE ELECTROTHERMAL THRUSTER

By

Stanley Joseph Whitehair

A DISSERTATION

Submitted to
Michigan State University
in partial fulfillment of the requirements
for the degree of

DOCTOR OF PHILOSOPHY

Department of Electrical Engineering and System Science

1986

ABSTRACT

EXPERIMENTAL DEVELOPMENT
OF A MICROWAVE ELECTROTHERMAL THRUSTER

By

Stanley Joseph Whitehair

This dissertation reports on the experimental investigation and application of high pressure microwave plasma discharges in helium, nitrogen and oxygen. Initial experiments examined the generation and maintenance of microwave plasma discharges in a cylindrical microwave cavity at high pressure using different gases. Coupling efficiency, plasma density and cavity Q versus pressure and gas type were measured along with other discharge properties. The microwave discharges were formed separated from any metal electrodes at all pressures and formed wall stabilized discharges free from contact with any surface at high pressures. Measured microwave coupling efficiencies into the discharges were in excess of 95% for all gases, accounting for cavity wall losses of less then 5%. In addition power densities of up to 640 W/cm^3 were measured.

Further experiments investigated the development and use of a microwave electrothermal thruster concept. Two different high pressure microwave coupling devices were developed. The first of these coupling devices used a coaxial microwave discharge to heat the propellant and a quartz nozzle to convert it into thrust. The device operated at a frequency of 2.45 GHz in a TEM mode over a power range of 200 to

jects.

ng eff

scc

a. The s

harge t

a Ty

pellant

d maxim

power

between

with

ference

ormance

other

other

600 Watts. Experimental measurements for thrust, specific impulse and energy efficiency were obtained for nitrogen gas with flow rates of up to 6000 sccm. Measured thruster energy efficiency varied from 30% to 60%. The second coupling device used a cylindrical cavity microwave discharge to heat the propellant. The cavity was operated in a TM_{011} and TM_{012} mode at 2.45 GHz with powers of up to 2000 Watts. Nitrogen propellant was tested yielding energy efficiencies between 10% to 25% and a maximum specific impulse of 280 sec. Helium propellant was tested with power levels of up to 1200 Watts. Measured energy efficiencies were between 10% and 50% with specific impulses between 200 to 600 sec. Tests with a metal nozzle produced similar results in nitrogen gas with efficiencies of up to 20% at a specific impulse of 425 sec. The performance of these thrusters compared favorably with other electrothermal thrusters and demonstrated the feasibility of a microwave electrothermal concept.

DEDICATION

This thesis is dedicated to the memory of Cloy and Stan McKeegan

ACKNOWLEDGMENTS

The author is thankful for the encouragement and guidance received from Dr. Jes Asmussen throughout this investigation. Additional thanks is given to Mr. Shigeo Nakanishi for his help with experiments presented in this thesis. Thanks is expressed to Mr. Ben Boyle for his help setting up and running the experiments. Special thanks to my parent for their encouragement in completing this degree.

This research was supported in part by fellowships from Michigan State University and by grants from the National Aeronautics and Space Administrations Lewis Research Center.

TABLE OF CONTENTS

TABLE OF CONTENTS

LIST OF FIGURES

LIST OF TABLES

Nomenclature

C_c	= Capactance of Excited Mode Near Resonance
e	= Electron Charge
$(Eff)_1$	= Overall Microwave Coupling Efficiency
$(Eff)_2$	= Applicator Microwave Coupling Efficiency
E	= Electric Field
E_r	= Radial Electric Field
E_{ro}	= Empty Cavity Radial Electric Field
ϵ_0	= Permittivity of Free Space
μ_0	= Permeability of Free Space
F	= Thrust Force
F_c	= Cold Propellant Thrust Force
F_H	= Hot Propellant Thrust Force
g	= Gravitational Acceleration ($9.8 m/s^2$)
G_c	= Conductance of Excited Mode Near Resonance
GHz	= Gigahertz
G_L	= Conductance of Discharge
H	= Magnetic Field
I_o	= Total Input current on the Coupling Probe
I_{sp}	= Specific Impulse
I_{spc}	= Cold Specific Impulse
I_{spH}	= Hot Specific Impulse
jB_L	= Susceptance of Discharge
jX	= Reactance of Modes Away From Resonance
jX_{in}	= Cavity Input Reactance
kW	= Kilowatt
L_c	= Inductance of Excited Mode Near Resonance
L_p	= Tuning Probe Length
L_s	= Tuning Short Length
MHz	= Megahertz

$\dot{m}$ = Mass Flow

$\dot{m}_H$ = Mass Flow of Hot Propellant

$\dot{m}_C$ = Mass Flow of Cold Propellant

M = Molecular Weight

$m:1$ = Transformer Turns Ratio

m_e = Mass Electron

N_0 = Electron Density

η = Thruster Efficiency

ω = Excitation Frequency

ω_p = Plasma Frequency

p_C = Cold Chamber Pressure

p_H = Hot Chamber Pressure

P/F = Power to Thrust Ratio

$\langle p \rangle$ = Power Density

$\langle p_e \rangle$ = Power Density per Electron

P_a = Power Absorbed in the Discharge

P_b = Power Absorbed in Cavity Walls

P_i = Incident Power

P_r = Reflected Power

P_t = Total Power Absorbed in the Microwave Cavity

P_{to} = Empty Cavity Absorbed Power

Q = Cavity Q

Q_u = Loaded Cavity Q

Q_{uo} = Empty Cavity Q

R = Intrinsic Resistance of the Cavity Walls

R_{in} = Cavity Input Resistance

S = Interior Cavity Wall Surface

TE = Transverse Electric Mode

TEM = Transverse Electric Magnetic Mode

TM = Transverse Magnetic Mode

T_o = Gas Temperature Prior to Expansion

ν_{eff} = Collision Frequency

v_c	=	Exhaust Velocity of Cold Propellant
v_H	=	Exhaust Velocity of Hot Propellant
v_p	=	Exhaust Velocity of Propellant
V	=	Cavity Volume
V_L	=	Plasma Volume
W_e	=	Time Average Magnetic Energy Stored in the Electric Field
W_m	=	Time Average Magnetic Energy Stored in the Magnetic Field
Z_{in}	=	Cavity Input Impedance
Z_0	=	Transmission Line Characteristic Impedance

CHAPTER I

INTRODUCTION

1.1 INTRODUCTION

This dissertation is concerned with the experimental investigation and application of high pressure microwave plasma discharges in helium, nitrogen and other gases. Initial experiments studied the generation and maintenance of microwave plasma discharges in a cylindrical microwave cavity at high pressure in different gases with no gas flow. Coupling efficiency vs. pressure and gas type and other discharge properties are measured. Further experiments deal with the development and testing of a microwave electrothermal thruster concept. This microwave electrothermal thruster concept is the application of a high pressure microwave plasma discharge to heat a gaseous propellant to a high temperature, and then using a nozzle, convert the thermal energy of the propellant into thrust.

Experimental research developed two different coupling devices which produce the desired high pressure microwave plasma discharges. The first of these devices is a coaxial microwave applicator and the second is a cylindrical microwave applicator. Thrusters using both coupling devices were used to measure thrust efficiency and other properties for several different gases.

This thesis summarizes the experimental research and development that lead to a successful demonstration of a working microwave electrothermal thruster. Some of this work has already been published

in scientific publications[1,2], at international scientific conferences[3,4,5,6,7,8], and in patent disclosures[9,10]. The experimental devices that were developed, represent an early prototype of an electrothermal thruster engine concept that has the potential for improvement and further study. These prototype thrusters were designed primarily to lend themselves to the experimental and theoretical investigation of electromagnetic-plasma interactions, microwave discharge energy balance, emission spectroscopy, etc..

1.2 RESEARCH

The research described in this thesis was carried out by the author over the period of 1982 to 1986 at Michigan State University under the direction of Dr. Jes Asmussen. The experimental work described in this thesis (except Chapter 6) took place primarily at the Michigan State University Plasma Research Laboratories. Mr. Shigeo Nakanishi of NASA Lewis Research Center provided additional aid in the design, operation and testing of the actual electrothermal thruster. Experiments with the initial coaxial microwave electrothermal thruster were carried out at Lewis Research Center using vacuum tank #8 under the direction of Mr. Nakanishi and are presented in Chapter 6. These experiments were carried out at Lewis Research Center because of the availability of a low pressure vacuum tank and thrust stand allowing direct thrust measurement.

The research described in this thesis builds directly on previous research carried out by Dr. Fredericks[11], Dr. Mallavarpu[12] and Dr. Rogers[13]. The success of this thesis is dependent upon these earlier experimental and theoretical studies of microwave discharges inside

microwave cavities. Indeed the theoretical knowledge used to build and understand the cavity and coaxial applicators were developed by these earlier experiments. The thesis research of Dr. Rogers, concerned with the properties of high pressure argon discharges, formed much of the background for the cavity research presented in this thesis. Further the basic microwave applicator the coaxial thruster is based on, was designed and built by Dr. Rogers.

1.3 RESEARCH OBJECTIVES

The objectives of this thesis research are primarily experimental. The main objective in the first experiments were to: (1) generate and maintain high pressure microwave plasma discharges in several different gases in a no flow situation, (2) take measurements of coupling efficiency versus pressure, and (3) take additional measurements of other plasma properties such as power density and cavity Q versus pressure etc.. The main objective in the second set of experiments were to: (1) generate and maintain high pressure microwave discharges in several different gases in a gas flow situation with different types of microwave couplers, (2) using this information produce a working microwave electrothermal thruster based on each type of microwave coupler studied earlier, (3) take measurements of these thrusters such as energy efficiency and specific impulse, and (4) conduct experiments to improve these thrusters by improving their performance characteristics such as increasing specific impulse and energy efficiency.

While the main topic of this thesis is microwave generated plasma discharges, a related experiment is presented in the appendix. This experiment involves the measuring of coupling between a microwave field in a cylindrical cavity, to a plasma flame generated by the burning of a gas. The purpose of this experiment is to show that energy in the form of microwaves can be coupled into a conventional combustion flame. The interest in doing this is that the coupled energy may be able to change the flame characteristics in a beneficial manner.

1.4 THESIS OUTLINE

This dissertation is organized as follows. Chapter II presents a background and review of previous work on electrothermal thrusters and provides a introduction to the concept of a microwave electrothermal thruster. Chapter III presents a brief review of previous work on high pressure discharges and describes the microwave applicators used in these experiments to couple energy into the discharge. Chapter IV describes the basic experimental setup used to conduct the experiments and measure data. Chapter V presents an experimental demonstration of coupling to high pressure microwave discharges and the measurements of the properties of these discharges. Chapter VI contains the experimental demonstration of a working microwave electrothermal thruster and its measured performance characteristics. Chapter VII presents experiments with cavity type applicator thrusters. Chapter VIII presents experiments with metal nozzle type thrusters. Chapter IX presents the conclusions and some speculation on improvements that could be made in thruster design.

CHAPTER II

MICROWAVE ELECTROTHERMAL THRUSTERS

2.1 INTRODUCTION

This chapter presents an introduction to the concept of a microwave electrothermal thruster. The first section of this chapter reviews previous work in the area of electric propulsion, specifically in the area of electrothermal thrusters. A short introduction to electric propulsion is presented along with a description of electrothermal thrusters and their application. Two main types of electrothermal thrusters, the resistojet and the arcjet, are currently being considered for use in space. A review of these two concepts is presented along with other experimental concepts. A summary of the performance of these thrusters is presented. In Chapter 6 this summary will allow a comparison between earlier electrothermal work and the microwave electrothermal thruster experimental data presented in this thesis. The second section of this chapter gives an introduction to the concept of a microwave electrothermal thrusters.

2.2 ELECTRIC PROPULSION

Chemical, electrical and nuclear are the three principle types of spacecraft propulsion under study today. Chemical propulsion[14], which is by far the oldest, best studied and best developed type of propulsion, provides large amounts of thrust necessary in missions such as those that have to overcome gravity. However for long-term missions, a chemical engine's rapid use of fuel limits its usefulness. Nuclear propulsion[15], by conversion of mass into energy has the potential of providing large amounts of thrust on a long term basis. However nuclear propulsion is a new concept, still under development and with potential questions of safety and cost not yet answered.

Electrical propulsion, in its different forms, uses electricity to increase the exit velocity of propellant. If this exit velocity can be raised to a higher value than possible in a chemical engine, then a electric engine could provide the same amount of thrust while using up less propellant in the process.

There are three main types of electric propulsion, electrostatic, electromagnetic and electrothermal. They differ in the method that is used to convert the electric power into thrust. An electrostatic thruster uses an electric field to accelerate ions to produce thrust. It is typically referred to as an ion thruster. An electromagnetic thruster uses a magnetic field interaction to convert electric power into thrust. Two types of electromagnetic thrusters are the MPD thrusters and the pulsed inductive thrusters. An electrothermal thruster uses electric heating to convert electrical power into thrust via a nozzle. An additional concept for electric propulsion is the free radical concept[16,17] using dissociated hydrogen to produce thrust. All further discussion of electric propulsion will be limited to electrothermal thrusters since the thruster concept described in this thesis uses this energy transfer method.

While electric propulsion is not as well developed as chemical engines, substantial research and development has been done on

electrical engines over the last thirty years. Jahn[18] gives an excellent description of basic principles of electrical propulsion, its advantages and disadvantages, and examples of working electrical propulsion concepts. He also provides descriptions for the many different types of electrical propulsion that are currently being studied. Because of this, this thesis will provide descriptions of only those concepts that most closely relate to the microwave electrothermal thrusters and the reader should refer to Jahn for more information on other concepts.

2.3 ELECTROTHERMAL PROPULSION

A diagram of a generic electrothermal thruster is shown in Figure 2.1. A propellant that could be a gas, liquid or a solid in some transportable form is fed into a thermal absorption region. In this region the propellant is heated to a higher temperature. The propellant is then exhausted through a converging-diverging nozzle that converts the high temperature propellant into thrust. The greater the temperature increase in the thermal absorption region, the better the operation of the thruster. However limitations in materials restrict operation of such thrusters to certain design configuration to produce working electrothermal thrusters and will be discussed in the following sections.

For a given mission, the type of thruster that one would select would be based on a great number of considerations. While the performance of the thruster alone would an important factor, it would not be the only factor. Other factors such as weight, volume, power requirement, propellant requirement, etc., must be considered also. The

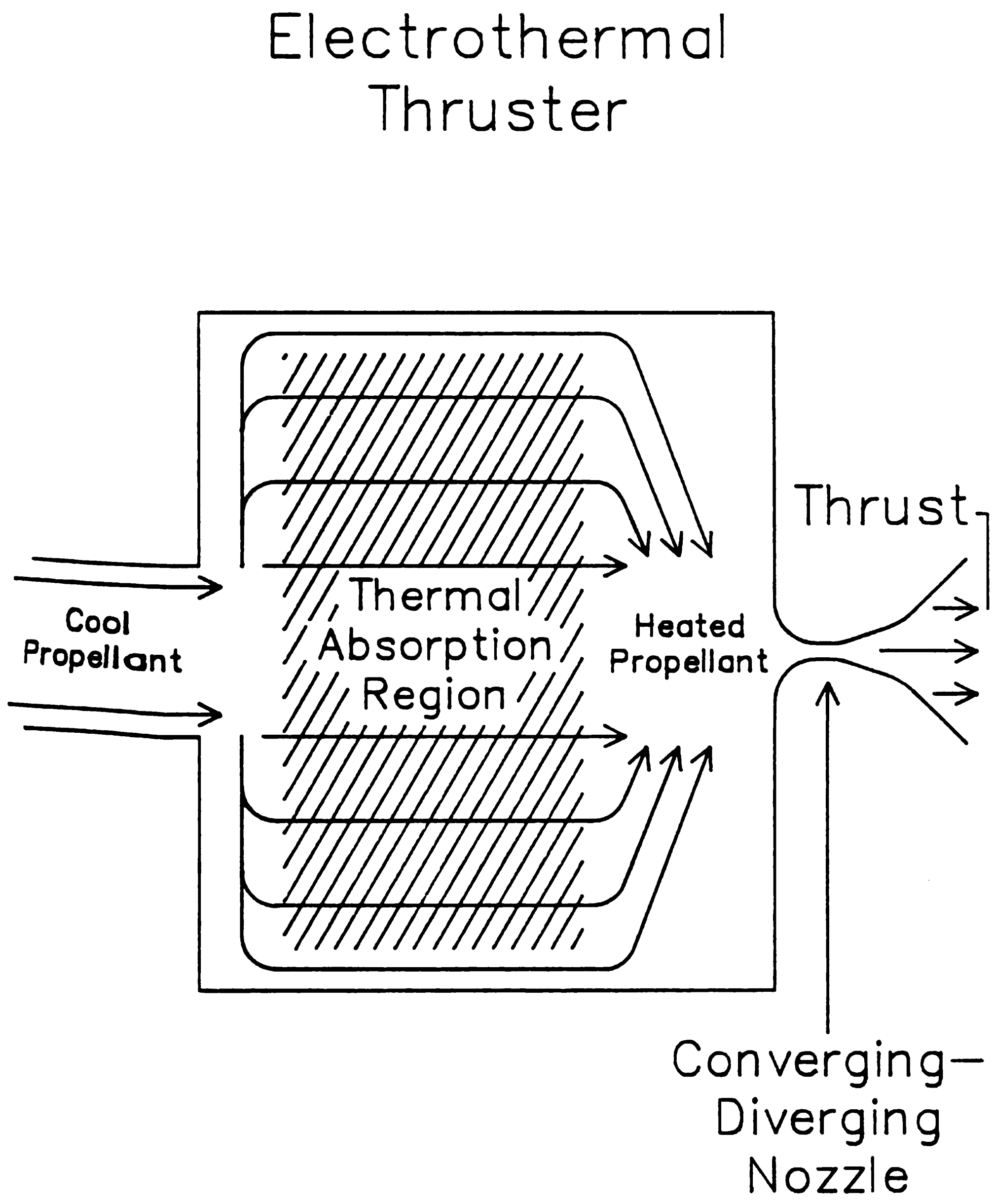

Figure 2.1 Electrothermal Thruster

actual decision would be based on a combination of all of these factors. Because of all the factors that could be considered, this thesis will restrict the performance discussion and comparison to primarily the performance of just the thruster, while some discussion of the general thruster system will be given. Primarily this means that the criteria of performance for this thesis will be based on several numerical quantities derived from experimental measurement of actual thruster performance and will be discussed in section 2.3.1.

The most developed types of electrothermal thrusters are mainly the resistojet and the arcjet. Both of these concepts have potential applications in space missions. Sections 2.3.2 and 2.2.3 describe in more detail advantages and disadvantages of each of these types of thrusters. The last section presents descriptions of some other potential types of electrothermal propulsion. This section also provides a summary of results for latter comparison to other thrusters.

2.3.1 THRUSTER PERFORMANCE EQUATIONS

The evaluation of thruster performance involved the experimental determination and calculation of several figures of merit. These quantities are generally recognized as the standards for thruster performance comparison and can be found elsewhere, but because of variation in the definitions of these quantities, especially energy efficiency, the definitions used in this thesis are briefly outlined in this section. The first of these is thrust force, F, and is defined as being equal to exhaust mass flow rate times the exhaust velocity relative to the thruster. Thrust is measured directly or calculated from other measured quantities. The overall energy efficiency, η, the specific impulse, I_{sp}, and the power to thrust ratio in are described in detail in this section.

The specific impulse is defined as the ratio of the thrust to the propellant mass flow expressed in units of seconds. Thus,

$$I_{sp} = \frac{F}{\dot{m}g} \qquad (2.1)$$

where $\dot{m}$= mass flow rate of propellant

g= gravitational acceleration (9.8 m/s^2)

F= thrust force

Overall energy efficiency is defined as the time rate with which kinetic energy is imparted to the hot propellant exhaust divided by the sum of the input power and the rate of kinetic energy flow of the initially cold propellant. Thus,

$$\eta = \frac{\frac{1}{2}\dot{m}_H v_H^2}{P_a + \frac{1}{2}\dot{m}_C v_C^2} \qquad (2.2)$$

where $\dot{m}_H$= mass flow rate of hot propellant,

v_H= exhaust velocity of heated propellant,

P_a= microwave power absorbed by the discharge,

v_C= cold gas exhaust velocity,

$\dot{m}_C$=mass flow rate of cold gas.

From momentum considerations, the thrust force is given by $F=\dot{m}v$, assuming all mass particles have a uniform velocity, v_p, parallel to the

thrust vector but in the opposite direction. Thus,

$$\eta = \frac{\dfrac{F_H^2}{2\dot{m}_H}}{P_a + \dfrac{F_C^2}{2\dot{m}_C}} \tag{2.3}$$

where F_H = hot condition thrust,

F_C = cold condition thrust.

Note that when the input absorbed power is zero, output conditions correspond to the cold flow input, yielding an efficiency of 100 percent. In the experimental results presented in this thesis, the mass flow rate was held constant during the hot and cold measurements, so that $\dot{m} = \dot{m}_C = \dot{m}_H$. Thus, from equations 2.1 and 2.3, the efficiency can be expressed as,

$$\eta = \frac{I^2{}_{spH}}{\dfrac{2P_a}{g^2\dot{m}} + (I_{spc})^2} = \frac{\left[\dfrac{I_{spH}}{I_{spc}}\right]^2}{\dfrac{2P_a}{g^2\dot{m}(I_{spc})^2} + 1} \tag{2.4}$$

This definition of energy efficiency is not universal, some definitions do not consider the cold gas kinetic energy and some definitions do not include all the input power in the definition of input energy.

The power to thrust ratio is simply the total input power divided by the thrust force. Using the definition of energy efficiency given above, the power to thrust ratio can be written,

$$\frac{P}{F} = \frac{g}{2}\left[\frac{I_{spH}}{\eta} - \frac{(I_{spc})^2}{I_{spH}}\right] \tag{2.5}$$

2.3.2 RESISTOJETS

Figure 2.2 shows the basic operating principle of a resistojet thruster. In this type of electrothermal thruster the thermal absorption region is produced by resistive heating of a electric element. This heating raises the temperature of the propellant passing through the region. The propellant then passes through a nozzle producing thrust.

Different types of resistojets have been built and tested. They differ mainly in the flow configuration used to heat the gas, the amount of power they can handle and the type of propellant they use. Several examples of experimental resistojets are presented.

One example is of a 3 kW concentric tubular resistojet.[19] The input propellant is fed through a series of concentric tubular resistance heating elements heating the gas and minimizing the heat loss from conduction and radiation. The thruster was tested with H_2 as a propellant with a input power level of 3 kW. It produced a maximum specific impulse of 830 sec with a mass flow of 79×10^{-6} kg/s and had a best system efficiency of 79%. In continued experiments with this type of thruster[20], the energy efficiency vs. specific impulse are presented in Figure 2.3 as the points designated A, for H_2 and NH_3 propellant.

A second example of a working resistojet is referred to as a HiPEHT (High Performance Electrothermal Hydrazine Thruster) type device.[21] The HiPEHT is a hybrid type device that combines a chemical engine with an electrothermal augmentation device to increase the specific impulse of the engine. When tested as a resistojet the chemical portion of the thruster was not used and the propellant was directly added into the electrothermal stage. This electrothermal stage

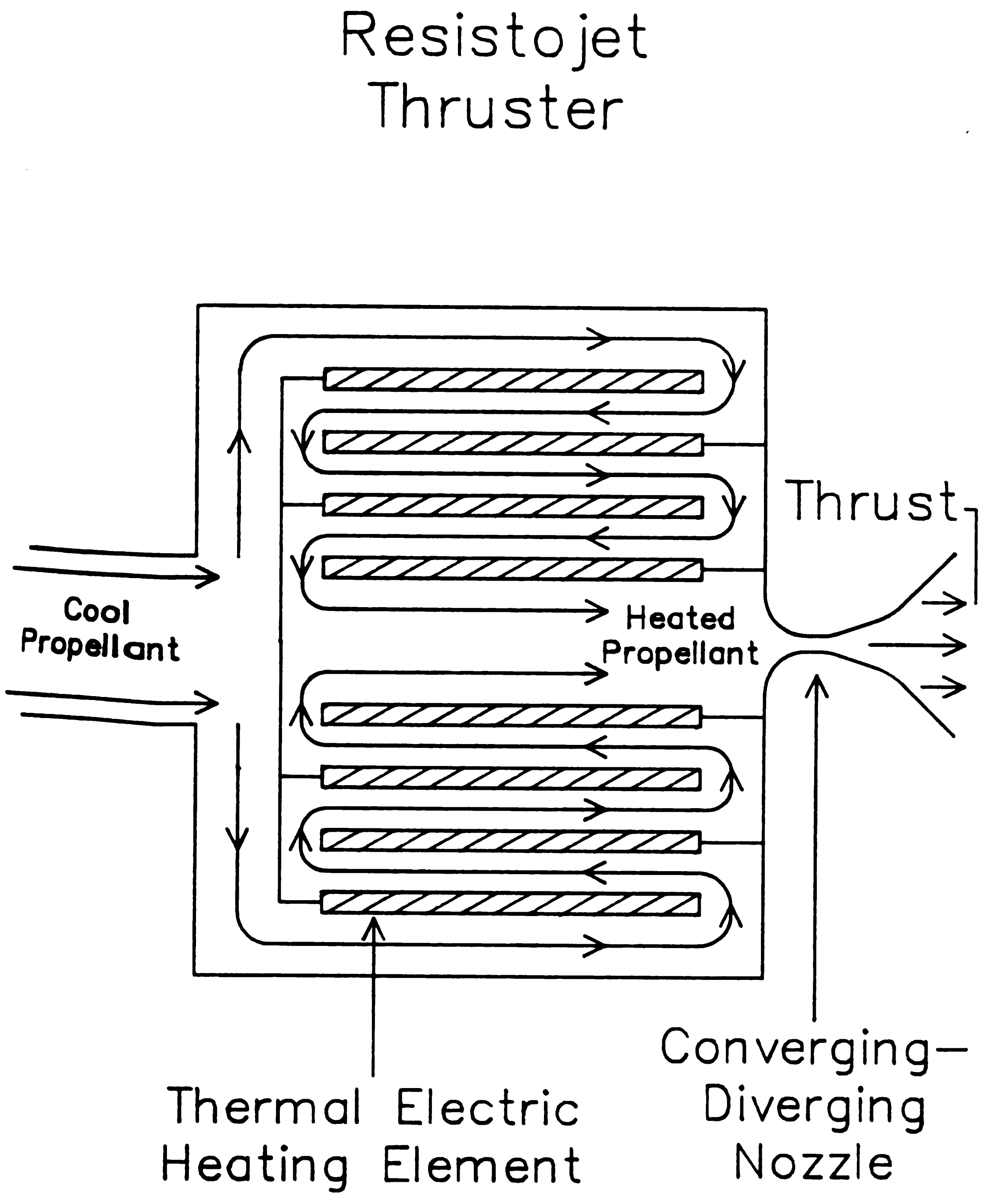

Figure 2.2 Typical Resistojet Thruster

Comparison of Several Electrothermal Thrusters Operating Below 5kW

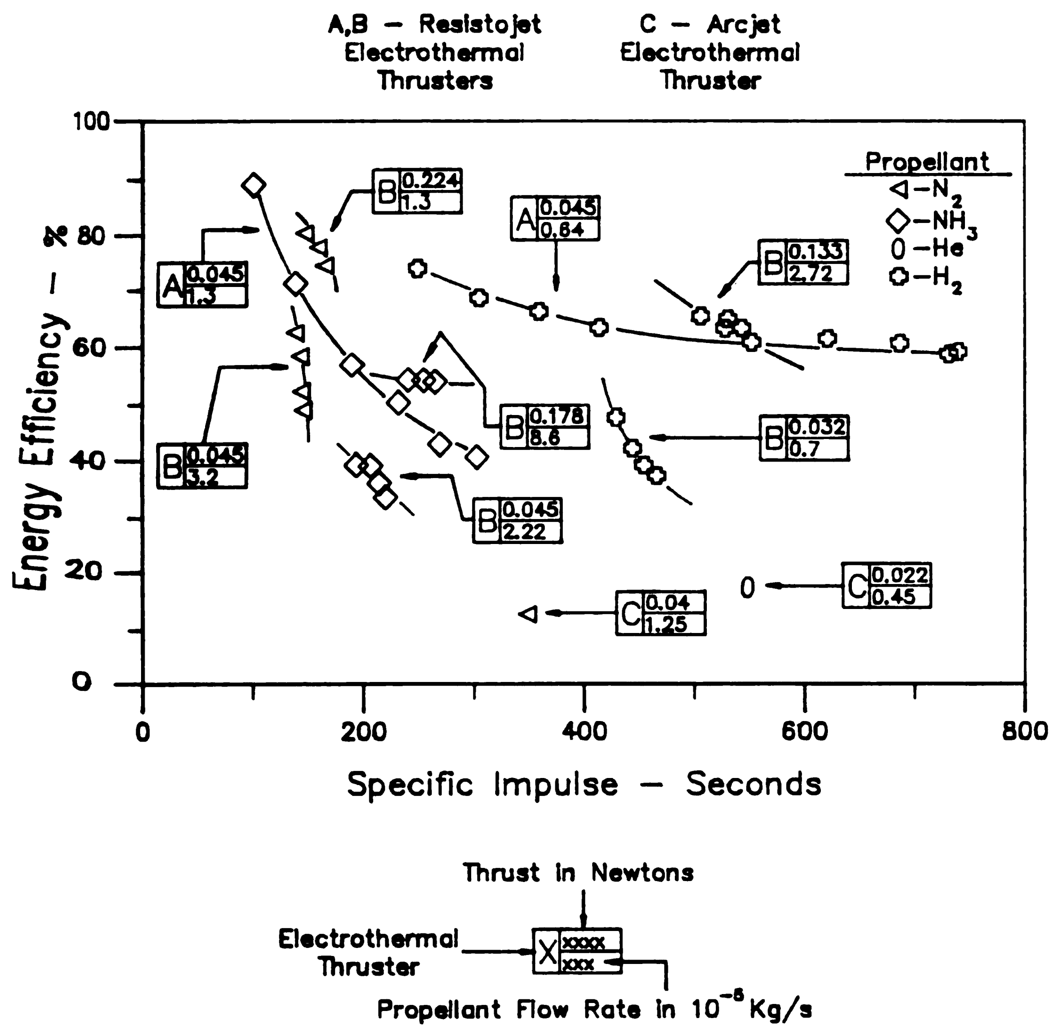

Figure 2.3 Comparison of Different Electrothermal Thrusters

used a vortex heat exchanger to increase the temperature of the propellant. N_2,H_2 and NH_3 gases were tested as propellant. Typical results for H_2 were I_{sp} of 550 sec with 5 kW of input power and an overall efficiency of 61%. Results for all three gases are presented in Figure 2.3 as points with the designator B.

A resistojet was the first electrothermal thruster to be tested on an actual spacecraft in orbit.[22] This was a small device using only 90 Watts of power, and with N_2 as propellant, generated a specific impulse of 123 sec. The device was use on board a Vela satellite to adjust the orbital position.

These experiments indicate that resistojets are valid electrothermal thrusters and have been used in real spacecraft applications. They posses several advantages for their use in an actual applications. They are easy to start, can use a broad range of power inputs in terms of both voltage and frequency, are simple to operate and can use a wide variety of propellants, although O_2 and H_2O could present lifetime problems. However they suffer from a temperature limitation in materials used to heat the gas, limiting the maximum specific impulse to below 1000 sec.

2.3.3 ARCJETS

Figure 2.4 shows the basic operating principle of a arcjet thruster.[23] The thermal absorption region in this thruster is produced using a dc electrical arc discharge. In this manner the the propellant flowing through the discharge region is heated by the arc discharge and then exhausted through a nozzle producing thrust.

An example of a working arcjet is given by John.[24] This thruster

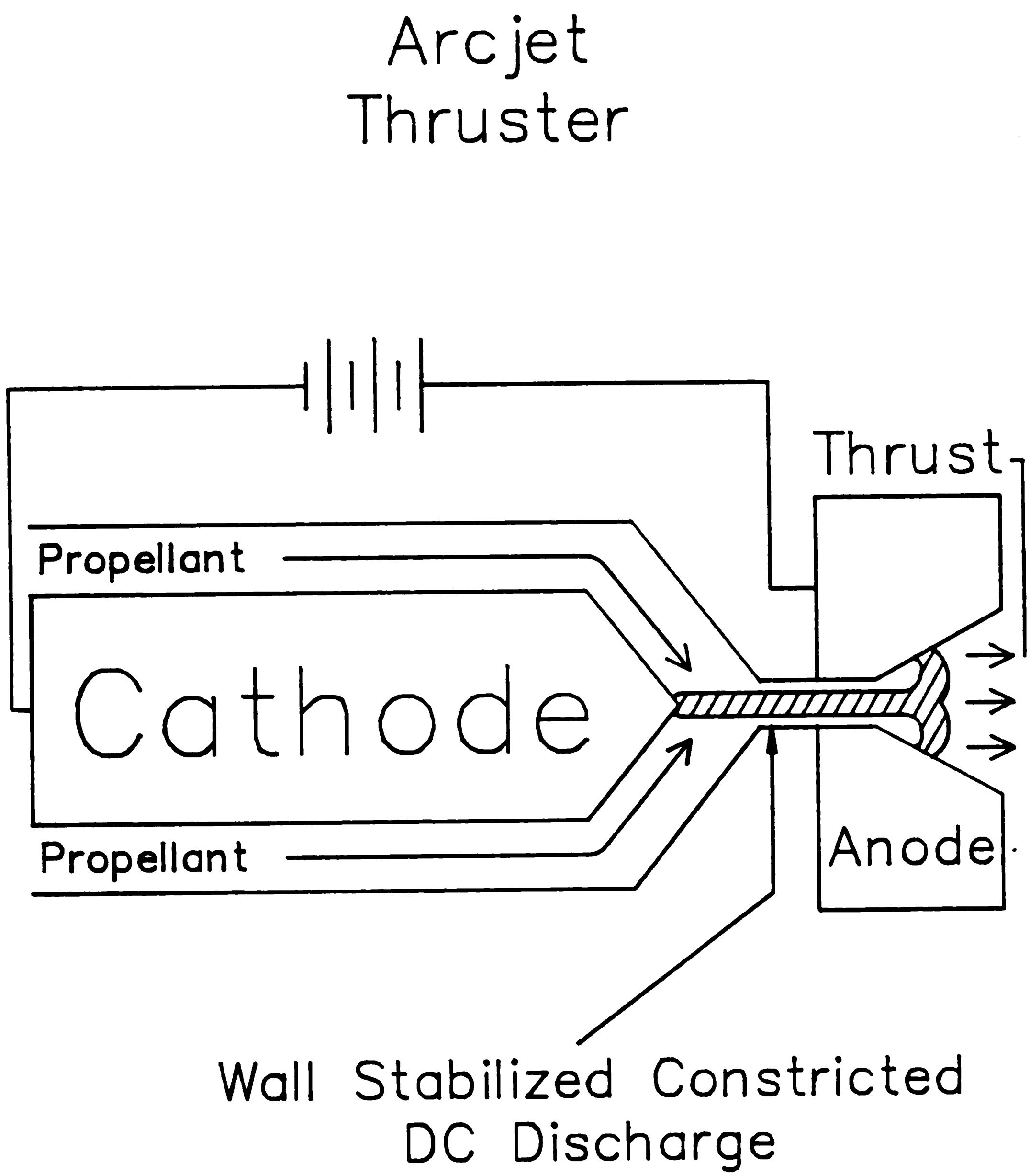

Figure 2.4 Typical Arcjet Thruster

is referred to as a radiation cooled arcjet engine having a constricted arc configuration. The constricted arc configuration means that a Laminar column arc is formed so that it passes through the narrowest portion of the nozzle and it uses the constriction to maintain arc stability through thermal energy interactions with the constriction walls, i.e. a wall stabilized arc is formed. This engine was tested in both H_2 and NH_3 propellants and and at power levels of 30 and 215 kW. For 30 kW of input with H_2 as a propellant a specific impulse of 1550 sec with a mass flow rate of 100×10^{-6} kg/s, and a efficiency of 38% was reported. For 215 kW with H_2 a specific impulse of 2200 sec with a mass flow rate of 330×10^{-6} kg/s, and a efficiency of 35% was reported. A one month lifetime of useful operation is reported due to cathode mass loss.

McCaughey[25] presents results for a 1 kW arcjet thruster. This thruster used both a short constriction and a magnetic field to maintain arc stability. The thruster was tested in a wide variety of gases including H_2, He, N_2, argon, ammonia, methane, air, etc.. Results for N_2 and He are shown in Figure 2.3 for this thruster and are designated as C. Lifetime results of these experiments were reported as good for propellants not containing oxygen or carbon. Use of propellants containing oxygen and carbon led to severe material problems.

Resistojets have limited specific impulse, but as can be seen from these examples, arcjets have the capability for large specific impulse since the arc can produce much higher temperatures. Arcjets on the other hand have limited lifetime problems and suffer from low efficiencies. In terms of power handling, arcjets of over 200 kW have been built and tested.[26] At these power levels the efficiency of the

arcjet improves from that reported to over 40%.[27]

2.3.4 OTHER CONCEPTS

The resistojet and arcjet are the two best developed electrothermal concepts. A third concept would be to use high power laser energy from a remote location to power a thruster.[28] The laser power could be beamed from earth or from another satellite in earth orbit eliminating the need for a heavy onboard power source. This laser thermal thruster engine would operate in a pulsed mode or continuous wave mode where laser energy is focused into a small chamber heating a gaseous, liquid or even solid propellant to many thousands of degrees then expanding it out a nozzle to produce thrust. At this time it has not been experimentally demonstrated, but stable laser supported plasmas have been demonstrated in the laboratory[29,30] and the question of stability and energy coupling are currently being studied[31,32].

The main problem with the arcjet thruster is the arc-cathode-anode interaction results in both lower efficiency and in erosion. One hypothetical concept that could be used to eliminate this problem would be to develop a induction arcjet thruster operating at RF frequencies. Such a thruster would not have electrodes in the discharge zone and thus might be able to combine the advantages of the resistojet and arcjet. Considerable experimental work has been done on induction arcs[33,34] and industrial applications have been studied[35].

2.3.5 SUMMARY

The results summarized above indicate that electrothermal thrusters operate at high specific impulse when compared to chemical

thrusters, and operate at higher levels of thrust than current ion thrusters. Recent studies have shown that for near Earth orbit transfer missions, the electrothermal thrusters show the best trip time performance values of specific impulse of from 1000 to 5000 sec.[36] These advantages have resulted in the identification of electrothermal thrusters as a technology for satellite station keeping and as auxiliary propulsion of large platforms in low earth orbit.[37] Specifically a thruster with the efficiencies of the resistojet but able to operate at higher specific impulse (over 1000 seconds) and higher thrust output would be desirable.[38] The ability to use waste products from space station operations, containing O_2 and other chemically active gases, as propellant[39] without the decreasing the thruster lifetimes would also be highly desirable.

2.4 MICROWAVE ELECTROTHERMAL THRUSTERS

From the discussion in the previous section it can be concluded that there is a need for an electrothermal thruster capable of operating at specific impulse levels above 1000 seconds with higher efficiencies and longer operational lifetimes. This section presents the microwave electrothermal thruster concept which has the potential to overcome these problems. The basic concept is first presented, next its advantages and disadvantages, a discussion of the power supply is then presented and last the potential for beamed power supply is discussed.

2.4.1 CONCEPT

The principal elements of a microwave electrothermal thruster system are shown in Figure 2.5. The system receives its electrical energy from a source such as solar cells and converts it into microwave power via a power conditioner such as a magnetron, klystron or gyrotron. Once converted into "microwaves", the electric energy is coupled into an energy absorption chamber where a low molecular weight gaseous propellant is heated as it flows through the chamber. The heated, propellant then exits via a conventional nozzle producing thrust.

2.4.2 ADVANTAGES AND DISADVANTAGES

The principle advantage of a microwave electrothermal thruster is that a microwave discharge does not require the electrodes of a DC arcjet to operate. This provides several potential advantages for this concept over the resistojet and the arcjet. Since there are no hot electrodes in contact with the discharge, chemically active gases such as O_2 can be used as propellant. A second benefit of this is that there is no erosion of the electrodes with the potential of longer thruster lifetime. If the discharge can be formed completely away from all solid components of the thruster, there will be fewer problems with material lifetimes and the energy losses from the discharge will be reduced. In addition, if the discharge can be maintained away from solid materials in the thruster, it could be operated at higher temperature than otherwise possible, thus increasing the rate of energy transfer to the propellant. Elimination of the electrodes also allows new freedom in thruster design.

The principle disadvantage of the concept of a microwave

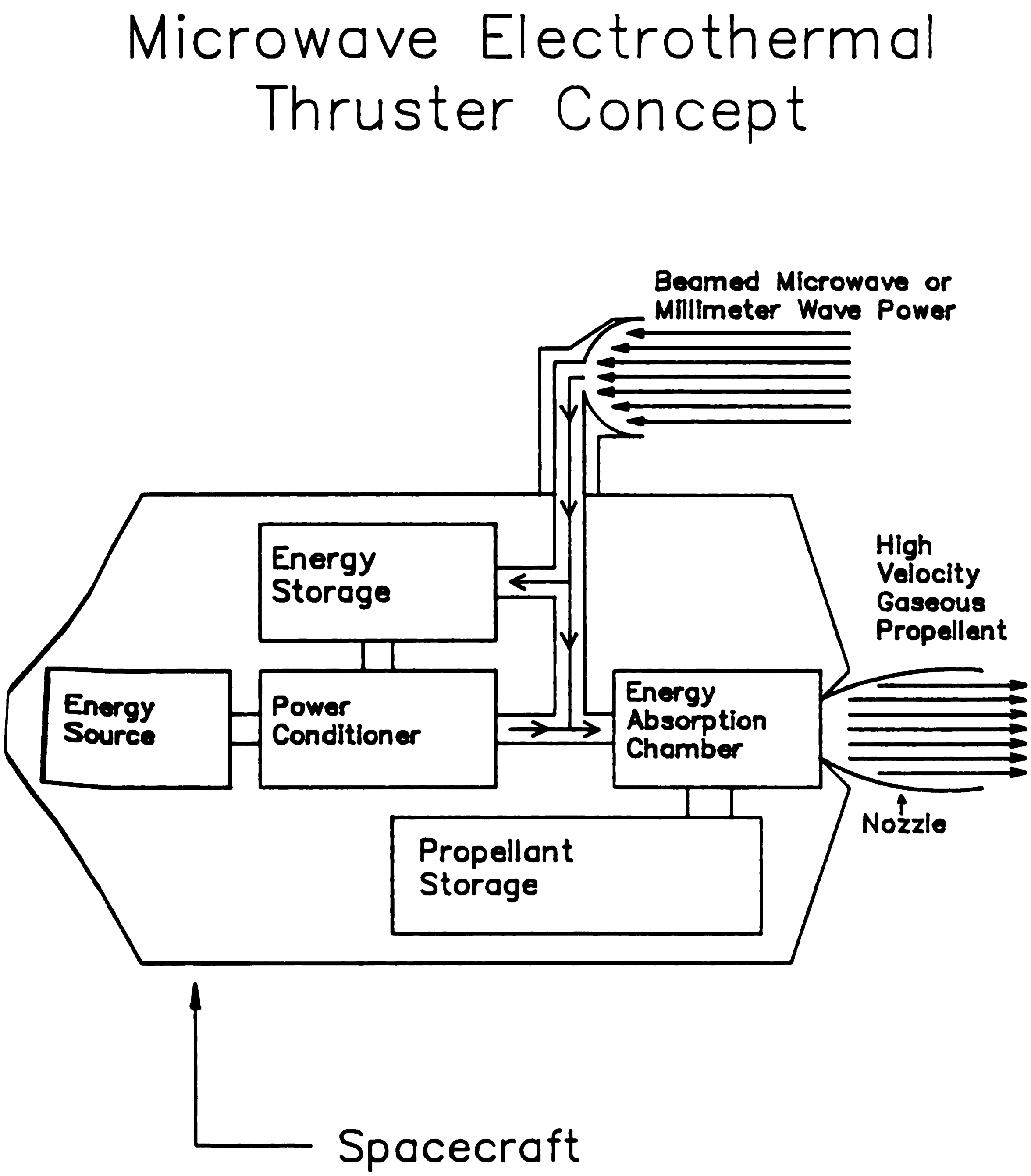

Figure 2.5 Microwave Electrothermal Thruster Concept

electrothermal thruster is that it is highly experimental, and at this time, still under development with other potential problems not even identified. A further potential advantage or disadvantage is that the energy absorption chamber requires microwave frequency power to operate. If microwave power is available for other uses in a spacecraft this is a advantage, but if it is not the total thruster system (including the microwave power conditioner) must be compared to other thruster systems to determine if it is a potential advantage or disadvantage.

This thesis deals with the development of the microwave electrothermal thruster, however a short discussion of the problem of the microwave power conditioning will be given in the next two sections. Two different microwave energy supply systems are described in these sections to provide this power. The first system describes the necessary components to generate the microwave power on board and the second system would function on power beamed to it from a external source.

2.4.3 ONBOARD POWER CONDITIONING

Electrical power would be provided by a onboard source of electricity such as solar cells, fuel cells, nuclear reactor, solar thermal reactor, etc.. At this time the only high power source of microwave power are tube devices that require high voltages. Thus the electrical power would have to be raised in voltage to supply power to these tubes implying power loss in the conversion.

Tube devices have existed for many years and are well studied and understood.[40,41] Tube efficiencies of up to 83% with power levels of up to 25 kW at 2.45 GHz have been reported for magnetrons.[42] Experimental amplitrons have reported efficiencies of up to 90% with power levels of up to 400 kW.[43] Depressed collector klystrons have reported efficiencies of over 80% with power levels of up to 1 MW.[44]

Thus, in any microwave electrothermal thruster system that uses a onboard power source, the efficiency of the entire system, not just the thruster, must be considered. If the high voltage power or even the microwave power is available on board for other purposes, the use of a microwave thruster may be advantageous. It should be noted that solid state devices are being developed that can operate at these frequencies. These devices currently operate at 2.45 GHz with power levels of up to 100 Watts with direct conversion from low voltage power into microwave power. At 1.85 GHz, commercial solid state power supplies are available that can produce power output of up to 1.25 kW continuous and 2.5 kW units are under development.[45]

2.4.4 BEAMED POWER SUPPLY

As shown in Figure 2.5 there is the potential for the use of beamed microwave or millimeter wave electricity to supply energy to the thruster. Such a system may be practical, probably at very high microwave or millimeter wave frequencies, where the antenna size/weight is not too large thereby allowing the beaming of 30-100 GHz energy thousands of miles. This concept has the potential advantage, similar to laser thermal thrusters[28], of not requiring a heavy onboard power source and of coupling beamed energy directly into the energy absorption chamber.

There has been great interest in beaming electricity for solar power stations to Earth for some time.[46] However in these applications low frequency power, 60 hz, is desirable and energy losses result in the conversion. Beaming to a spacecraft using a microwave electrothermal thruster may not require conversion and thus could prove to be very beneficial.[47] However at this time the beaming of microwave energy is still experimental and there are many questions regarding its use and operation.

CHAPTER III

MICROWAVE APPLICATORS AND ARCS

3.1 INTRODUCTION

Conversion of microwaves into high temperature thermal energy requires the use of a microwave applicator and a microwave plasma discharge or arc. The applicator serves to couple microwave energy into the arc and the arc heats the propellant gas. The basic types of applicators are described in section 3.2. Two different energy coupling structures or microwave applicators were used in the experiments presented in this thesis. The first of these is a coaxial type applicator based on a TEM type electromagnetic mode and is described in the section 3.3. The second type is a cavity type applicator which uses a classical type resonant cavity and is described in the section 3.4. The basic operation of the microwave arc and how it transfers energy to the propellant is described in section 3.5.

3.2 MICROWAVE APPLICATORS

The practical realization of any electrothermal concept requires the energy absorption chamber to be designed to perform several interrelated functions. First, it must efficiently couple electric energy into a low molecular weight propellant and must heat this propellant to extremely high temperatures. In addition, the energy absorption chamber must be designed to prevent significant energy losses from the heated propellant by radiation and heat conduction and convection to the chamber walls before it exits the nozzle. These several interconnected functions must be performed simultaneously within the energy conversion chamber without imposing chamber wall, electrode, heater element, nozzle material and life limitations. The final design of the energy conversion chamber results after the trade off between these several interrelated functions.

Applicators can be classified into groups by the type of phenomenon they use to sustain the microwave arc.[48] The first are resonant applicators that use a resonant, or standing wave, field pattern to sustain the plasma discharge. The second group sustains a discharge with propagating electromagnetic energy. Thus, in a propagating wave applicator the discharge is sustained by evanescent fields or by radiating type fields. Examples of each of these is presented in the following sections.

3.2.1 RESONANT APPLICATORS

In resonant type applicators two different types of discharges can be identified, fast wave and slow wave. In fast wave discharges the phase velocity of the EM wave is faster than the speed of light. In slow wave discharges the phase velocity of the EM wave is less than the speed of light.

Examples of resonant applicators that produce fast wave high pressure discharges are given by Babat[49] and Asmussen[50]. The coupling structure used in these examples, is formed by a cylindrical resonant cavity. This cavity is basically a length of waveguide terminated by two shorting planes set to certain resonant eigenvalue lengths.

Microwave power is coupled into the cavity by either a coaxial coupling structure or by a waveguide aperture coupling structure. At high pressures (above ~10 Torr) the discharge will fill only part of the cavity and is separated from all surfaces if properly designed. The discharge alters the field pattern of the resonant mode thus changing the resonant frequency of the structure. The structure can be retuned by altering the position of one of the shorting planes[51] or by changing the input frequency of the microwave energy[52]. This process is nonlinear since changing the cavity tuning changes the plasma properties requiring the cavity to be further retuned, etc..

There are several advantages for using this type of energy applicator in a thruster system. Because it is a resonant device, the discharge it produces is stable in position irregardless of the rate of propellant flow, and if properly excited, this discharge can be maintained away from the chamber walls. The input power level this device could be maintained at is limited mainly by the input coupling structure and not by the applicator. An additional advantage of this applicator is that it can also produce slow wave discharges. Its main disadvantage is that its structural size relates directly to the excitation frequency. At higher microwave frequencies its reduction in size limits the input power it can handle and at lower frequencies its size may become to bulky for practical use.

An example of a resonant applicator that produces a slow wave high pressure discharge is given by experiments with the surface wave launcher shown in Figure 3.1.[53,54] This coupling structure is referred to as a coaxial reentrant cavity and is operated with a quartz tube located inside the center conductor. The gap in this structure

Coaxial Reentrant Cavity

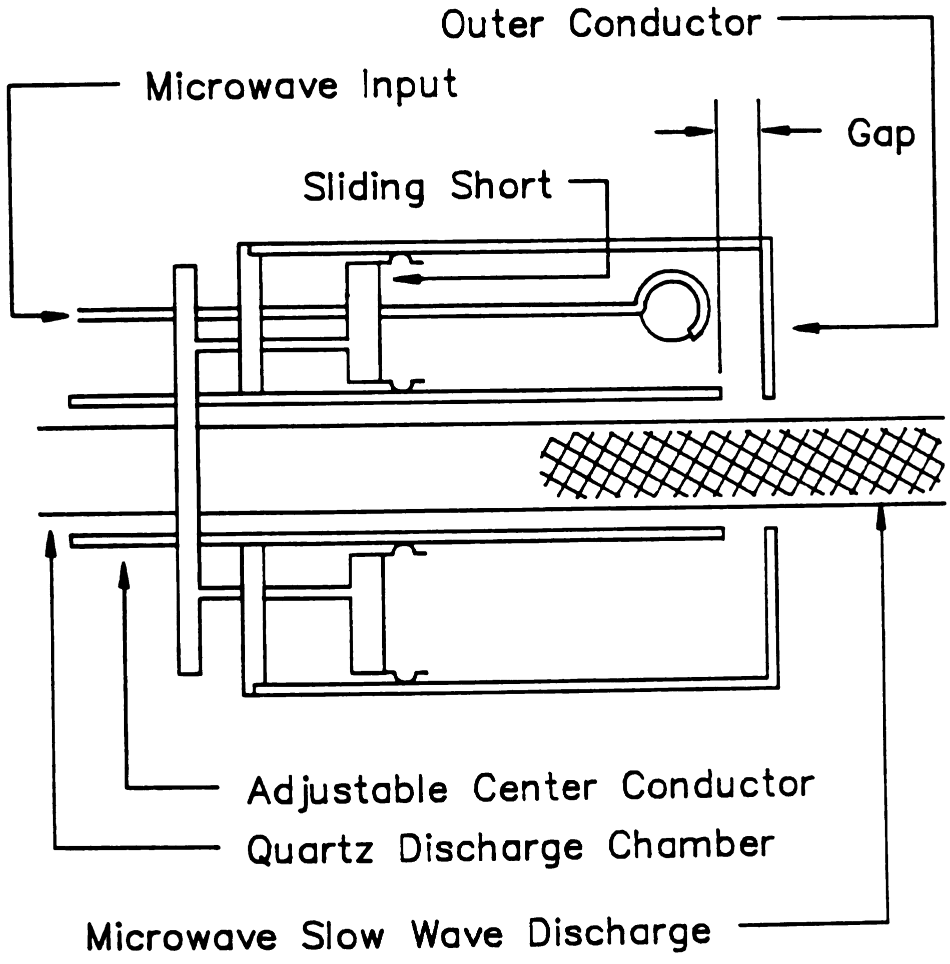

Figure 3.1 Coaxial Reentrant Cavity

generates strong fields that launch a surface wave discharge in the gas inside the quartz tube. This surface wave discharge extends in both directions from the gap. Energy is transferred to the discharge by the slow surface wave propagating, thus heating the discharge and attenuating the surface wave. Increasing the input power to the coupler has the primary effect of lengthening the discharge.

An advantage of this type of coupler is that it is capable of operating down to low frequencies (100 MHz) without the need of a large coupling structure. The coupling gap however presents a problem in terms of limiting the maximum input power. This is due to possible breakdown in this region. Another problem is the power handling abilities of the input coupling structure. The potential for breakdown limits the maximum value that the input coupling structure can handle.

3.2.2 PROPAGATING WAVE APPLICATORS

Propagating wave applicators can also be divided into two different types according to how they operate. The first type presented, uses a evanescent field to sustain a discharge and the second type presented uses a radiating field.

An example of a coupling structure that uses a evanescent electromagnetic field is the coaxial microwave "torch".[55] A similar device is presented in great detail in section 3.4 of this chapter. A microwave discharge is formed attached to a center conductor of a coaxial matching structure. Gas flow is used to keep the discharge from arcing to the outer conductor and in the process forces the discharge to form out straight from the center conductor.

At higher microwave frequencies EM modes other than a TEM mode can form if the diameter of the device is made too large (4 cm for 3 GHz). But making a smaller device limits the power it can handle without having unwanted breakdown in the applicator. At lower frequencies this is not a problem since the diameter can be increased to handle more power. In fact, since this device uses a TEM mode, it could probably operate down to low frequencies although changes in the matching circuit would be necessary. One of the main disadvantages is that the discharge is attached to the center conductor, possibly causing thermal loss, melting and limiting the discharge temperature.

An example of a coupling structure using a radiating electromagnetic field is described in experiments by Moriarty[56] and is shown in Figure 3.2. This structure is basically a quasi-optical microwave coupling system. This system used a ellipsoidal antenna 10 feet in diameter to focus propagating microwave radiation into a discharge chamber. A microwave discharge was formed at the focus of antenna inside the discharge chamber. The system had a coupling efficiency of 20% with a input peak power of 1 MW at 3 GHz.

For space applications this system is rather bulky but at higher frequencies it could be small enough to be practical. In fact it is similar to the proposed laser thruster[28] and would be capable of operation up to light frequencies as a laser thruster. The matching is a serious problem and it would have to be improved for real use. The potential for handling radiation using lenses would allow this coupler to operate a very high power levels.

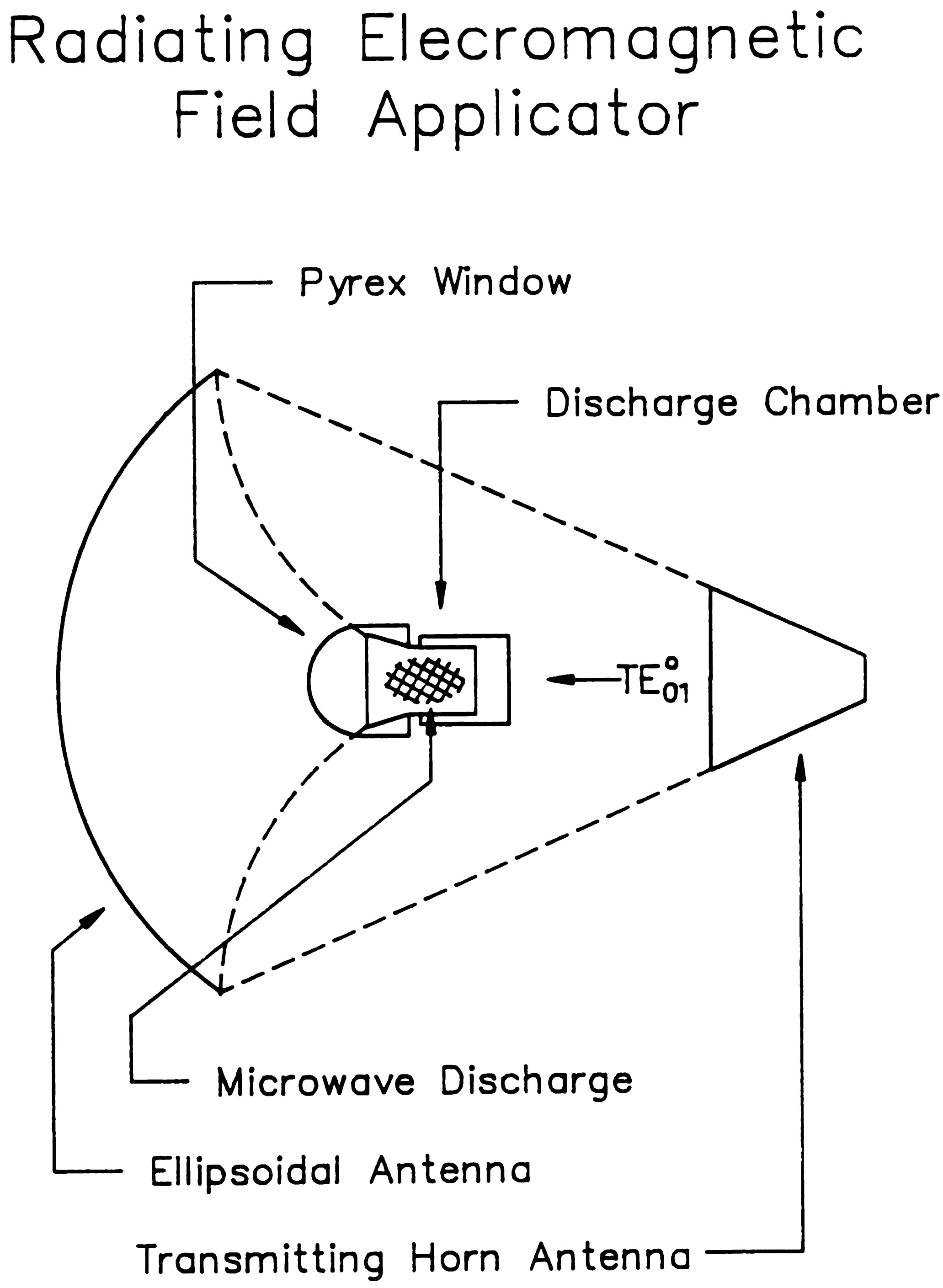

Figure 3.2 Radiating Wave Applicator

3.3 COAXIAL APPLICATORS

The basic design and construction of the coaxial applicator presented in this section was by Rogers[57] and was based on earlier work.[55,58] First a detailed description of the basic coupling structure is given and next a description of the working applicator based on this coupling structure is presented.

3.3.1 APPLICATOR DESCRIPTION

As shown in the Figure 3.3 the applicator consists of a coaxially fed microwave discharge located at the end of a 4.8 cm i.d. cylindrical, brass microwave coupling system. Microwave power is fed in through, the input microwave port (1), thus entering into a coaxial coupling system (2) in a transverse electromagnetic mode (TEM). A cylindrical microwave discharge (3) is formed and maintained at the end of a 2 cm diameter adjustable center conductor (4). A adjustable sliding short (5) and the adjustable center conductor allow the coaxial coupler to be tuned so that all of the incident power is coupled into the discharge structure (6) located at the end of coaxial applicator. The center conductor of the applicator is hollow and sealed so that water can flow through it to cool the tip. Water cooling is also provided for the outside wall of the coupler although experiments suggest it was not needed. The discharge structure located at the end of the coupler was designed so it could be removed and different types of discharge structures could be tested.

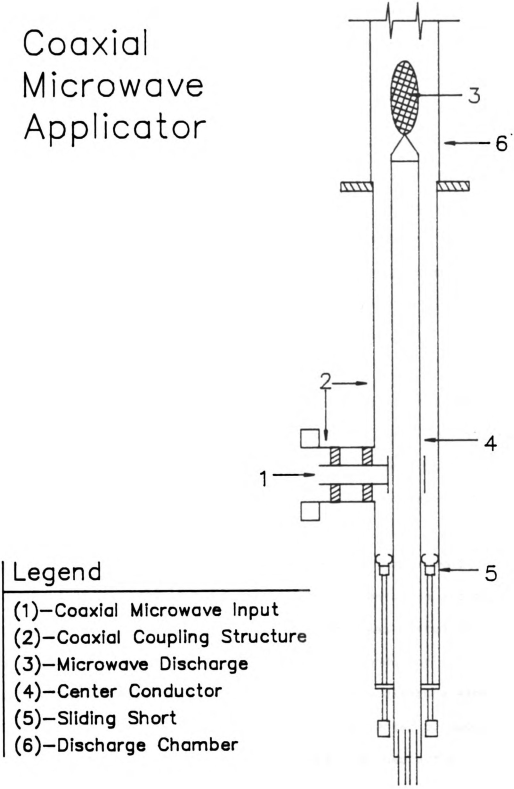

Figure 3.3 Coaxial Microwave Applicator

3.3.2 APPLICATOR OPERATION

Figure 3.4 shows the basic applicator that was tested by Rogers.[13] This figure continues the numbering system used in Figure 3.3 with the following additions. A teflon gas seal (6), seals the discharge chamber (8) from the atmosphere. The test propellant enters through (7) and enters into the discharge chamber (8). A microwave screen (9) continues the outer wall of the coupling system. In these experiments the applicator was not connected to a vacuum system. The discharge chamber was sealed and the input gas added to the discharge chamber. A vent allowed the gas to be removed at the top of the discharge chamber, thus all experiments were conducted at atmospheric pressure. A piece of tungsten carbide wire was shorted from the outside conductor to the inside conductor starting the discharge.

Rogers obtained discharges in helium and nitrogen with a input power level of 500 Watts and the applicator in a horizontal position. Reflected power was low indicating good matching. These experiments demonstrated the use of the torch and the ability to generate high pressure discharges with it.

Experiments by Rogers with this applicator were continued by this author. The applicator was changed to a upright orientation and a 0-2.5 kW microwave system was used. The applicator was tested in mixtures of nitrogen and helium. Short and center conductor tuning positions were established. The most critical tuning distance was found to be the distance from the short to the tip of the center conductor. If this distance was maintained, the short/probe combined action could be adjusted over a range of values with little change in matching. As such the torch had no single mode of operation, but rather a range of

Experimental
Coaxial
Microwave
Applicator

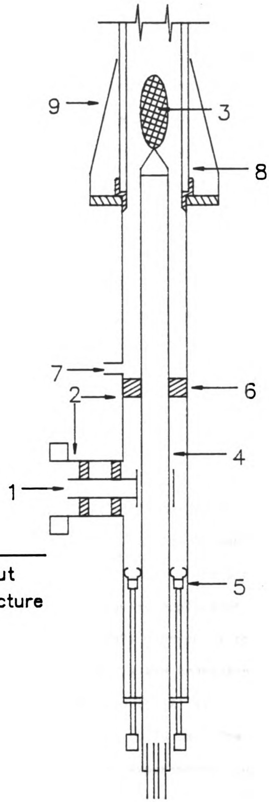

Legend

(1)—Coaxial Microwave Input
(2)—Coaxial Coupling Structure
(3)—Microwave Discharge
(4)—Center Conductor
(5)—Sliding Short
(6)—Teflon Plug
(7)—Gas Input
(8)—Discharge Chamber
(9)—Conducting Screen

Figure 3.4 Experimental Coaxial Microwave Applicator

operatic

Th

s). I

sed an

he app

spacers

port

nput

3.4 CA

resona

appli

and t

3.4.1

shown

expe

is m

seco

by 1

bras

adj

sec

rem

dis

operation.

The best match that could be obtained with this applicator was 95%. In order to simplify construction, unmatched teflon spacers were used and it was felt that these spacers were limiting the matching that the applicator could achieve. It was found that the position of these spacers was very critical. If they were placed close to the sliding short they would get very hot and also cause arcing between the coaxial input and the fingers on the short.

3.4 CAVITY TYPE APPLICATORS

The second type of applicator that was used in experiments was a resonant type cavity applicator. The first section details the basic applicator design, the next section describes its electrical operation and the last section describes the circuit tuning of this applicator.

3.4.1 APPLICATOR DESCRIPTION

A diagram of the cavity applicator used in these experiments is shown in Figure 3.5 and utilizes the same design philosophy of earlier experiments.[51,12,59] The energy absorption chamber shown in this figure is made up of two interdependent parts; First, a cavity applicator and second, a discharge chamber. The resonant ("cavity") portion is formed by 17.8 cm inside diameter cylindrical brass pipe (1) and transverse brass shorting planes (or "shorts"). One of the shorts (2) is adjustable to provide a variable cavity length of 6 to 16 cm. The second short (3) was fixed in position, but in some experiments could be removed to allow different discharge chambers (6) to be tested. The discharge (4), which could be viewed through a copper screen window (5)

Cross Section of Microwave Cavity Applicator

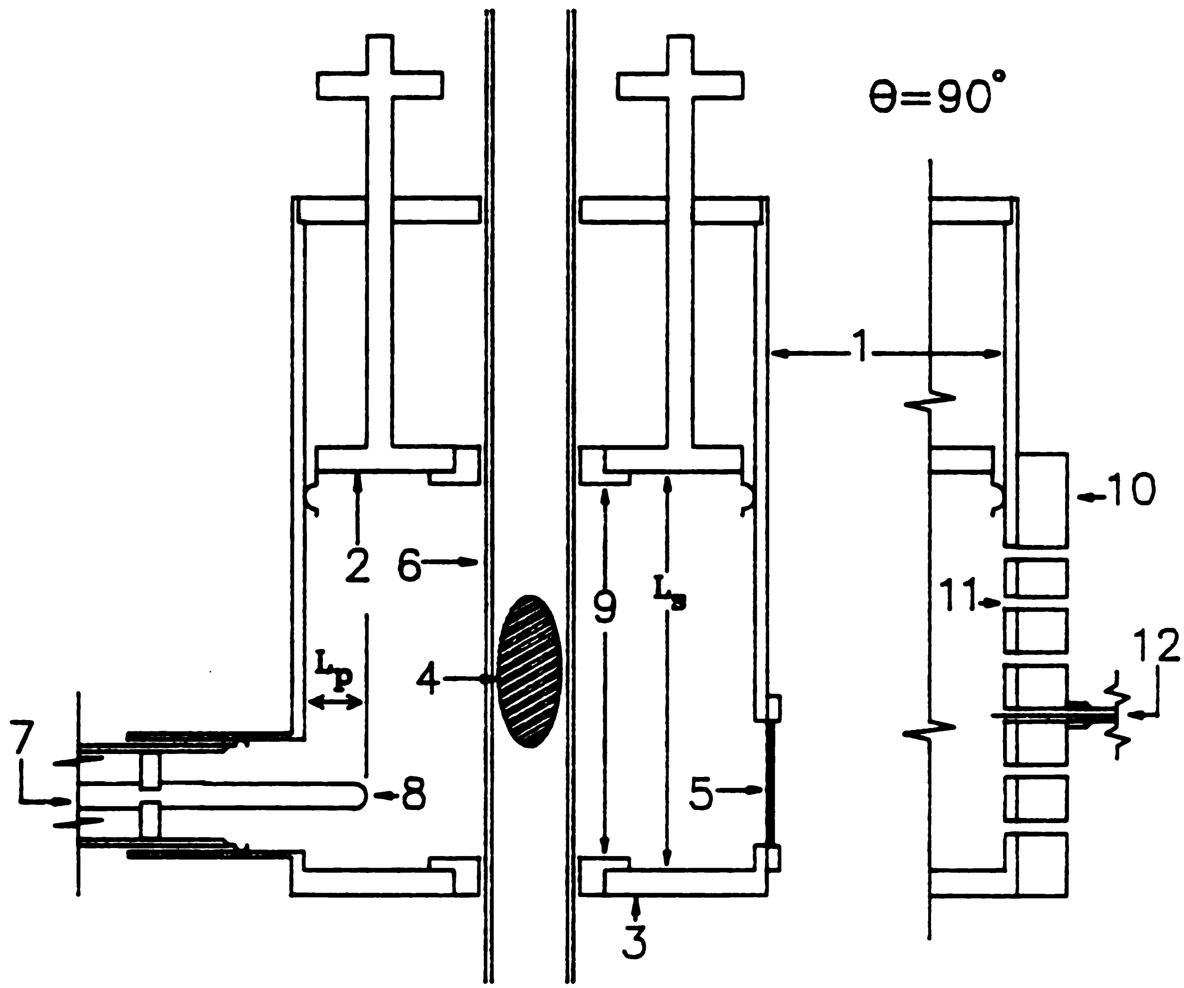

Legend

(1)—Cavity Walls	(7)—Coaxial Microwave Input
(2)—Sliding Short	(8)—Input Coupling Probe
(3)—Base Plate	(9)—Brass Collars
(4)—Plasma Discharge	(10)—Microcoax Block
(5)—Viewing Window	(11)—Microcaox Probe Hole
(6)—Discharge Chamber	(12)—Microcoax Probe

Figure 3.5 Cross Section of Cavity Applicator

is form
stable
cylindr
chamber
input p
The ad
tuned
discha
microw

cylin
Sever
and t
probe
diagr
would
meas

appl
disc
a qu
inco
The
3.6
cav
tun

is formed inside a cylindrical discharge chamber and is maintained in a stable fashion contracted away from the walls of the chamber. The cylindrical quartz discharge chamber was removable so that different chambers could be tested. Input microwave power is fed into the coaxial input port (7) and coupled into the cavity by the adjustable probe (8). The adjustable probe and the adjustable short allow the cavity to be tuned so that the maximum amount of power is transferred into the discharge. Brass collars (9) were used to increase cavity Q and reduce microwave leakage.

A rectangular brass bar (10) was soldered onto the outside of the cylindrical outer shell of the cavity parallel to its center axis. Several small, diagnostic holes (11) were drilled through this piece and the cavity wall at known axial locations. Small electrical E field probes (12) made from 2 mm o.d. microcoax were inserted into the diagnostic hole to measure the radial E field near the wall. The probe would couple out a small amount of power proportional $|E_r|^2$ and then be measured with a power meter.

Figures 3.6 and 3.7 show photographs of the microwave cavity applicator. Figure 3.6 shows the applicator assembled but lacking a discharge chamber. Figure 3.7 shows the applicator disassembled with a quartz discharge chamber (D). This discharge chamber has a nozzle incorporated in it and was used for experiments presented in chapter 7. The cavity body (A) shown in Figure 3.7 is the same as the one in Figure 3.6 and the microcoax block is visible in the lower right side of the cavity of both pictures. The same sliding short actuator (B) and the tuning probe actuator (C) were used in both figures.

Initial experiments with the cavity applicator used a simple type

Picture of Assembled Microwave Cavity Applicator

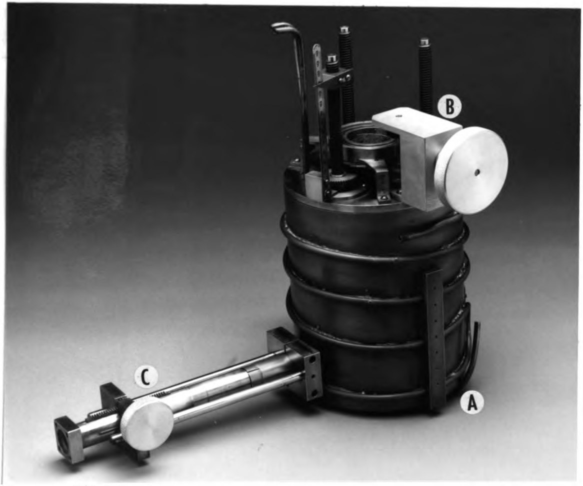

Legend

(A) –	Brass Microwave Cavity Body (note microcoax block in lower corner)
(B) –	Sliding Short Actuator
(C) –	Tuning Probe Actuator

Figure 3.6 Picture of Assembled Microwave Cavity Applicator

Picture of Disassembled Microwave Cavity Applicator

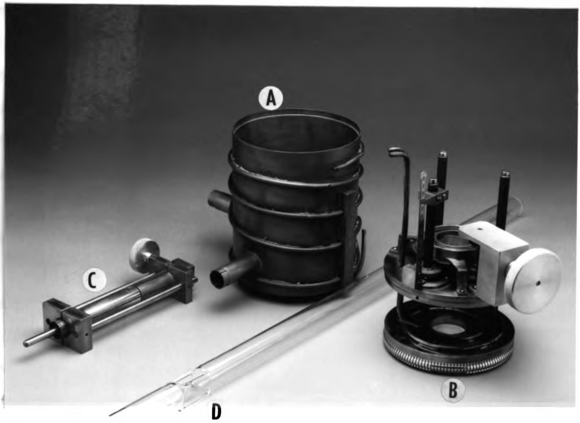

Legend	
(A) –	Brass Microwave Cavity Body (note microcoax block in lower corner)
(B) –	Sliding Short Actuator
(C) –	Tuning Probe Actuator
(D) –	Quartz Discharge Chamber with Nozzle

Figure 3.7 Picture of Disassembled Microwave Cavity Applicator

ctuator f

robe. Th

atter exp

odified a

port was

his actua

rive to m

ctuator w

his actua

ossible b

3.4.2 APPL

In ex

f the dis

ylindrica

atterns a

3.8. The e

axis produ

he center

shown in F

discharge

with a coc

he discha

he discha

Exper

ode to cr

The electr

actuator for the sliding short and no actuator for the variable length probe. The tuning accuracy of measurement was limited due to this so in latter experiments the sliding short and variable length probe were modified and are the actuators shown in Figure 3.6 and 3.7. The sliding short was attached to a jack type actuator as shown in the figures. This actuator used 3 ACME threaded screws and a coaxial planetary gear drive to move the sliding short back and forth. A rack and pinion actuator was added to the variable length probe as shown in the figures. This actuator allowed the probe to be moved in finer increments than was possible by hand adjustment.

3.4.2 APPLICATOR OPERATION

In experiments a microwave discharge (4) was created in the center of the discharge chamber (6) by exciting the cavity in the single, TM_{012} cylindrical cavity mode (L_s = 14.4 cm). The electric and magnetic field patterns and the associated discharge for this mode are shown in Figure 3.8. The electric field has an axial standing wave maximum along the axis producing an intense, approximately half wavelength discharge in the center of the cavity and the center of the discharge chamber. As shown in Figure 3.8, the discharge is "contracted" or separated from the discharge chamber walls. Thus, the discharge has a hot central core with a cooler gaseous outer layer adjacent to the quartz tube walls. If the discharge is allowed to touch the quartz walls heat transfer from the discharge to the walls increases resulting in wall melting.

Experiments described in this thesis also used the TM_{011} cavity mode to create a plasma discharge, which is also shown in Figure 3.8. The electric and magnetic field patterns are similar to the fields of

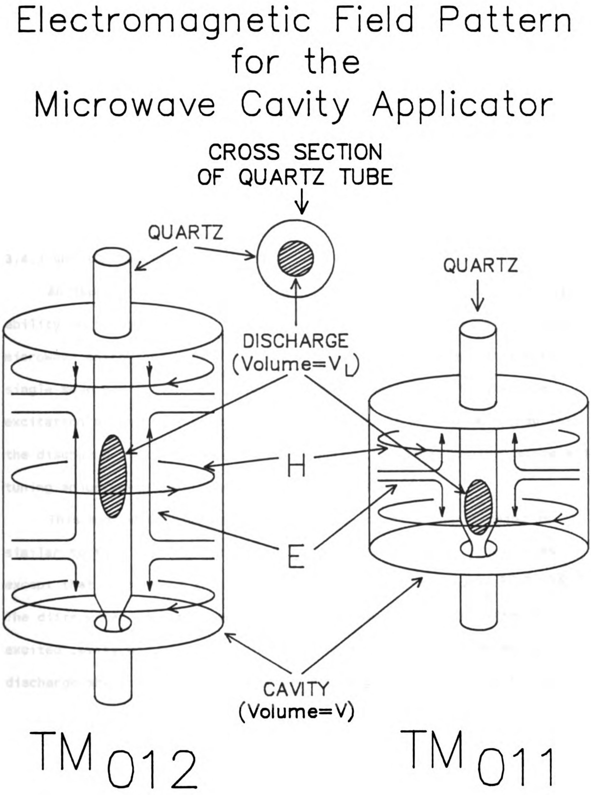

Figure 3.8 Electric and Magnetic Field Patterns for the Cavity Applicator

the
len
adj
len
can
dis
min

3.

ab
mic
sin
exc
the
tur

si
ex
Th
ex
di
hi

the TM_{012} mode except the cavity is adjusted to one half the resonant length, i.e., 7.2 cm. The discharge is formed at one end of the cavity adjacent to the nozzle and its length is approximately a quarter wave length long. Advantages of this configuration are that the discharge can easily be brought close to or in contact with the nozzle and the discharge has a smaller volume and hence, smaller surface which minimizes radial energy losses.

3.4.3 APPLICATOR TUNING

An important feature of the cylindrical cavity applicator is its ability to focus and match (little or no reflected power) the incident microwave energy into the discharge zone. This is accomplished with single mode excitation and "internal cavity" matching. Single mode excitation allows the focusing and control of the microwave energy into the discharge zone. The matching is labeled "internal cavity" since all tuning adjustments take place inside the cavity.

This method of electromagnetic energy focusing and matching is similar to that employed in recently developed microwave ion sources except that it is used at higher discharge chamber pressures.[60,61,62] The differences with this application are associated with different excited cavity modes and the discharge itself; i.e. differences in discharge shape and location and the discharge properties due to the higher operating pressures.

where

incl

disc

elec

curr

resi

seen

adju

adju

the

the

vari

thes

are

res-

tran

with

figu

conn

vic-

The input impedance of a microwave cavity is given by

$$Z_{in} = \frac{P_t + 2j\omega(W_m - W_e)}{\frac{1}{2}\,|I_o|^2} = R_{in} + jX_{in} \quad (3.1)$$

where P_t is the total input power coupled into the cavity (which includes metal wall losses as well as the power delivered to the discharge). W_m and W_e are, respectively, the time averaged magnetic and electric energy stored in the cavity fields and $|I_o|$ is the total input current on the coupling probe. R_{in} and jX_{in} are the cavity input resistance and reactance and represent the complex load impedance as seen by the feed transmission line. At least two independent adjustments are required to match this load to a transmission line. One adjustment must cancel the load reactance while the other must adjust the load resistance to a value equal to the characteristic impedance of the feed transmission system. In the cavity applicator the continuously variable probe (8) and sliding short (2 of Figure 3.5) tuning provide these two required variations, and together with single mode excitation are able to cancel the discharge reactance and adjust the discharge resistance to equal the characteristic impedance of the feed transmission line.

This internal cavity matching technique can best be understood with the aid of the equivalent circuit shown in Figures 3.9. These figures display a standard circuit representation for a cavity which is connected to a feed waveguide or transmission line and is excited in the vicinity of a single mode resonance.[63] G_c, L_c, and C_c represent the

Equivalent Circuit of the Microwave Cavity Applicator

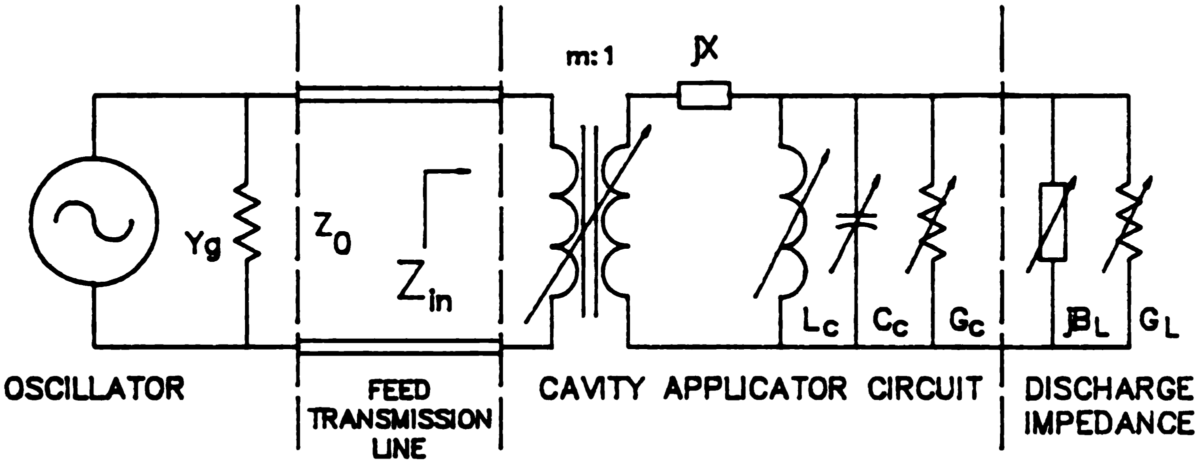

$$\hat{\epsilon} = \epsilon' + j\epsilon'' = \epsilon_o\left[1 - \frac{\omega_p^2}{\left(\nu_{eff}^2 + \omega^2\right)}\right] + j\epsilon_o\left[\frac{\nu_{eff}}{\omega}\frac{\omega_p^2}{\left(\nu_{eff}^2 + \omega^2\right)}\right]$$

Losses in Single Mode Cavity

$$G_C \propto R \oint\!\!\oint_S |H|^2 ds = P_b \qquad G_L \propto \frac{\omega}{2}\iiint_{V_L} \epsilon''|E|^2 dV = P_a$$

Stored Energy in the Field

$$C_C \propto \frac{1}{2}\iiint_{V-V_L} \epsilon_o|E|^2 dV \qquad L_C \propto \frac{1}{2}\iiint_{V-V_L} \mu_o|H|^2 dV$$

$$jB_L \propto \frac{1}{2}\iiint_{V_L} \epsilon'|E|^2 dV + \frac{1}{2}\iiint_{V_L} \mu_o|H|^2 dV$$

Figure 3.9 Equivalent Circuit of the Cavity Applicator

conductance, inductance and capacitance respectively of the excited mode near resonance and jX represents the reactive effect of the evanescent modes far from resonance. The relationships between the cavity fields and these equivalent lumped circuit elements is shown in Figure 3.9. In a cavity without a discharge, $\varepsilon' = \varepsilon_0$, and $V_L = 0$ and integrations for C_c, and L_c are over the entire cavity volume V. At resonance, the capacitive and inductive susceptance cancel, resulting in a pure conductive input admittance. The coupling probe (or aperture) is represented in Figure 3.9 as the ideal transformer of turns ratio m:1. Both circuit elements and the transformer are drawn with arrows to indicate their variability during the tuning process.

The discharge is ignited by first adjusting the probe and cavity length positions to excite a specific empty cavity resonance (i.e., TM_{012} or TM_{011}) and to match the empty cavity applicator to the input transmission system. Microwave power is then applied, absorbed into the cavity without reflection and a discharge is ignited even with low input powers of 20-50 W if the pressure in the discharge zone is reduced to 0.5 to 10 Torr. The presence of the discharge changes L_c, G_c, and C_c and adds an additional discharge conductance G_L and susceptance, jB_L, to the circuit. That is, in the presence of a discharge ε'' and V_L are no longer zero and hence jB_L and G_L are also not zero.

As indicated by the equations in Figure 3.9, these equivalent circuit elements are nonlinear functions of many experimental variables. These include discharge gas mix and type, pressure and flow rate, discharge geometry, absorbed microwave power (i.e., $|E|^2$) and discharge properties such as electron density, and collision frequency. The nonlinear behavior of the discharge (and hence the behavior of the equivalent circuit elements) is exhibited as hysteresis[64] in experimental variables such as input power, tuning, and operating pressure.

The discharge admittance shifts the resonance, unmatching the plasma loaded cavity from the feed transmission line. If the cavity length and coupling probe remain fixed, further increases in incident power result in only a slight increase in absorbed power and a small change in discharge admittance since the cavity is further detuned from resonance. Thus, the presence of the discharge allows only a small portion of additional incident power into the cavity causing a large increase in reflected power. This limited variation in discharge properties is a fundamental problem associated with sustaining microwave discharges in fixed size and fixed coupling cavities.[54] Discharges in these cavities can be only maintained over a very narrow range of discharge loads (discharge densities, volumes, pressures, flow rates, etc.) and thus these cavity applicators often operate with large reflected powers.

The variable "internal cavity" matching employed in this applicator provides the variable impedance transformation that allows the discharge to be matched over a wide range of discharge loads. The tuning together with variation of the incident microwave power "pulls" the discharge properties along a discharge "loss line" similar to that described elsewhere for cylindrical discharges.[48,64] For a given incident power, gas type, gas flow rate, and discharge pressure, i.e., for a given operating condition, the length and probe tuning are varied in iterations until reflected power is reduced to zero. Typical tuning distances are of the order of several millimeters and thus the tuning process can be quickly performed either manually or with small motors and can also be utilized as a simple discharge power control technique.

The matching is accomplished without altering either the plasma shape and position or the mode electromagnetic field patterns and without losing microwave power in external (conventional) tuning stubs. Increases in input power increase the electric and magnetic field strengths. However, the geometry of field patterns as shown in Figure 3.8, i.e. the electromagnetic focus, remains approximately constant throughout the tuning process keeping the location of the plasma in the center of the cavity away from external walls. Thus, the cavity system can be tuned to a match as the experimental conditions, such as flow rate, pressure, discharge configuration etc., change.

This tuning provides another important practical function. Certain stabilizing gas flows require the insertion of a quartz center body into the discharge chamber and into the cavity excitation region. The position of the body was varied to optimize performance. Its presence and position inside the cavity would tend to detune the cavity. However, only a slight length tuning is required to compensate for its presence and to return the system to a power match.

3.5 MICROWAVE ARCS

This section will describe the discharge itself and the mechanism by which it is sustained and transfers energy to the propellant. First the energy paths that convert microwave energy into thrust are presented. The descriptions in these sections are brief and very general. For further information on microwave discharges the reader should refer to MacDonald[65] and Marec[66] and for information on general

arc
pea
pre
fic

pro
The
mi

3.

in
el
el
Ch
tr
en
st
ap
su
th

mo
mo
el
ga
(e

arc properties the reader should refer to Pfender[67]. Actual measurements of the energy distribution of a microwave discharge at pressures below 10 Torr, sustained by a cavity applicator and using flowing hydrogen gas, are presented in Chapman[68].

In the last section experiments with these discharges are presented under the conditions necessary for an electrothermal thruster. The coupling structures presented in the section serve to match the microwave power into the microwave discharge.

3.5.1 DESIRED ENERGY PATHS

The energy paths of a microwave electrothermal thruster are shown in Figure 3.10. Microwave energy is transferred to the electron gas via electromagnetic force interactions between the electrons and the electromagnetic field in the applicator and is described in Cherrington[69] and Marec[66]. Ideally all of the microwave energy is transferred to the electron gas but in a real applicator some of the energy is always lost due to resistive heating of the applicator structure. The rate at which the energy is transferred to the applicator walls is given as P_b in Figure 3.9 and is equal to the surface integral of the tangential magnetic field over the interior of the cavity surface. Chapter 5 presents measurements of this loss.

Due to the large differences in mass, electrons are accelerated much more than the ions and therefor energy transfer to the electrons is much greater than the energy transfer to the ions. Thus the electromagnetic energy is transferred almost entirely to the electron gas and the electromagnetic interactions with the ions can usually (except at special ion resonances) be ignored.

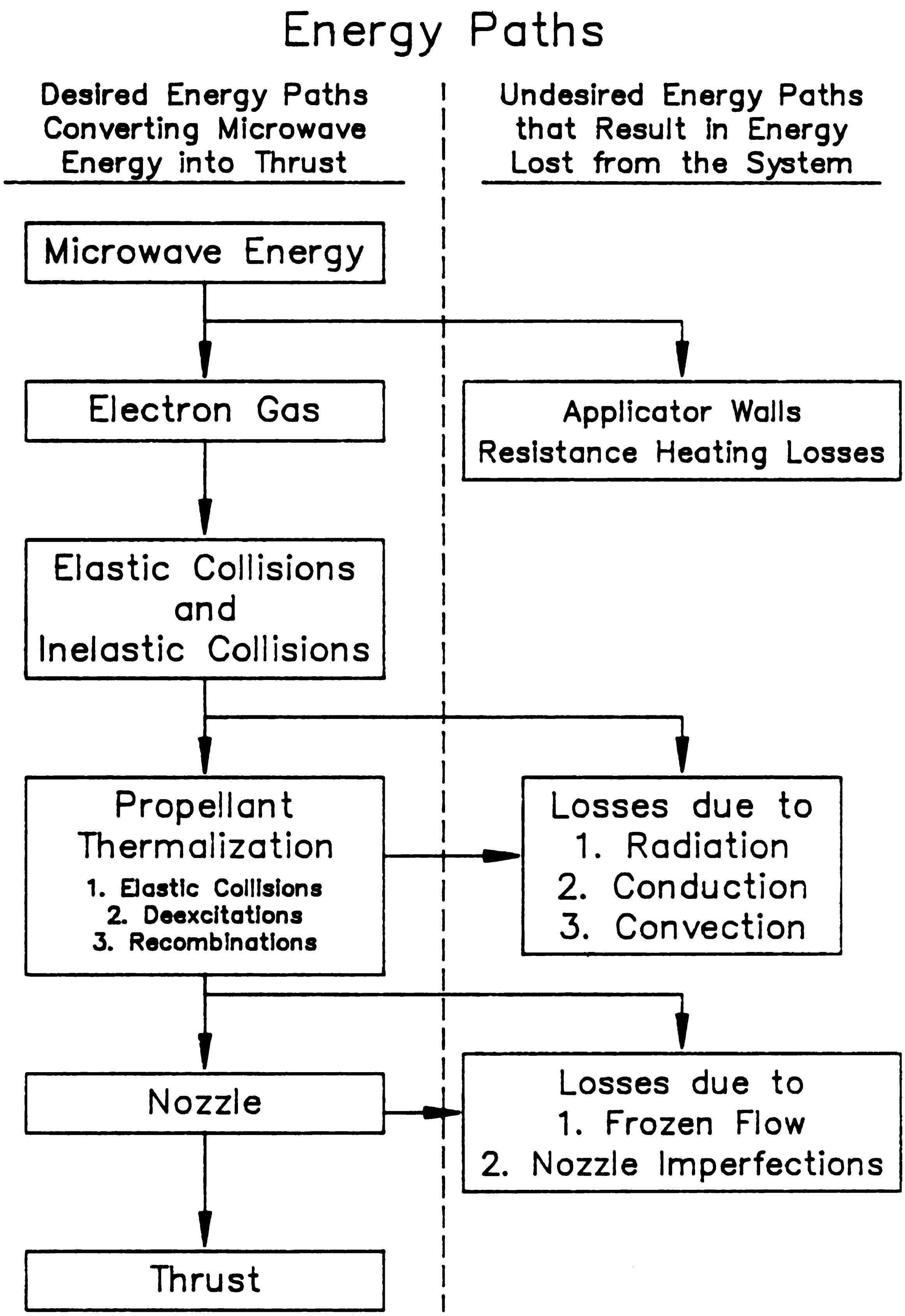

Figure 3.10 Energy Paths Converting Microwave Energy into Thrust

If the direction of the electromagnetic field changes every half cycle, the direction of force on the electron also changes every half cycle causing the electron to oscillate with the electric field. If the electron does not collide with a heavier neutral or ion or the walls of the discharge chamber, it just oscillates out of phase with the field and there is zero net energy transfer to the electrons over a complete cycle. This means that no net energy is supplied to a particle in a steady state time harmonic electromagnetic field when there are no collision processes.

However, when there are elastic collisions with heavier particles present the transfer of electromagnetic energy to the electron gas is enhanced. Thus in a plasma where neutral and ion gases interact with the electron gas, the electrons on the average gain energy after each elastic collision and hence a net transfer of energy from the electromagnetic field to the electron gas takes place. The time average power density delivered to the plasma from the electromagnetic field is given by

$$\langle p \rangle = \frac{1}{2} \frac{\nu_{eff} N_0(r) e^2}{m_e(\nu_{eff}^2 + \omega^2)} |E|^2 \qquad (3.2)$$

where $N_0(r)$ = electron density

ω = excitation frequency

ν_{eff} = effective electron - neutral collision frequency

$|E|$ = magnitude of the electric field

e = electron charge

or per average electron

$$\langle p_e \rangle = \frac{1}{2} \frac{\nu_{eff} e^2}{m_e(\nu_{eff}^2 + \omega^2)} |E|^2 \qquad (3.3)$$

Thus the time average power delivered to the discharge is given by the equation for P_a from Figure 3.9.

The heated electron gas transfers its energy to the heavier ion and neutral gases via elastic and inelastic collisions. Each typical elastic collision, similar to a collision between two elastic balls of unequal mass, transfers a small amount of energy (proportional to m_e/M per collision) from the higher energy electrons to the heavier, cooler ion and neutral gases. This energy is converted quickly into thermal energy of the heavier gases after inter-ion and inter-molecular collisions.

Inelastic collision also transfer energy from the electron gas to the heavier gases by such inelastic processes as excitation, ionization and dissociation. This energy is stored in the heavier gases until additional inelastic collisions occur. Some of these inverse inelastic processes are collisional recombination and deexcitation. These deexcitation and recombination collisions release the ionization, dissociation and excitation energy to the interacting particles. By further collisional processes this energy is converted into the thermal energy of the propellant.

Thermalization of the propellant results directly from elastic collisions and indirectly from inelastic collisions through deexcitation and recombination of ionized and dissociated species. A converging-diverging nozzle then serves to convert the thermalized energy to thrust energy. Ideally all of the electron gas energy is converted to thermal energy and is available for the nozzle to convert into thrust energy.

In a real thruster, radiation, convection and conduction prevent all of the electron gas energy from being available for conversion by the nozzle.

Addition energy losses occur in the conversion of the thermalized propellant in to thrust. Frozen flow losses occur when excited, dissociated and ionized species flow out the nozzle without being thermalized. Non ideal nozzle conversion of thermal energy into thrust energy results in further energy losses.

3.5.2 DISCHARGE PROPERTIES

The particle and energy flow with respect to the surrounding boundaries are shown in Figure 3.11. For this engine to operate cold input propellant is fed into the discharge chamber. Microwave energy is provided via the energy applicator. The microwave discharge serves to couple this energy into the thermalization of the propellant. The previous section discussed how the microwave energy in the electromagnetic field is converted into thrust. This section discusses properties of the discharge itself and where the energy transfer is occurring.

The transfer of microwave energy into the electron gas occurs within the discharge zone via the energy paths discussed in the last section. This electromagnetic energy transfer and resulting energy paths inside the discharge zone result in a large amount of thermalization within the discharge zone and downstream from this zone. At high pressures when the discharge is separated from the discharge chamber walls, the discharge is at a considerably higher temperature than the gas outside the discharge zone. Thus the microwave discharge,

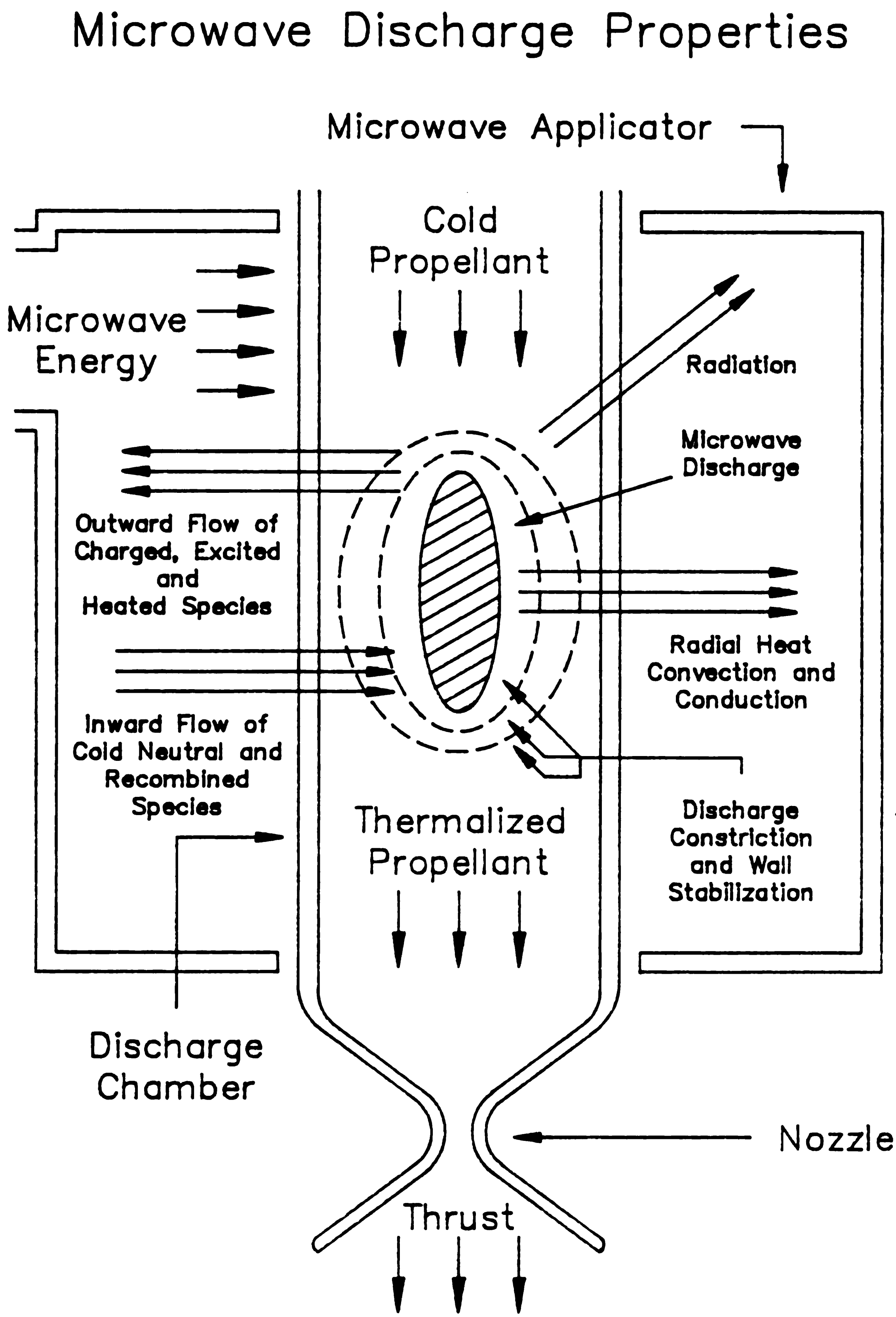

Figure 3.11 Microwave Discharge Properties

like low frequency arcs, is a thermally inhomogeneous discharge with a hot central core and sharp temperature gradients between the center and the surrounding cooler gas outside the discharge region. If the pressure is assumed to be uniform across the discharge chamber, the density in the discharge must be lower than the density outside the discharge because of the high temperature in the discharge zone.

As shown in Figure 3.11, there is a flow of cold neutral and recombined species into the discharge zone. At the same time there is net outward flow of ions, electrons, dissociated atom and thermally excited atoms. Under steady state conditions the density remains constant so that these two flows must be equal. In addition, because of temperature gradients, there will be convection flow from the hot center to the cool surrounding gas and heat conduction to the surrounding gas. Further if there is gravitational forces present, convection currents can occur because of buoyancy effect of the lighter heated gas verses the heavier cold gas. These flows are important because they bring cold neutral atoms into the discharge to be heated and they transport energy out of the discharge heating the propellant. At the same time these flows, along with radiation from the discharge, present a energy loss to the boundary walls.

At low pressure ($\leq$10-100 Torr) the ions, electrons and disassociated atom will diffuse to the wall of the discharge chamber where wall recombination takes place. At low pressures the particle density is not large enough for volume recombination to occur at a high rate. As the pressure is increased the rate of volume recombination increases. The increase in recombination together with the large thermal gradients causes the discharge to constrict.[70] This constriction is very important in the presence of a flowing propellant since the farther the discharge is away from the wall, the lower the energy losses to the walls and the greater the transfer to the propellant as it passes around and through the discharge.

In the applicators described in this thesis, the constricted discharges are held in place regardless of the rate of propellant flow by wall stabilization and the proper exciting electromagnetic field (mode in a cavity applicator) configuration. The maximum energy transfer to the discharge occurs with the discharge centered in the chamber by design of the applicator. If the discharge moves off center the energy into the discharge is reduced and the applicator is detuned. At the same time the thermal energy loss to the chamber walls is increased. Thus any movement off center reduces the energy of the discharge, this reduction increases the particle density in the direction of movement which intern forces the discharge back to the center. This stabilization allows the discharge to be maintained off the chamber wall again reducing the energy loss.

3.5.3 DISCHARGE INITIATION

The description above describes the discharge operation in steady state condition. The methods used to start the discharge are also important. Two methods, and combinations of them, were use in these experiments. In the first method, the pressure of the discharge chamber was reduced to the point where the effective collision frequency, ν_{eff}, of the free electrons in the neutral gas, was equal to the radiation frequency, ω, of the microwave field. The applicator was then tuned for maximum E field and a discharge was initiated by tuning for minimum reflection. The pressure for this was between 0.5 Torr and 10 Torr for most gases.

If a high enough electric field could be generated, a second method was used at higher pressures. The applicator was tuned to maximum E field and a Tesla coil was used to inject extra free electrons in to the discharge chamber and breakdown occurs.

3.5.4 DISCHARGE EXPERIMENTS

This section describes research into the generation of high pressure microwave discharges and the properties of these discharges. The applicators described in this section produced discharges in several gases at high pressures. Experiments with other gases showed the ability to generate discharges in them, but were not studied at high pressure.

Experiments with hydrogen microwave discharges at atmospheric pressures were conducted by Kapitza.[71,72] These experiments used a cylindrical resonant cavity 20 cm in diameter operated in a TM_{01n} mode. A variable power supply could provide power levels of up to 174 kW at 1.55 GHz although the maximum absorbed power was 20 kW. Filaments of hydrogen about 1 mm in diameter and up to 10 cm long (at full power) were formed inside the cavity. Measurement of electron density and temperature were taken. Dymshits[73] calculated a gas temperature of 9000 K from this data for the hydrogen discharge.

Experiments with both hydrogen and nitrogen were conducted by Arata.[74,75] These experiments used a rectangular resonator with a variable power microwave source that was capable of power levels of up to 30 kW at .915 Ghz. Power absorption was reported to be greater than

80% into the discharge. For a input power of 20 kW, nitrogen was reported to have a gas temperature of 6300 K with a 4 cm discharge chamber and a gas temperature of 6800 K with a 2 cm chamber. Hydrogen, at a input power level of 20 kW, had a gas temperature of 9000 K.

Experiments with argon were conducted by Rogers[76] using the cylindrical resonator described in section 3.4 of this chapter. In a typical experiment input power was 500 Watts at 2.45 GHz and a 12 mm diameter quartz tube, running through the center of the cavity, was used as a discharge chamber. For a typical experiment a 0.2 mm filament discharge was produced with a power density of 130 W/cm^3. The inferred gas temperature was given as 1400 K with a collision frequency of 1.2×10^{10} sec^{-1}.

Experiments with argon were conducted by Hubert[77] in a surface wave coupler. For input power of 100 Watts at 1.7 Ghz and a 5 mm diameter quartz discharge chamber, a 14 cm long discharge was produced with a diameter of 1 mm. This discharge was at one atmosphere of pressure and gas temperature was given as 2500 K.

Experiments with nitrogen were conducted by Miyake[58] in a microwave torch. A gas temperature of 6700 K at high pressure was given for a input power of 2 kW at 2.45 GHz. At these conditions the discharge was 10 cm long and about 0.5 cm in diameter. Further experiments with a torch were conducted by Batenin.[78,79] For a atmospheric discharge in hydrogen, with a input power of 2 kW at 2.45 GHz, a gas temperature of 8500 K was measured. For a atmospheric discharge in helium, with a input power level of 900 Watts at 2.45 GHz, a gas temperature of 6500 ± 500 K was measured.

These experiments show that high pressure discharges can be generated and sustained by microwaves. They also show that these discharges are very hot and thus provide great potential for electrothermal use.

There is some interest in using more complex materials as propellants. These materials are left over from other spacecraft processes and would otherwise go to waste. Bandel[80] was able to generate a microwave discharge in a mixture of air and water. Mertz[81] used a microwave discharge of a mixture of CO and H_2 to produce methane. While these experiments were at low pressure, they demonstrate that discharges can be produced in complex molecular gases.

CHAPTER IV

EXPERIMENTAL SYSTEMS AND MEASUREMENTS

4.1 INTRODUCTION

This chapter describes the experimental systems that were used to generate and measure the data presented in this thesis. The first section presents a general overview of the entire system. The second section describes the experimental procedure and calculations used to take measurements of properties of the high pressure discharges. The third section describes the experimental procedures, measurements and calculations used to evaluate the properties of microwave electrothermal thrusters.

4.2 GENERAL EXPERIMENTAL SYSTEM

In order to experimentally create and control the microwave discharge and make measurements of thruster properties, several experimental measurement and control systems were necessary. The first measured and controlled the flow rate and pressure of the test gases used in the experiments. The second system measured and controlled the microwave energy and the third system measured the plasma volume size.

4.2.1 GAS FLOW, PRESSURE AND VACUUM MEASUREMENT

A diagram of the basic gas flow system is shown in Figure 4.1. As shown in this figure the system could be divided into two parts. The

Gas Measurement System

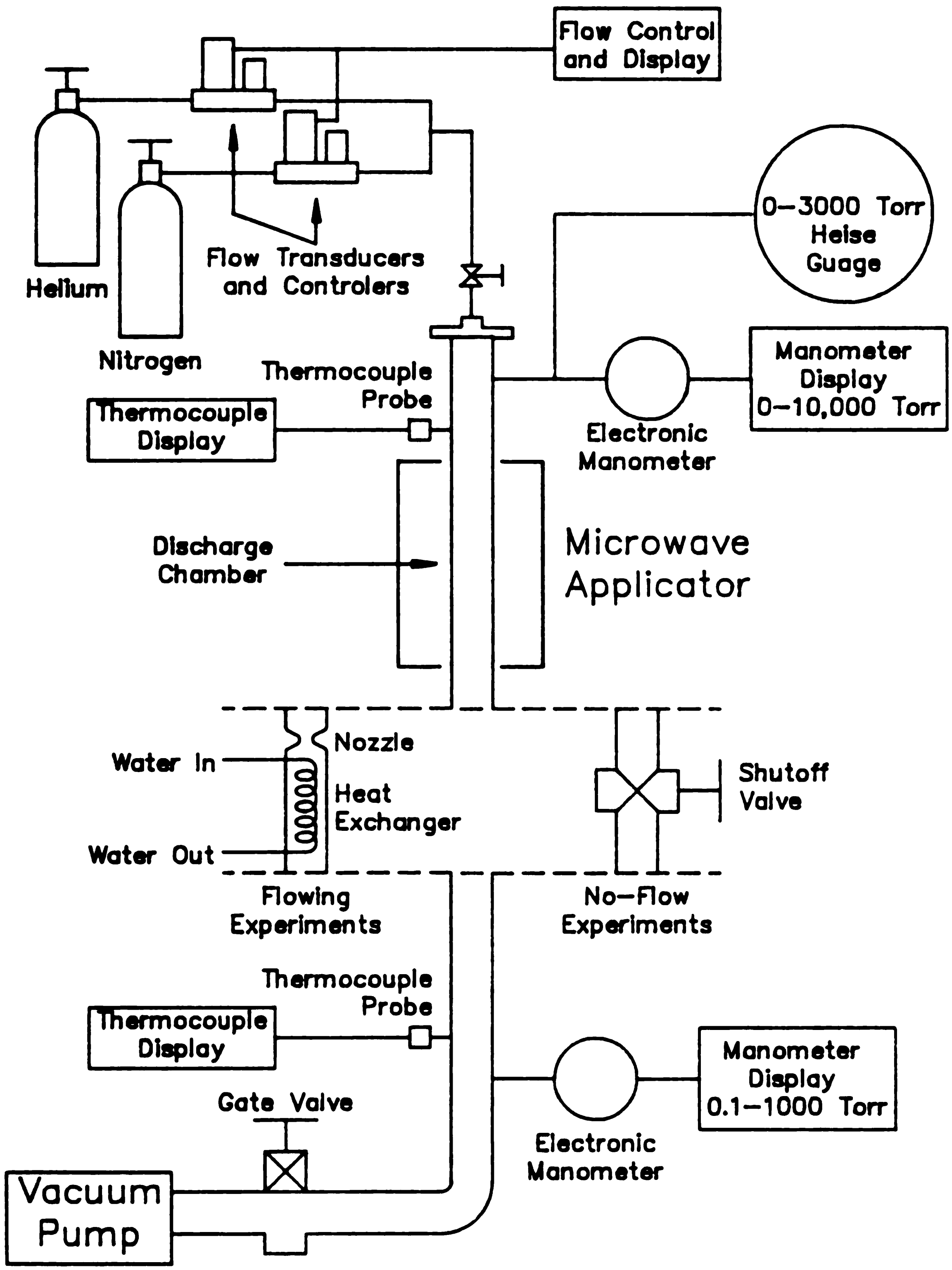

Figure 4.1 Gas Flow, Pressure and Vacuum Measurement System

rst p
serves
n this
gases,
pressur
usable
A
measure
this wa
control
experi
Figure
differe
10,000
the cha
electro
the gas
F
measure
dependi
a elect
pressur
manomet
for con
to meas
chamber
Th

first part supplies the gas to the discharge chamber and the second part serves to evacuate the discharge chamber. For all experiments presented in this thesis the propellants used were helium, nitrogen and oxygen gases, and were supplied to the system from high pressure cylinders with pressure regulators attached on cylinders to reduce the pressure to usable levels.

As shown in Figure 4.1 the system was capable of providing flow measurement of the propellant if it was required. In early experiments this was provided by a rotometer but was this found to be difficult to control and calibrate and is not shown in the Figure 4.1. For latter experiments a MKS 3 channel flow controller was used and is shown in Figure 4.1. This controller could measure the mass flow of three different gases into the discharge chamber, in a range of 50 to 10,000 sccm for each gas, and could also give the total gas flow into the chamber in sccm. By use of a electronic feedback circuit and electronic valves it could maintain a constant value of gas flow when the gas pressure or other conditions in the discharge chamber changed.

For all experiments discharge pressure was a necessary measurement. As shown in Figure 4.1 two different systems were used depending on the experimental conditions. For conditions above 1 Torr, a electronic MKS manometer and a Heise gauge were used to measure the pressure in the discharge chamber, and a 0.1-1000 Torr Datametric manometer was used to measure the pressure in the evacuation system. For conditions below 1 Torr, a Hastings thermocouple type gauge was used to measure the pressure in both the vacuum line and in the discharge chamber.

The vacuum was provided by a two stage mechanical roughing pump as shown in

the disc

rate of

system w

system w

allowed

might be

system f

vacuum s

nozzle,

experime

was used

system f

4.2.2 M

Th

function

microwav

microwav

the amou

The S-ba

these ob

As

componen

filtered

made by

microwav

shown in Figure 4.1 and a gate valve allowed the pump to shut off from the discharge chamber evacuation line. In order to provide the maximum rate of pumping, 2" vacuum Pyrex glass piping was used in the vacuum system wherever possible. In experiments with no gas flow, the vacuum system was used to evacuate the tube and a small amount of gas would be allowed to flow through the system to flush out any impurities that might be present. Then a valve is closed and gas is added to bring the system to the desired experimental pressure. In flowing experiments the vacuum system serves to keep the pressure low on the exhaust side of the nozzle, and thus also serving to exhaust the propellant from the experiment. In the experiments that required gas flow a heat exchanger was used to cool the gas near the nozzle exit to protect the vacuum system from the high temperature propellant.

4.2.2 MICROWAVE SYSTEM

The microwave system used in these experiments had two important functions. The first of these was to deliver a controllable source of microwave power to the microwave applicator and to safely handle this microwave power. The second was to provide an accurate measurement of the amount of power being coupled to the applicator and the discharge. The S-band, rectangular waveguide microwave system that accomplished these objectives is shown in Figure 4.2.

As shown in Figure 4.2, the system consisted of the following components. A 2.45 GHz microwave source was used to provide a well filtered continuous wave supply of microwave power. Different supplies made by several manufacturers were used to provide different amounts of microwave power needed in the experiments. The output of the microwave

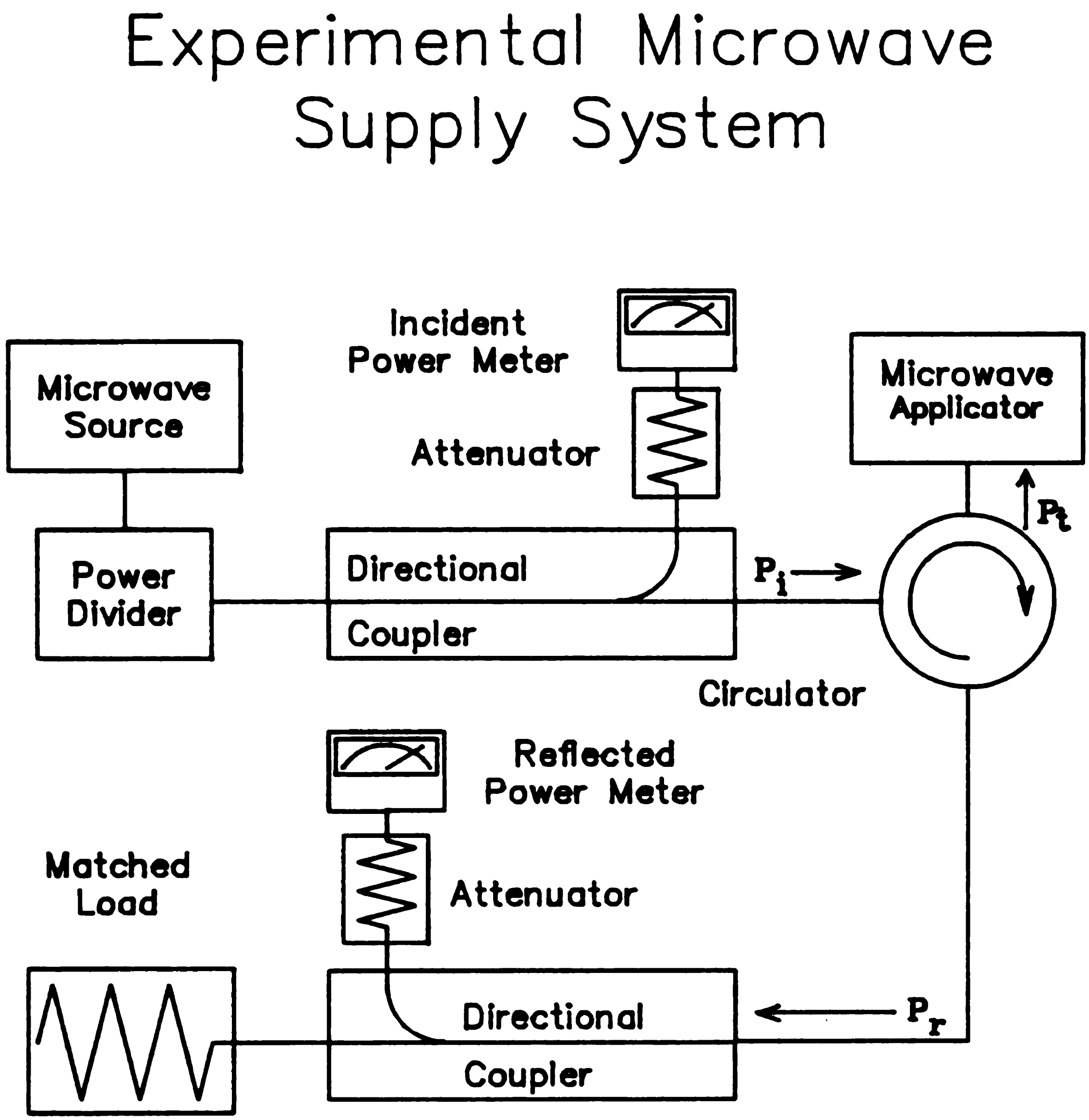

Figure 4.2 Experimental Microwave Supply System

source was connected into a microwave power divider. This device allowed a variable portion of the microwave signal to be absorbed into an internal load. This proved necessary since some of the microwave sources provided a stable, clean signal only near full power.

As shown in Figure 4.2 the output of the power divider was attached to the input of a waveguide broadwall directional coupler. This device couples a small amount of the input signal into the secondary arm where a precision attenuator and a microwave power meter are attached. By careful calibration with a source of known power and frequency, the power reading on the power meter gives a very accurate measurement of the incident microwave power.

Next the signal was inputted into the first port of a 3-port waveguide microwave circulator. The second port in the circular coupling structure was attached to the transmission system to the microwave applicator. The transmission system to the applicator used two different systems. For some early experiments a coaxial type system was used, but for all later experiments a flexible waveguide system was used because of less power loss and increased power handling capability.

The circulator provided at least 40 db of isolation between the incident and reflected coupling signals. This isolation protected the source from damage due to reflected signals and increased the accuracy of the incident and reflected power measurements by eliminating the back coupling into the directional couplers. The circulator also minimizes frequency pulling of the magnetron by variations in the plasma load.

The third port of the circulator was attached to a second broadwall type directional coupler. A precision attenuator and microwave power meter again were used to measure reflected signal power.

The output of the directional coupler terminated in a water cooled dummy load. This load served to absorb the microwave power not coupled in the energy absorption chamber.

By inputting a microwave test signal of known power and measuring both at the incident power meter and replacing the applicator with a second power meter an accurate calibration of the input power P_i can be made. By attaching a microwave source of known power in place of the energy absorption chamber and measuring the power at both the reflected power meter and a power meter attached in place of the water load, a very accurate calibration of reflected power P_r was made. Thus the power absorbed in the energy applicator is given by $P_t = P_i - P_r$.

4.2.3 DISCHARGE VOLUME MEASUREMENTS

The size of the plasma volume was a desired measurement in some experiments. A modified technique of Rogers[13] was used to make these measurements. A diagram of the setup is shown in Figure 4.3. As shown a camera is used to take a picture of the plasma discharge. In order to reduce the amount of aberration distortion in the resulting picture, Rogers technique was modified. Instead of a singlet close up lens, a rectilinear wide angle lens with a extension tube was used to take the picture. As shown in the figure this allowed the camera lens to be placed against the window of the cavity applicator and yet because of the wide angle lens the entire discharge was visible in the picture. Typically a 24 mm or 28 mm lens was used to take the picture and from 1 mm to 10 mm of extension tube was necessary depending on the focusing ability of the lens. For all gases the same exposure was used, EV12 with a f/stop of 4 and a speed of 1/250 of a second or a f/stop of 2.8

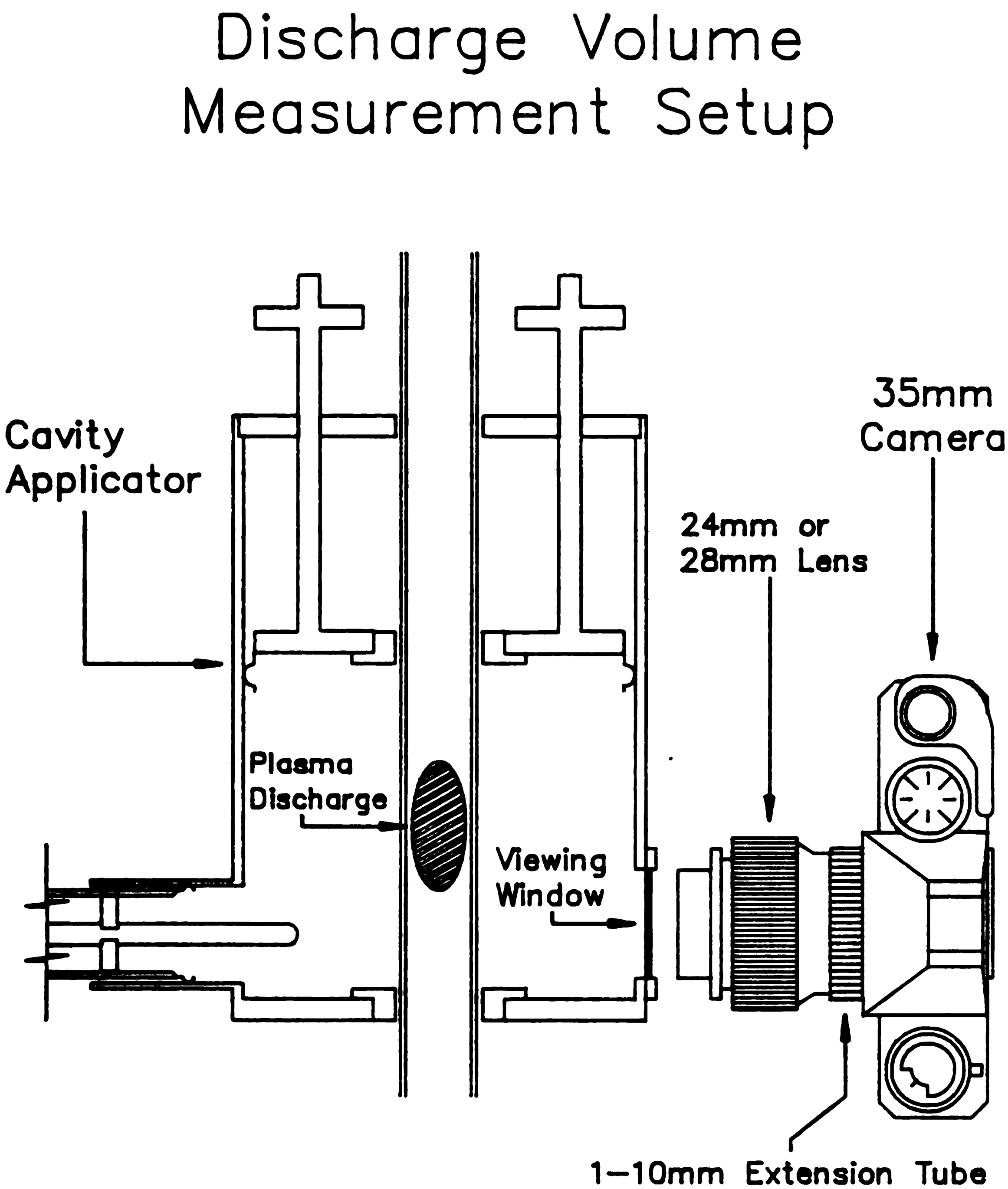

Figure 4.3 Experimental Setup for Discharge Volume Measurement

at 1/500 of a second.

In order to calculate the area of the plasma, slide pictures were taken using Ektachrome 200 film. With no discharge present a piece of graph paper was inserted into the discharge chamber in approximately the same position as the discharge. A picture of this graph paper was taken and used to correct for spherical distortions due to the wide angle. Then the plasma volume was calculated by first taking a picture of the discharge with the camera set up as mentioned earlier. Next the slide was projected onto a large piece of graph paper with the discharge enlarged as much as possible. The discharge was then divided into equal height solid disks and the diameter of each disk was measured. These diameters were then corrected for the distortions mentioned earlier. Then the volume of each disk was calculated by computing its volume as a solid cylinder and the total plasma volume was computed by summing the volume of all the disk sections.

4.3 HIGH PRESSURE CAVITY DISCHARGE CRITERIA

Experimental quantities of interest in the evaluation of applicator coupling performance are the power absorbed in the discharge, the microwave coupling efficiency to the discharge and the loaded cavity Q. By limiting the discussion to a single mode in a cavity type applicator, namely the TM_{012}, and by using the technique of Rogers[13], the coupling efficiency, loaded cavity Q and microwave power absorbed in the cavity walls can be calculated from the empty cavity Q and empty cavity absorbed power. A brief review of this technique is presented in the next sections.

4.3.1 COUPLING EFFICIENCY

The difference between the incident power, P_i, and the reflected power, P_r, measures the total power, P_t, delivered to the applicator. Power delivered into the applicator divides itself between the power delivered to the conducting cavity walls, P_b, and the power delivered to the discharge, P_a. Thus $P_t=P_b+P_a$. These two quantities can be related to the excited single mode cavity fields, discharge variables such as plasma frequency, ω_p, and the effective collision frequency, ν_{eff}, and the intrinsic resistance of cavity walls. The exact division of the power between the walls and the discharge depends on the relative lossyness of the discharge vs. the lossyness of the cavity walls.

It is useful to define a system "figure of merit" called coupling efficiency, which is concerned with the efficiency of coupling microwave power into the discharge. The overall coupling efficiency can be defined as

$$(Eff)_1 = \frac{P_a}{P_i} \times 100 \qquad (4.1)$$

where $P_i=P_r+P_t=P_r+P_a+P_b$. Viewing the applicator as an impedance transformer and focusing device, an ideal applicator will deliver all the incident power into the discharge with zero reflected power and applicator wall power loss. Thus the overall coupling efficiency will then be 100%. In most experiments the reflected power can be reduced to a very small amount by tuning adjustments, so that $P_r<<P_i$. Then the overall coupling efficiency is equal to just the applicator coupling

efficiency

$$(Eff)_2 = 100 \times \frac{P_a}{P_t} = 100 \times \frac{P_a}{P_a+P_b} \quad (4.2)$$

Despite the simplicity of this equation the coupling efficiency is a difficult quantity to determine experimentally since the wall losses are difficult to measure.

4.3.2 CAVITY LOADED Q

If the cavity applicator is assumed to operate in a single mode a general equation can be derived for the power absorbed in the plasma. The microcoax probes mentioned in a earlier section were used to sample the radial electric field at the wall of the cavity applicator. The small size of the microcoax probes allowed them to be inserted and removed during actual experiments with little detectable perturbation to the plasma or cavity fields. The measured loaded cavity axial field distribution agreed well with the theoretical TM_{012} mode distribution of $|E_r|$ and is shown in Figure 4.4.

It is assumed that the presence of the discharge does not significantly alter the spatial distribution of the cavity wall currents from those of the empty cavity TM_{012} mode. Evidence supporting this assumption is that only very small experimental changes in resonant length are required to match the plasma from the empty mode to the mode with the discharge present as shown in Figure 4.4. The field distribution with the plasma present varies only slightly when compared to the empty cavity as measured by the microcoax probes. The exact numerical solution for the cavity field distribution with the lossy

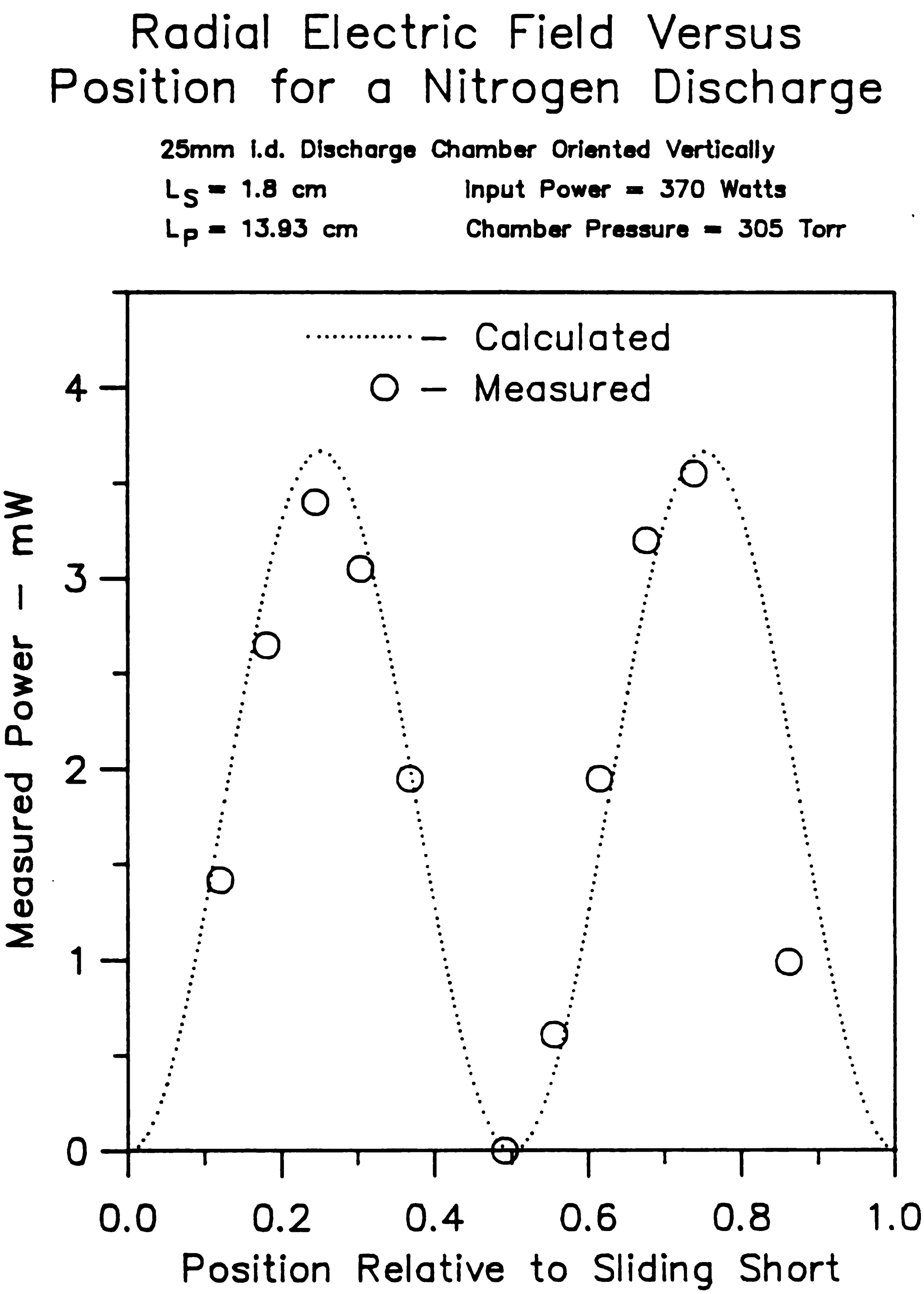

Figure 4.4 Radial Electric Field for a Nitrogen Discharge

plasma present only differs from the empty cavity distribution near the discharge in the center of the cavity[13]. Under these conditions, the ratio of the radial electric field measured at a fixed position on the cavity wall to the total power absorbed by the wall is a constant with and without a discharge. Thus

$$\frac{P_b}{|E_r|^2} = \text{constant} \qquad (4.3)$$

By measuring the power absorbed P_{to}, the cavity quality factor, Q_{uo}, and the associated radial electric field E_{ro} for the critically coupled empty cavity excited by a low power test signal, the absorbed power in the wall, P_b, and Q_u for a cavity loaded with a discharge can be determined from the following equations

$$P_b = \frac{|E_r|^2}{|E_{ro}|^2} P_{to} \qquad (4.4)$$

and

$$Q_u = \frac{Q_{uo}\, P_{to}}{|E_{ro}|^2} \, \frac{|E_r|^2}{P_t} \qquad (4.5)$$

where E_r and P_t are respectively the radial electric field and the cavity absorbed power with the discharge present. Since both of the equation require the ratio of electric fields, only the relative magnitudes of the electric fields are necessary. Thus the electric field probes do not have to be calibrated for these measurements.

4.4 THRUSTER PERFORMANCE CRITERIA

The performance of a thruster is measured in terms of thrust, specific impulse, and energy efficiency. The equations used to derive these quantities are presented in Chapter 2. All of these equations, 2.1-2.5, are derived from the measured thrust, therefore the method used to measure the thrust is of great importance since all other calculations will depend on it. The best method of thrust measurement would be direct thrust measurement using the vacuum of space under weightlessness conditions. However the availability of space shuttles and nonreusable boosters, and the their cost of operation limit almost all thrust measurements to ground experiments.

The experimental techniques for thrust measurement used in this thesis were developed by S. Nakanishi of NASA Lewis Research Center and described here. The next sections present two different ways to measure thrust. The direct thrust measurement system used a thrust stand to take direct thrust readings. The indirect thrust measurement system was used to take thrust readings when a thrust stand was not available.

4.4.1 DIRECT THRUST MEASUREMENT

For direct thrust measurement a high resolution, high sensitivity thrust stand was used. This system was set up in a vacuum tank at NASA Lewis Research Center so that a direct measurement of thrust could be taken with a test engine exhausting into a high volume tank and pumping system.

This system used a precision thrust stand shown in a front view in Figure 4.5. Figure 4.6 shows a side view and both views show the relationship of the center of the thrust target to the center of the 4 inch test port of the vacuum tank. The thrust stand is a torsional pendulum in which the target is balanced by the torsion in the suspension wire. A counterweighted arm with the target on one end and a

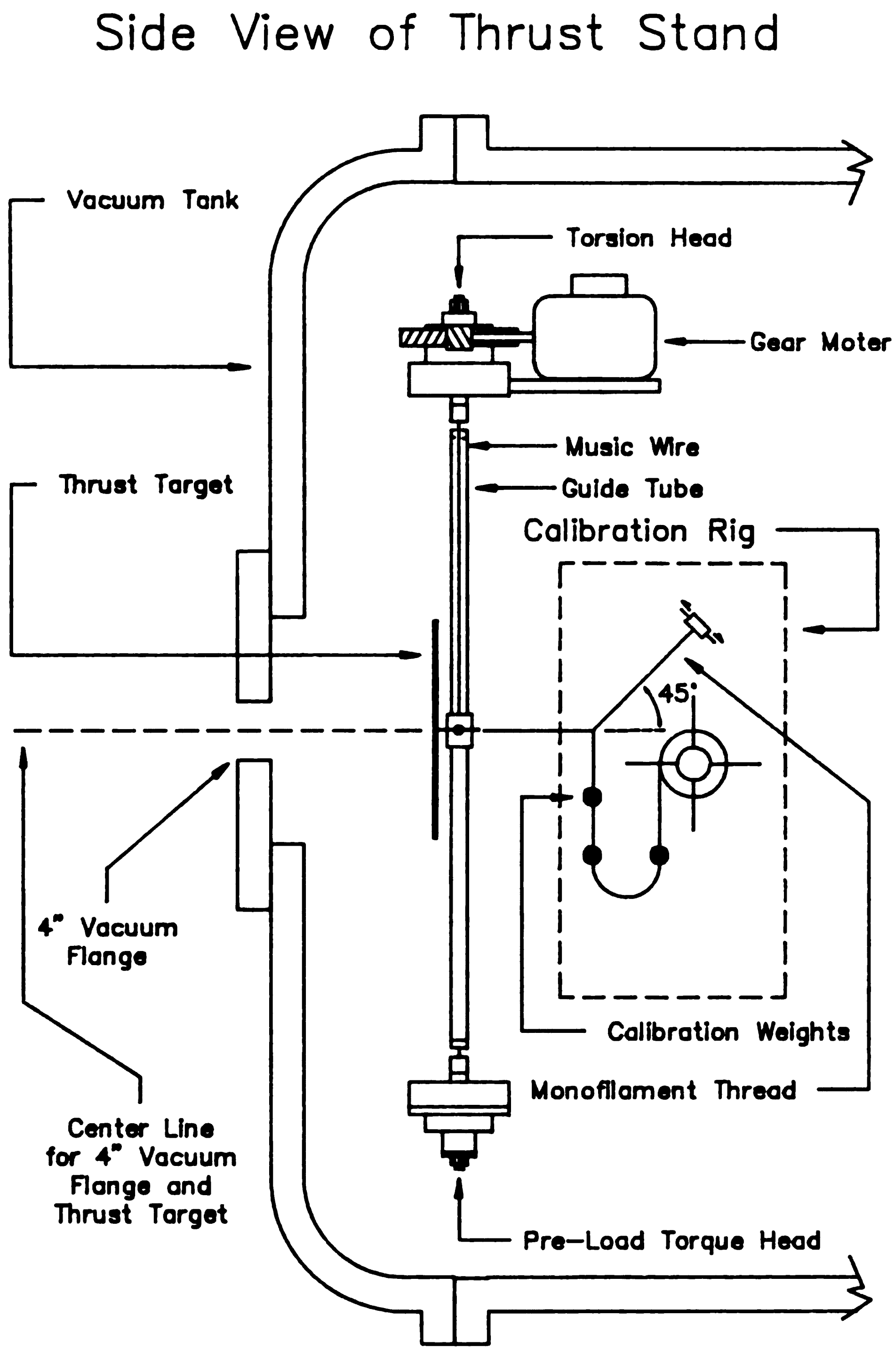

Figure 4.6 Side View of Thrust Stand

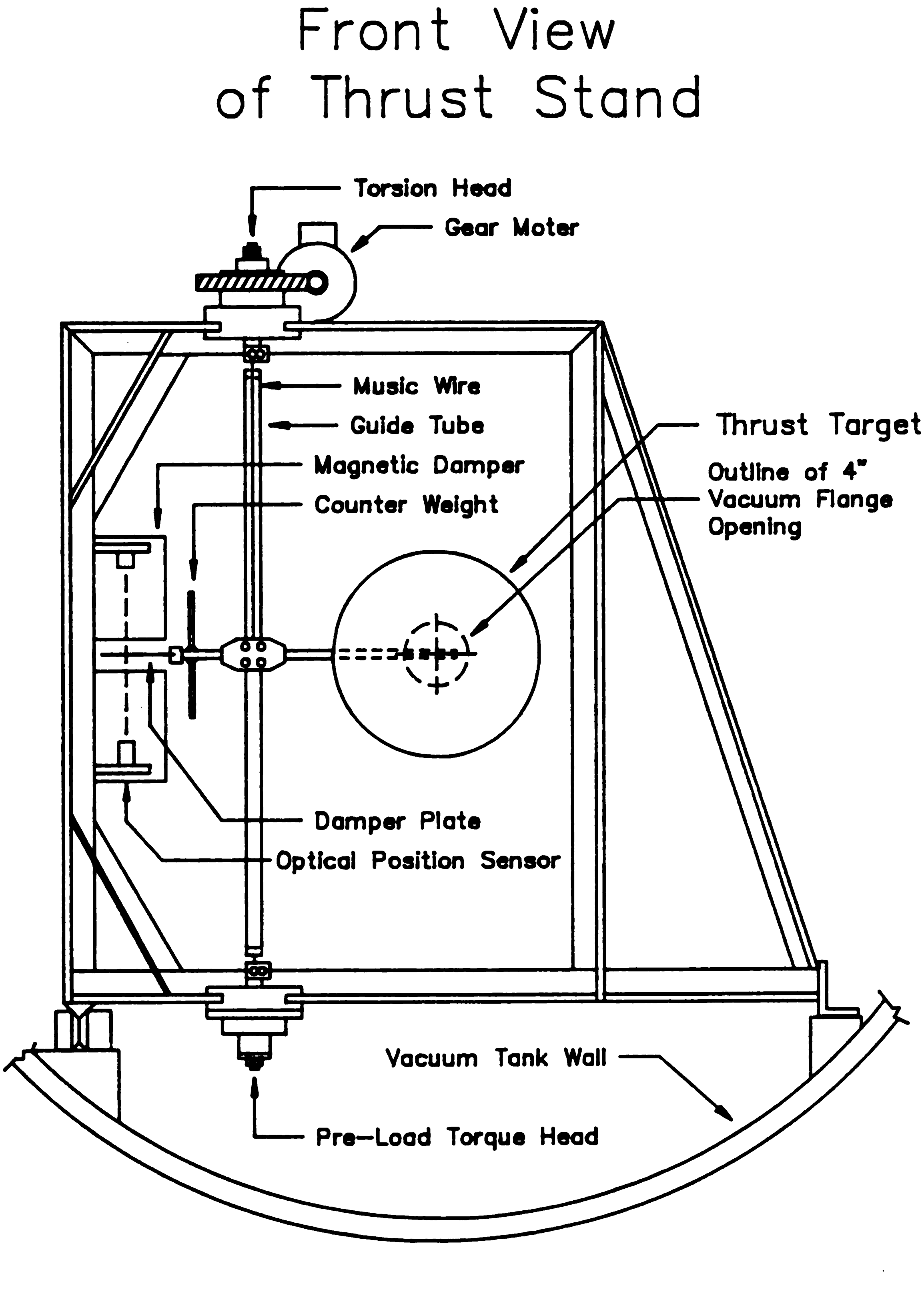

Figure 4.5 Front View of Thrust Stand

magnetic damper plate on the other end is suspended by a single strand of music wire clamped at the middle and selected according to the range of thrust to be measured. Initially a 0.76 mm in diameter wire was used, but due to an increase in the range of thrust measurement that was required, the wire size was increased to 1.04 mm to accommodate these higher thrust levels. Application of a counter torque by the upper torsional head driven by a gear motor restores neutral equilibrium to a reference position monitored by a optical position sensor sighting the damper plate. The reference position corresponds to a condition where the thrust vector is perpendicular to the target plate. The thrust can be measured as a function of the twist in the upper wire required to maintain neutral equilibrium under any thrust condition on the target.

Frictionless calibration of the thrust measurement system was accomplished by a rig which established an equilibrium of forces such that the horizontal force equals the vertical weight transmitted via a thin monofilament thread. A windlass permitted the application and removal of calibration weights to the back of the target. The wire twist was resolved by a 10-turn potentiometer attached to the worm shaft of a 20:1 reduction worm gear drive. Thrust measurement were always made with the worm driving in the same direction to eliminate back lash errors. The wire twist measurement corresponded to a 11.65 degree per Volt to permit a resolution of 0.01165 degrees when read on a 1 mV range on a digital voltmeter. The sensitivity of the optical position sensor was 0.47 V per degree of wire rotation. The target could be routinely adjusted to reference position within $\pm$5 mV or 0.0106 degrees. Since the thrust calibration constant with a 1.04 mm wire was 0.018 Newton per Volt on the worm shaft, or 0.018 N for 11.65 degrees of wire twist, the thrust equivalent of 1.545×10^{-5} N per degree of wire twist implies that a reference position error of $\pm 1.6 * 10^{-5}$ N.

4.4.2 POSSIBLE ERRORS IN DIRECT THRUST MEASUREMENTS

There are several possible sources of error with this thrust stand. The first possible source of error is due to the center of thrust of the test thruster not being properly aligned with the thrust target. To limit this problem the center of the thrust stand target was carefully aligned with the center of the vacuum port. Further, the target plate was carefully adjusted so that it was parallel with the mounting face of the vacuum port. Finally to test if the thruster was off center in its thrust axis, it was rotated through 90 degree turns and operated with a cold gas flow to test for variations in thrust. No variation could be measured, so it was assumed that the thruster was operating with its center of thrust axis properly aligned with the target plate.

The next possible source of error is from scattering between the exhausted propellant of the thruster and gas molecules in the vacuum tank. During thruster tests, it was impossible to maintain ideal vacuum facility conditions for thrust measurement. For some tests, direct thrust measurement was not obtainable at all. A short series tests were made to evaluate the affects of vacuum tank pressure on thrust measurement and to develop a method for calculating performance even without measurement of thrust. These tests consisted of thrust measurements made at a constant propellant flow rate and temperature while the facility pressure, as measured by an ionization gauge, was varied by bleeding in nitrogen gas at various rates. A set of thrust measurements were also made at a constant propellant flow rate and microwave power, while the facility pressure was varied.

Measured thrust as a function of facility pressure is shown in Figure 4.7 for several operating conditions. All curves except one are for isothermal flow of nitrogen gas with a temperature of 296 K. From the theoretical specific impulse equation, nitrogen at this temperature should yield an I_{sp} of 80 seconds. Using this I_{sp}, the theoretical thrust corresponding to each propellant flow rate has been calculated and they are shown as dashed lines in Figure 4.7. At the lowest flow rate of 29×10^{-6} kg/s, the lowest no bleed facility pressure of 6.3×10^{-4} Torr was obtained. The measured thrust was within 10^{-3} N of the theoretical thrust. As the facility pressure was increased with nitrogen bleed, the measured thrust decreased as much as 33% for a decade increase in pressure. Similar trends were observed at other flow rates and also for the case in which 294 Watts of microwave power was absorbed in the plasma discharge.

In the isothermal flow cases, a extrapolation of the curves allows the intersection of each with the theoretical thrust value line corresponding to that flow rate. It is observed that these intersections occur at pressures near 5×10^{-4} Torr. This implies that if facility pressure could be maintained below 5×10^{-4} Torr at all times, nozzles of the type used can be expected to achieve almost 100% efficiency. The curve shown for 294 Watts of microwave power by similar extrapolation produced a a thrust of 6.6×10^{-2} N to yield an I_{sp} of 113.4 seconds.

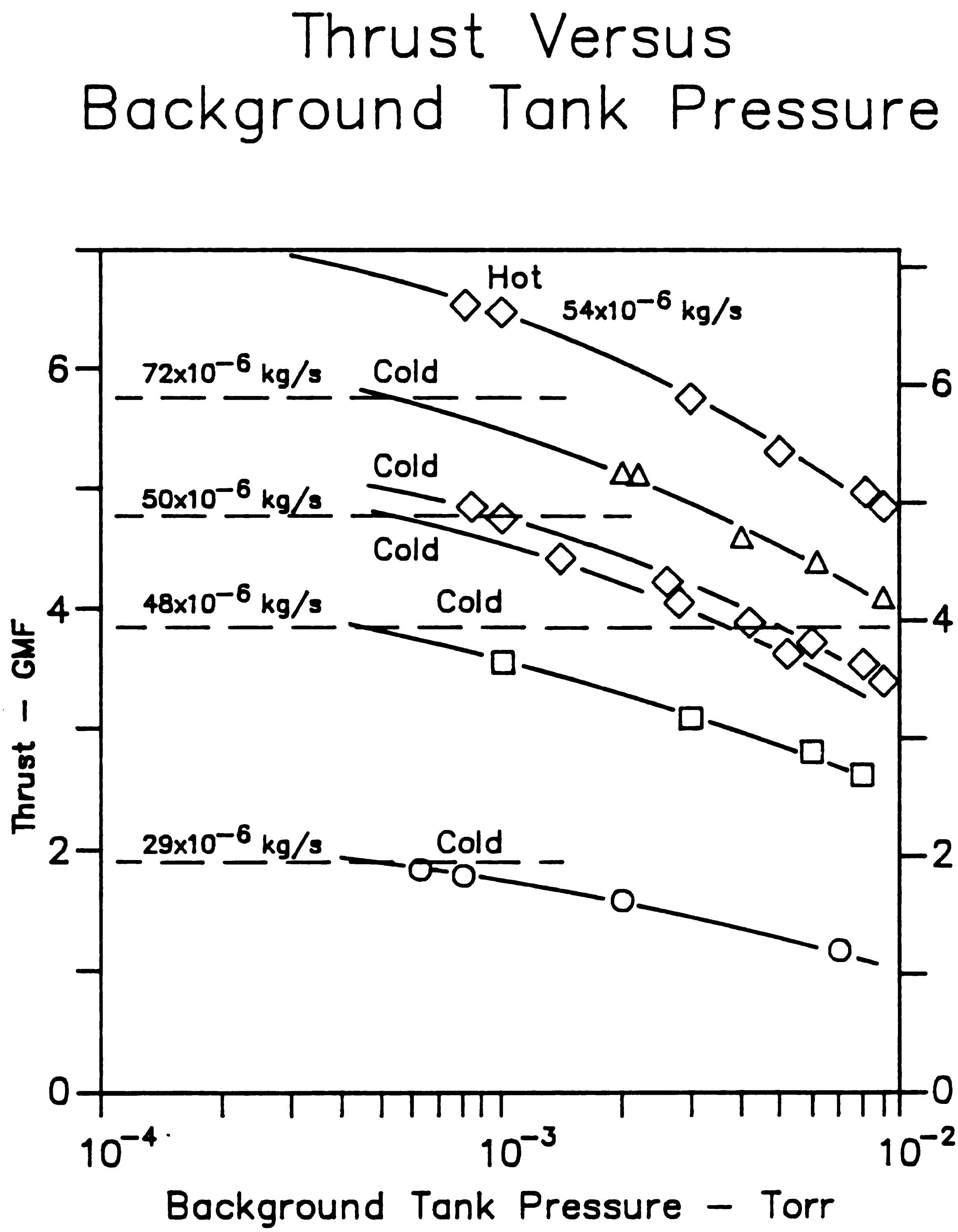

Figure 4.7 Thrust Versus Background Tank Pressure

4.4.3 INDIRECT THRUST MEASUREMENT

In some experiments direct thrust measurements are not available. For instance, in some experiments a high volume vacuum tank was not available, the nozzle could not be positioned to operate the thrust stand correctly, or the thrust stand did not have enough range. At these and other instances when direct thrust measurements are not available, an indirect means of thrust measurement was used. This section presents this indirect method of thrust measurement.

If it is assumed that a nozzle of fixed throat area is always choked at a given propellant flow rate, the upstream pressure varies as the square root of the gas temperature. Because specific impulse also varies as the square root of the gas temperature, the thrust at a given propellant flow rate varies directly as the upstream pressure. The assumptions inherent in the above reasoning is that the gas is in equilibrium and that the nozzle efflux is uniform and one dimensional.

Thus if the thrust is directly proportional to upstream pressure for a given constant flow rate, a linear relationship can be assumed between the hot to cold thrust ratio and the hot to cold pressure ratio. If a direct proportionality is assumed conservatively, the thrust and specific impulse of any gas can be calculated. The theoretical cold specific impulse can be calculated from the equations

$$I_{spc} = 24.6(T_0/M)^{1/2} \qquad (4.6)$$

for diatomic gases and

$$I_{spc} = 20.9(T_0/M)^{1/2} \qquad (4.7)$$

for monatomic gases. Where T_0 is the gas temperature prior to expansion and M is the molecular weight of the gas. A full isentropic expansion to vacuum conditions is assumed.

The hot specific impulse can be obtained from the measured hot to cold pressure ratio, because for a given propellant flow rate, the specific impulse is proportional to thrust. Thus,

$$\frac{I_{spH}}{I_{spC}} = \frac{p_H}{p_C} \tag{4.8}$$

Knowing the hot and cold specific impulse, and the thrust power, the efficiency can be calculated from equation 2.4 as,

$$\eta = \frac{\left[\dfrac{p_h}{p_c}\right]^2}{\dfrac{2P_a}{g^2\dot{m}(I_{spc})^2} + 1} \tag{4.9}$$

and the power to thrust ratio is given by substitution of this value of efficiency in equation 2.5.

4.4.4 VERIFICATION OF INDIRECT THRUST MEASUREMENTS

It is clear that because of pumping limits, facility pressures below 5×10^{-4} Torr will seldom be achieved, especially at high propellant flow rates. At these and other instances when direct thrust measurements are not available, the indirect thrust measurement technique is used. The applicability of the indirect thrust measurement technique for calculating thrust was examined by plotting the ratios of directly measured thrust and the tube pressures. The "hot" and "cold" conditions are with and without microwave power, respectively. The ratio of hot to cold measured thrust is shown plotted against the hot and cold pressure ratio in Figure 4.8. Data from both the cavity thruster and the coaxial thruster configuration (presented in latter chapters) are shown for a wide range of facility pressures. There is a linear relationship between the two hot to cold ratios. There is a tendency for the thrust ratio to be about 3% higher than a direct 1:1 proportionality with pressure ratio. It is not known whether or not the thrust measurement tended to be 3% high during hot conditions.

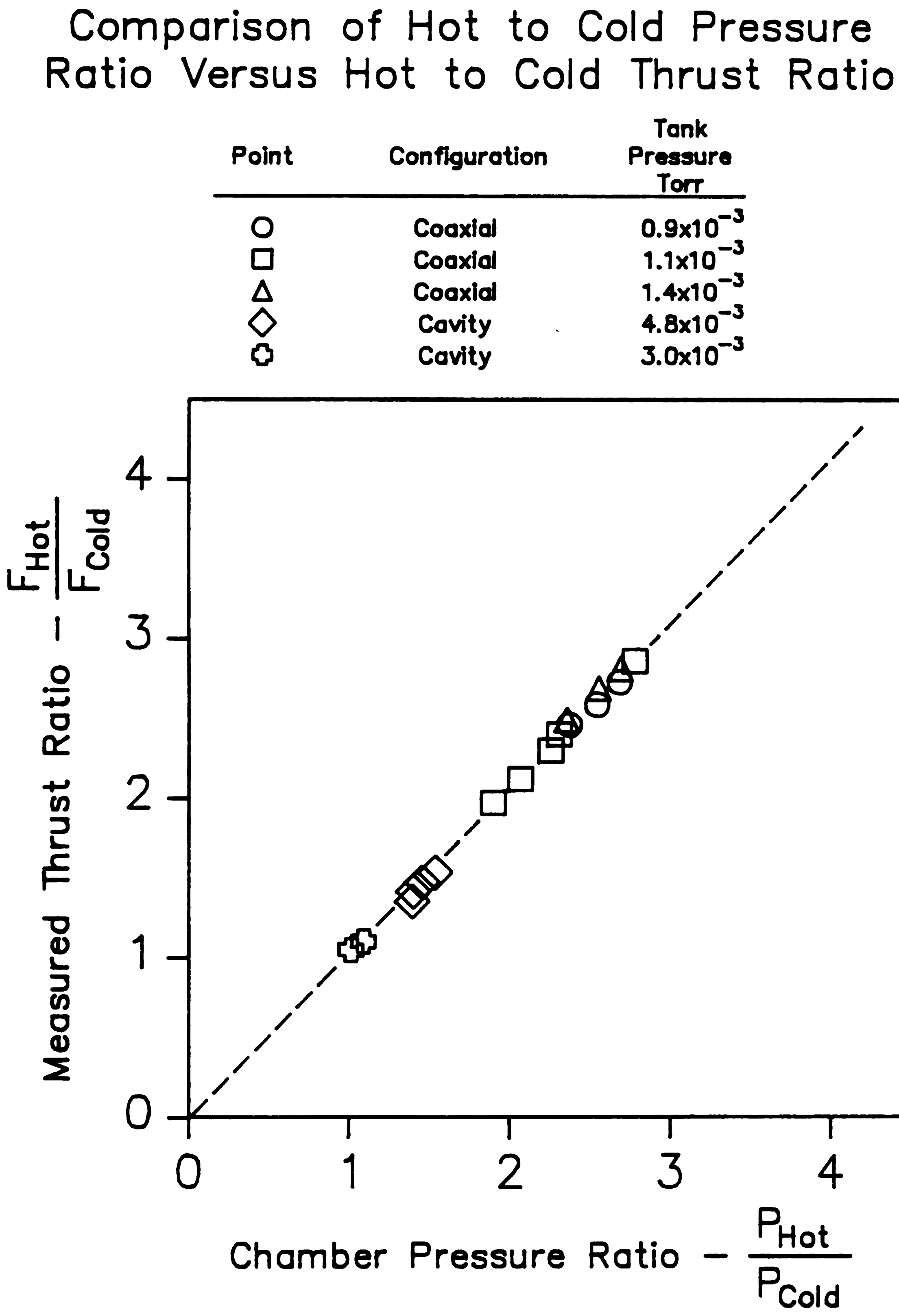

Figure 4.8 Comparison of Pressure Ratio to Thrust Ratio

CHAPTER V

HIGH PRESSURE MICROWAVE DISCHARGES

5.1 INTRODUCTION

The results of experiments with high pressure microwave discharges are presented in this chapter. These experiments were conducted for several reasons. First to experimentally produce high pressure microwave discharges in different gases and measure the microwave coupling efficiency to them. Second, to determine the tuning conditions necessary to produce and maintain these plasmas. Third to measure discharge properties vs. pressure for different diameter discharge chambers.

The experimental microwave energy coupling and measurement system variations from chapter 4 are first described along with a description of how the experiment was conducted. Measured properties such as pressure, power density, coupling efficiency and cavity Q are presented for variation in pressure and chamber diameter.

5.2 EXPERIMENTAL SYSTEM

The experiments were conducted using the general techniques and equipment described in chapter 4. However the specific setup and techniques used to conduct the experiments and measure the data is presented in the next two sections. The first section describes the microwave setup and use of the microwave applicator. The second section describes the general experimental setup and procedure.

5.2.1 MICROWAVE CAVITY TYPE ABSORPTION CHAMBER

The cavity type absorption chamber is shown in Figure 3.5, and its operation described in chapter 3. The cavity applicator was mounted in a vertical manner as shown in Figure 3.5. Fused quartz tubes running coaxially through the applicator served as discharge chambers for the experiments. The advanced short and probe actuator designs described in section 3.4.1, were not employed in these experiments. A variable power 500 Watt CW 2.45 GHz microwave source served as the source of microwave power for these experiments. For all data points shown the cavity was tuned to reduce the reflected power to its minimum valve. This was always a small value, so that power absorbed in the absorption chamber was approximately 500 Watts. The microcoax probes were employed to measure $|E_r|^2$. To increase the accuracy of these reading the probe was placed in each of the sample hole and a reading taken. These were averaged and used in the calculation of $|E_r|^2$.

The empty cavity measurement of $|E_{ro}|^2$ was conducted using a low power microwave source to prevent breakdown in the cavity. The reading were averaged in the same manner as the earlier reading of $|E_r|^2$. The empty cavity measurement of Q_{uo} was taken using a sweep generator and measuring bandwidth between the half power points on the applicator resonance curve.

5.2.2 MEASUREMENT SYSTEM AND EXPERIMENTAL PROCEDURE

The basic vacuum and gas handling systems used in these experiments were described in chapter 4. Cylindrical fused quartz tubes were used for discharge chambers as shown in Figure 3.5, and were designed to be interchangeable. For these experiments three different diameters were used. They were inside diameters of 12 mm, 25 mm, and 37 mm. The method of evacuation mentioned in chapter 4 was used to evacuate the discharge chambers. Gas was slowly added to the discharge chamber to reach the desired pressure level. A slight flow was added and the microwave power was turned on. A Tesla coil was used to start the discharge in the applicator. The flow was turned off and the pressure raised to the desired level. Until the pressure was above 40 Torr, the cavity tuning was set for 40 Torr to prevent the discharge from going out. The values of L_s and L_p for this are shown in Tables 5.1-5.3. Above 40 Torr the tuning was adjusted for maximum power absorbed in the applicator. Compressed air blowing on the discharge chamber from a second port was used to cool the chamber. The camera for the measurement of discharge area was attached to the cavity for stability and set up to measure plasma volume using the technique of section 4.2.3. Figure 5.1 shows photographs of a nitrogen discharge as the pressure is varied.

5.3 EXPERIMENTAL MEASUREMENTS

For these experiments the following measurements were taken. The discharge chamber pressure, microwave incident and reflected power, $|E_r|^2$, L_p (input probe length), L_s (input short length), and discharge size and are presented in Tables 5.1-5.3. Three different gases were tested, oxygen, nitrogen and helium. Using the equation 4.2 for coupling efficiency and the technique described in section 4.3, coupling efficiency was calculated for nitrogen and helium in each of the three tubes. Figure 5.2 shows the results for nitrogen. A coupling

Discharge Constriction Versus Pressure

Nitrogen Gas in a 12mm i.d. Cylindrical
Quartz Discharge Chamber

Pressure — Torr

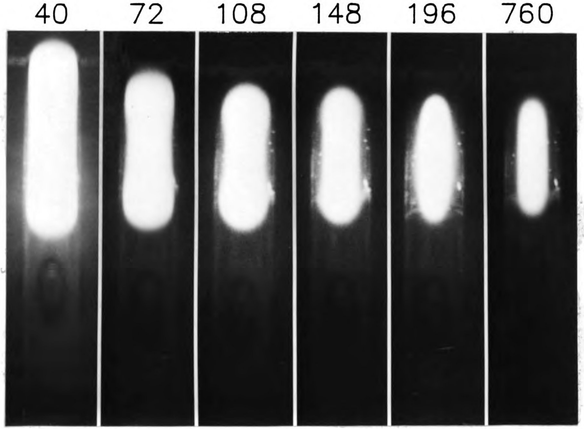

Figure 5.1 Picture of Discharge Constriction Versus Pressure

Table 5.1 Experimental Results in 12mm Discharge Chambers

Nitrogen in 12mm Tube, 1/29/1983

Pressure mm	P_t Watts	$\|E_T\|^2$ (Watts)	P_b Watts	Qu -	$(Eff)_2$ %	Volume cm^3	$\langle p\rangle$ W/cm^3	L_s cm	L_p cm
40	468	8.0	10.6	100.4	97.73	5.893	79.42	14.6	1.4
72	462	7.25	9.64	92.2	97.91	3.681	125.5	14.55	1.45
108	454	7.75	10.3	100.3	97.73	2.377	191.0	14.55	1.5
148	457	7.85	10.44	100.9	97.72	1.768	258.5	14.55	1.5
196	459	7.95	10.57	101.7	97.70	1.017	451.3	14.5	1.55
257	457	7.8	10.37	100.2	97.73	0.959	476.5	14.5	1.55
340	455	7.55	10.4	97.46	97.79	0.893	509.5	14.5	1.55
474	454	7.4	9.84	95.73	97.83	0.840	540.5	14.45	1.5
584	452	7.25	9.64	94.21	97.87	0.895	505.0	14.45	1.5
760	447	6.7	8.91	88.03	98.01	0.699	639.5	14.5	1.5

Helium in 12mm Tube, 1/29/1983

Pressure mm	P_t Watts	$\|E_T\|^2$ (Watts)	P_b Watts	Qu -	$(Eff)_2$ %	Volume cm^3	$\langle p\rangle$ W/cm^3	L_s cm	L_p cm
40	315	1.525	2.023	28.4	99.4	14.11	22.32	14.75	1.45
72	350	2.18	2.90	36.6	99.2	10.00	35.00	14.6	1.4
108	405	3.9	5.19	56.6	98.7	7.49	54.07	14.65	1.45
148	400	3.45	4.59	50.66	98.9	6.04	66.23	14.6	1.4
196	390	3.15	4.19	47.4	98.9	4.77	81.76	14.55	1.45
257	400	4.8	6.4	70.48	98.4	4.208	95.06	14.55	1.5
340	415	4.1	5.45	58.03	98.7	3.736	111.1	14.5	1.55
474	445	5.45	7.245	71.93	98.4	2.954	150.6	14.45	1.5
584	464	6.9	9.17	87.34	98.0	2.572	180.4	14.45	1.5
760	485	9.3	12.36	112.6	97.45	1.869	259.5	14.45	1.55

Oxygen in 12mm Tube, 2/3/1983

Pressure mm	P_t Watts	$\|E_T\|^2$ (Watts)	P_b Watts	Qu -	$(Eff)_2$ %	Volume cm^3	$\langle p\rangle$ W/cm^3	L_s cm	L_p cm
40	462	10.25	13.63	130.3	97.05	4.77	96.86	14.7	1.45
72	444	7.75	10.3	102.5	97.68	3.66	121.4	14.6	1.55
108	402	9.5	12.63	120.8	97.27	3.15	146.9	14.5	1.5
148	461	13	17.28	165.6	96.25	-	-	14.45	1.45
196	457	17.75	23.6	228.1	94.84	3.14	145.4	14.45	1.45
257	470	20.75	27.59	259.3	94.13	2.016	233.1	14.45	1.5

Table 5.2 Experimental Results in 25mm Discharge Chambers

Nitrogen in 25mm Tube, 1/9/1983

Pressure mm	P_t Watts	$\lvert E_T\rvert^2$ (Watts)	P_b Watts	Qu -	$(Eff)_2$ %	Volume cm^3	$\langle p\rangle$ W/cm^3	L_s cm	L_p cm
40	444	5.4	7.18	71.44	98.4	12	36.6	14.55	1.5
72	434	5.05	6.71	68.4	98.5	7.8	55.5	14.5	1.6
108	432	4.9	6.51	66.6	98.5	3.7	115.5	14.45	1.6
148	428	4.65	6.18	63.8	98.6	2.5	171.4	14.4	1.6
196	420	4.3	5.72	60.1	98.64	2.0	206.7	14.45	1.7
257	413	4.05	5.38	57.6	98.7	1.96	210.96	14.4	1.6
340	412	3.9	5.18	55.6	98.74	1.96	209.5	14.4	1.6
474	413	3.8	5.05	54.0	98.78	2.34	176.4	14.4	1.6
584	416	4.05	5.38	57.2	98.7	2.4	172.4	14.45	1.6
760	425	4.3	5.7	59.4	98.65	1.96	216	14.4	1.6

Helium in 25mm tube, 5/1/1983

Pressure mm	P_t Watts	$\lvert E_T\rvert^2$ (Watts)	P_b Watts	Qu -	$(Eff)_2$ %	Volume cm^3	$\langle p\rangle$ W/cm^3	L_s cm	L_p cm
40	310	1.45	1.92	27.47	99.4	23.3	13.3	14.7	1.5
72	360	2.25	2.99	36.7	99.17	23.4	15.4	14.55	1.4
108	365	2.35	3.12	37.8	99.14	19.0	19.16	14.5	1.6
148	375	2.65	3.52	41.5	99.06	15.1	24.8	14.5	1.5
196	390	3.1	4.12	46.69	98.94	10.9	35.8	14.4	1.6
257	410	3.75	4.99	53.7	98.78	7	58.8	14.35	1.6
340	435	4.65	6.18	62.8	98.6	4.8	90.0	14.35	1.45
474	450	5.7	7.58	74.4	98.3	3.815	118.0	14.3	1.55
584	470	7	9.3	87.5	98.0	3.26	144.0	14.3	1.6
760	485	8.8	11.7	106.5	97.6	2.58	187.6	14.3	1.7
1100	497	11.25	14.96	132.9	97.0	2.1	-	14.3	1.6

Oxygen in 25mm tube, 2/5/1983

Pressure mm	P_t Watts	$\lvert E_T\rvert^2$ (Watts)	P_b Watts	Qu -	$(Eff)_2$ %	Volume cm^3	$\langle p\rangle$ W/cm^3	L_s cm	L_p cm
30	432	5.5	7.312	74.78	98.31	20.27	21.3	14.55	1.4
72	465	8.1	10.77	102.3	97.68	9.92	46.88	14.45	1.5
108	468	9.85	13.09	123.6	97.2	8.35	56.06	14.4	1.5
148	478	12.25	16.29	150.5	96.59	6.92	69.06	14.4	1.5
196	478.5	15.25	20.27	187.2	95.76	6.12	78.2	14.15	1.55
257	468.5	18.75	24.93	235.1	94.68	6.31	74.26	14.15	1.5
340	448	24.0	31.91	314.6	92.88	5.9	75.83	13.9	1.6

Table 5.3 Experimental Results in 37mm Discharge Chambers

Nitrogen in 37mm Tube, 1/9/1983

Pressure mm	P_t Watts	$\lvert E_r \rvert^2$ (Watts)	P_b Watts	Qu -	$(Eff)_2$ %	Volume cm^3	<p> W/cm^3	L_s cm	L_p cm
40	431	5.0	6.65	68.2	98.46	24.32	17.72	14.55	1.4
72	433	5.0	6.65	67.8	98.46	11.06	39.15	14.5	1.5
108	427	4.55	6.05	62.6	98.58	9.259	46.12	14.45	1.5
148	414	4.3	5.72	61.0	98.62	6.416	64.52	14.45	1.7
196	406	3.8	5.05	54.97	98.76	5.887	68.97	14.45	1.65
257	400	3.55	4.72	52.1	98.82	4.973	80.43	14.4	1.65
340	400	3.35	4.45	49.2	98.89	4.18	95.76	14.4	1.65
474	410	3.7	4.92	53.0	98.8	3.378	121.4	14.4	1.65
584	420	4.0	5.32	55.94	98.73	4.562	92.07	14.4	1.65
760	450	6.5	8.641	84.84	98.08	4.549	98.93	14.4	1.65

Helium in 37mm Tube, 1/9/1983

Pressure mm	P_t Watts	$\lvert E_r \rvert^2$ (Watts)	P_b Watts	Qu -	$(Eff)_2$ %	Volume cm^3	<p> W/cm^3	L_s cm	L_p cm
40	310	1.18	1.57	22.36	99.5	42.03	7.375	14.75	1.4
72	325	1.53	2.03	27.65	99.4	29.75	10.92	14.55	1.4
108	350	2.0	2.66	33.6	99.24	23.31	15.01	14.45	1.55
148	370	2.525	3.357	40.0	99.1	17.54	21.09	14.45	1.4
196	385	2.975	3.955	45.38	98.97	13.04	29.52	14.4	1.5
257	403	3.55	4.72	51.7	98.8	10.24	39.36	14.45	1.5
340	424	4.35	5.78	60.26	98.6	7.831	54.14	14.45	1.5
474	447	5.55	7.38	72.92	98.35	5.638	79.28	14.4	1.5
584	462	6.45	8.575	82.0	98.14	4.715	97.99	14.35	1.5
760	477	8.05	10.7	99.12	97.76	3.706	128.7	14.35	1.5

Oxygen in 37mm Tube, 2/3/1983

Pressure mm	P_t Watts	$\lvert E_r \rvert^2$ (Watts)	P_b Watts	Qu -	$(Eff)_2$ %	Volume cm^3	<p> W/cm^3	L_s cm	L_p cm
25	412	3.9	5.185	55.6	98.74	30.0	13.72	14.65	1.4
40	430	5.4	7.18	73.76	98.33	29.15	14.75	14.55	1.45
72	448	6.6	8.77	86.5	98.04	17.25	25.97	14.45	1.5
108	470	8.65	11.50	108.1	97.55	17.37	27.06	14.45	1.55
148	481.8	10.5	13.96	128.0	97.1	17.69	27.23	14.4	1.5
196	490	13.25	17.61	158.8	96.41	18.15	27.0	14.35	1.5
257	487	16.25	21.6	196.0	95.56	19.93	24.43	14.35	1.5
340	478.5	19.0	25.26	233.2	94.72	17.82	26.85	14.4	1.55

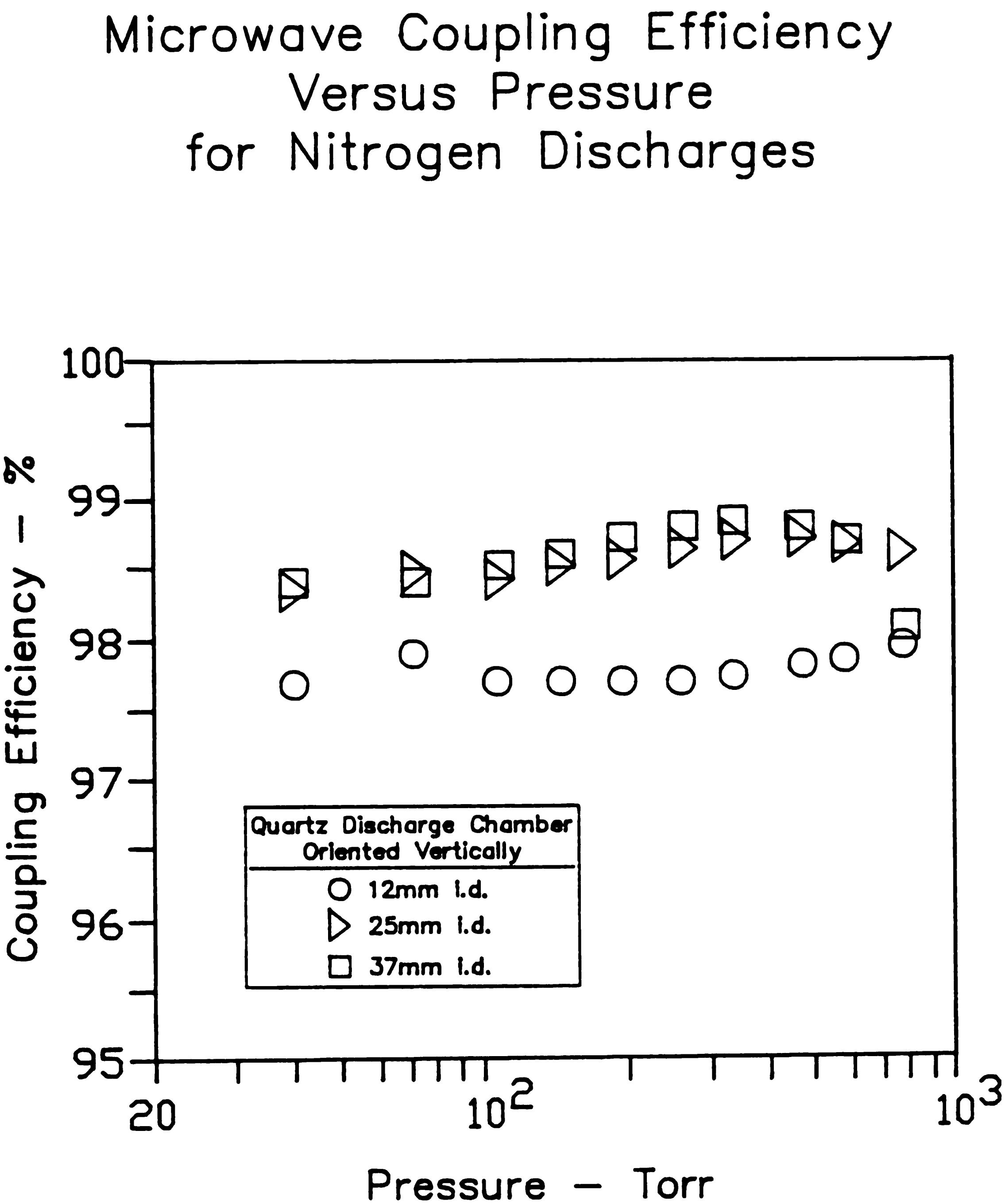

Figure 5.2 Microwave Coupling Efficiency for Nitrogen

efficiency of over 97% was maintained for all three tubes and for a pressure range of 40 to 800 Torr. Figure 5.3 shows the results for helium. A coupling efficiency of over 97.5% was maintained for all three tubes and in a pressure range of 40 to 800 Torr.

Using the equation for cavity Q described in chapter 4, the cavity Q was calculated for nitrogen and helium in each of the three different tubes. Figure 5.4 shows the Q for nitrogen discharges. The Q ranged from 50 to 105 over a pressure range of 40 to 800 Torr in the three tubes. Figure 5.5 shows the results of Q calculations for helium discharges. The Q varied from 20 to 115 over a pressure range of 40 to 800 Torr for the three different tubes. The low values of Q compared to the empty applicator case (about 5000) show that the majority of the power is being absorbed in the discharge resulting in lower fields in the cavity and thus lower wall loss.

Using the coupling efficiency, power absorbed, and discharge volume the absorbed power density was calculated for nitrogen and helium. Figure 5.6 shows these calculation for nitrogen. Values of 20 to 700 Watts/cm^3 were calculated for a pressure range of 40 to 800 Torr. Figure 5.7 shows these calculations for helium. Values of 7 to 300 Watts/cm^3 were calculated for a pressure range of 40 to 800 Torr. Figure 5.8 shows a comparison of these results of power density in the discharge to earlier work by Rogers.[13] This comparison is for 12 mm tubes using the nitrogen and helium results described earlier in this section compared to Rogers argon results. Rogers argon data was produced using equipment identical to that used to produce the results presented in this chapter. As can be seen in the figure, power density went from 11 Watts/cm^3 at 40 Torr to 120 W/cm^3 at one atmosphere.

Microwave Coupling Efficiency
Versus Pressure
for Helium Discharges

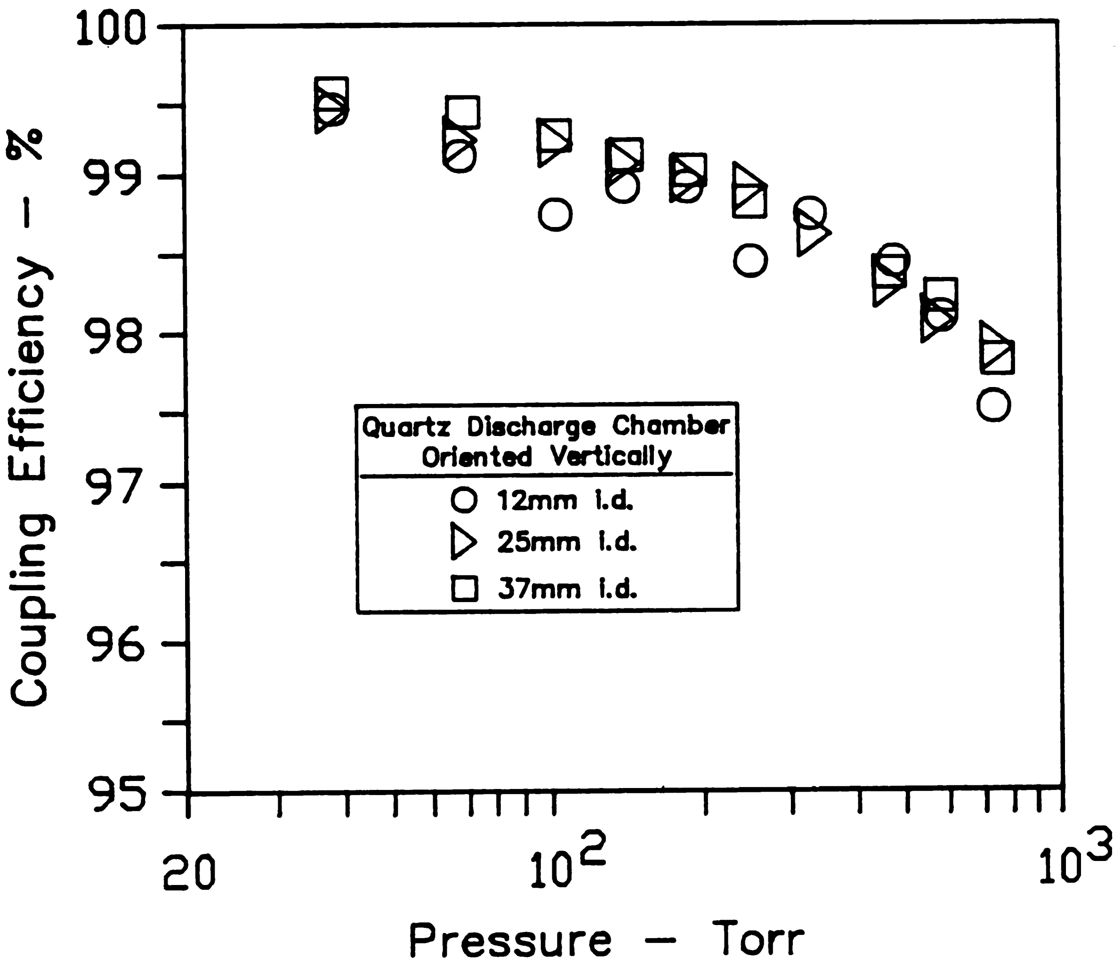

Figure 5.3 Microwave Coupling Efficiency for Helium

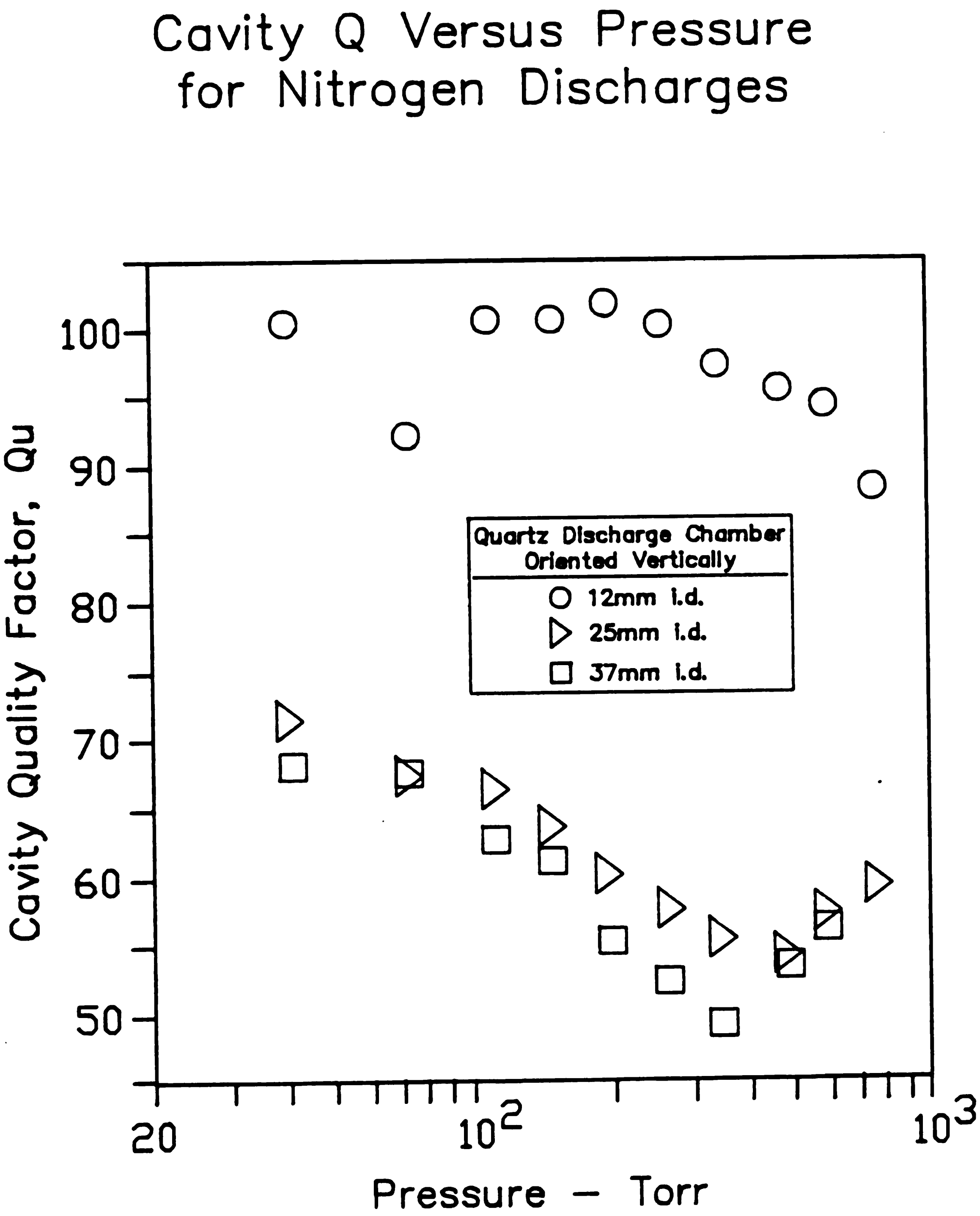

Figure 5.4 Cavity Q Versus Pressure for Nitrogen Discharges

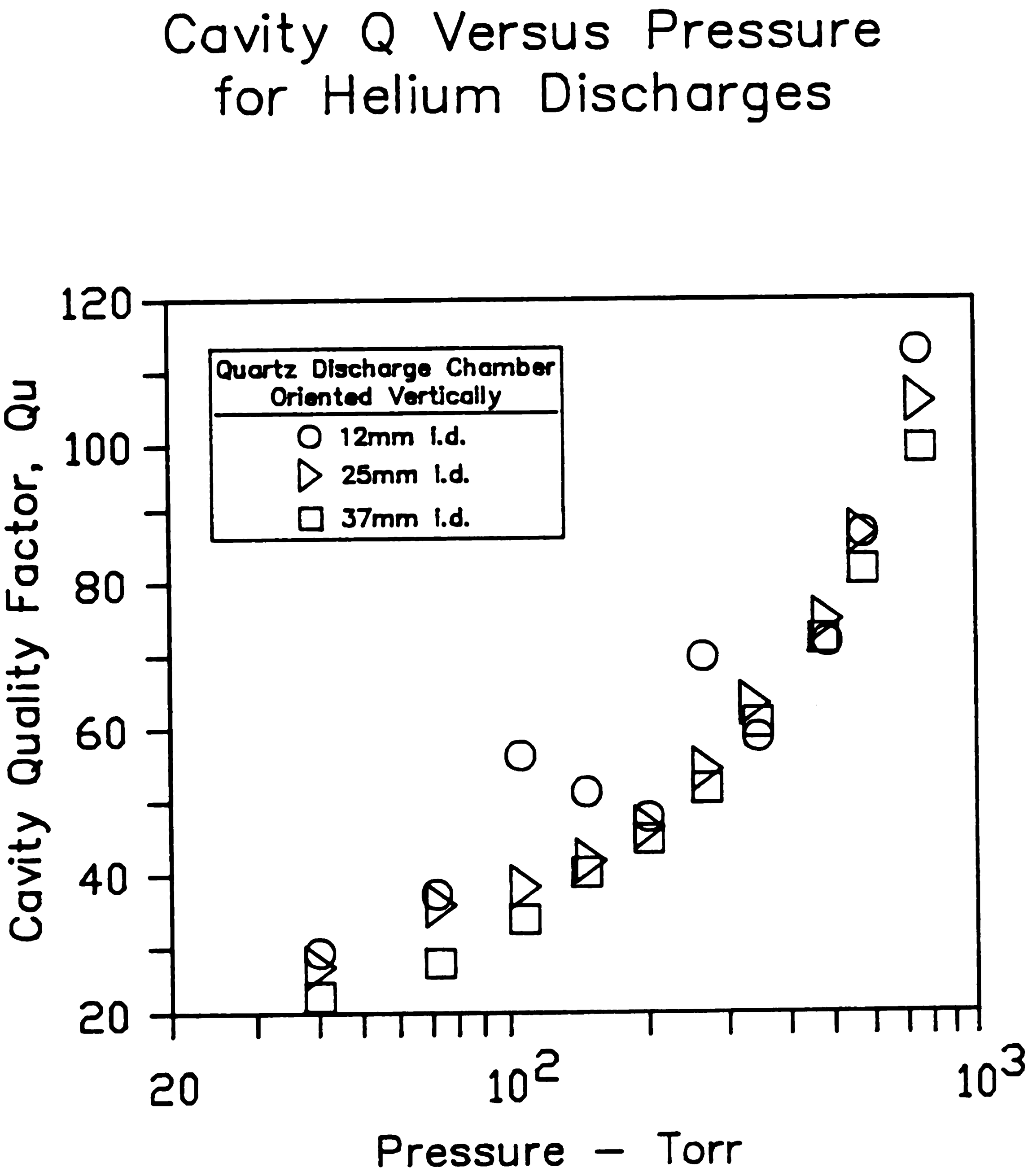

Figure 5.5 Cavity Q Versus Pressure for Helium Discharges

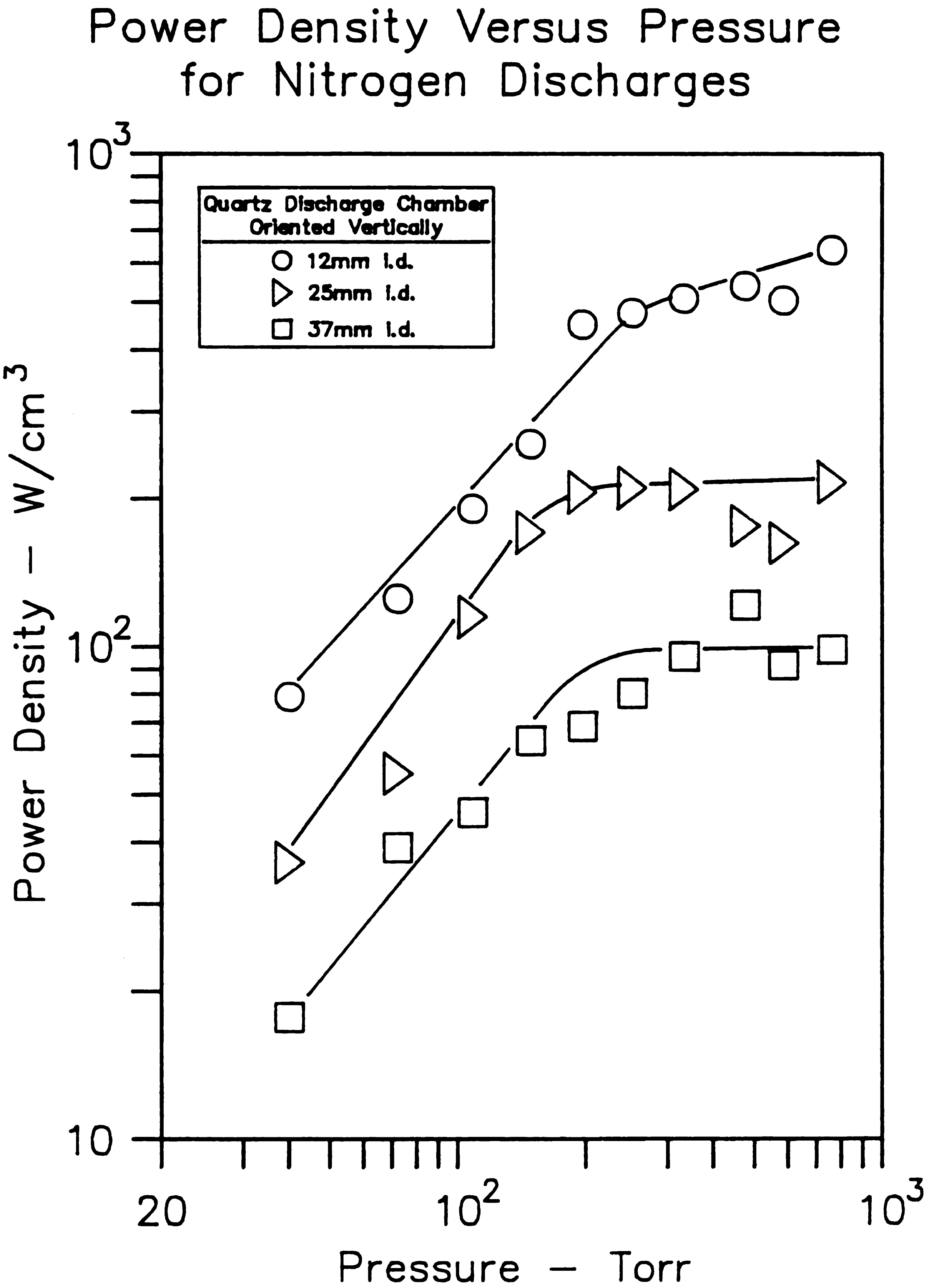

Figure 5.6 Power Density Versus Pressure for Nitrogen Discharges

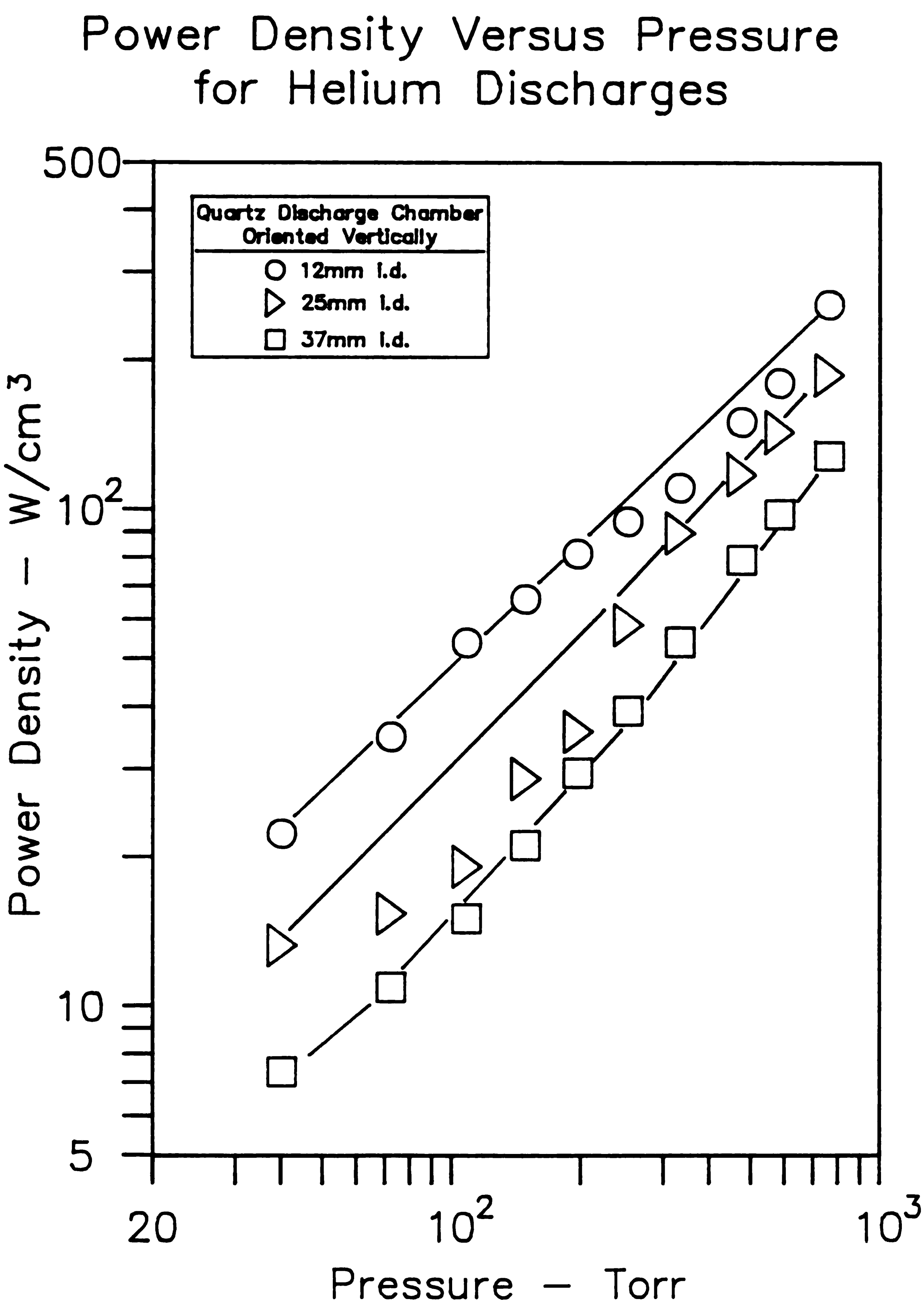

Figure 5.7 Power Density Versus Pressure for Helium Discharges

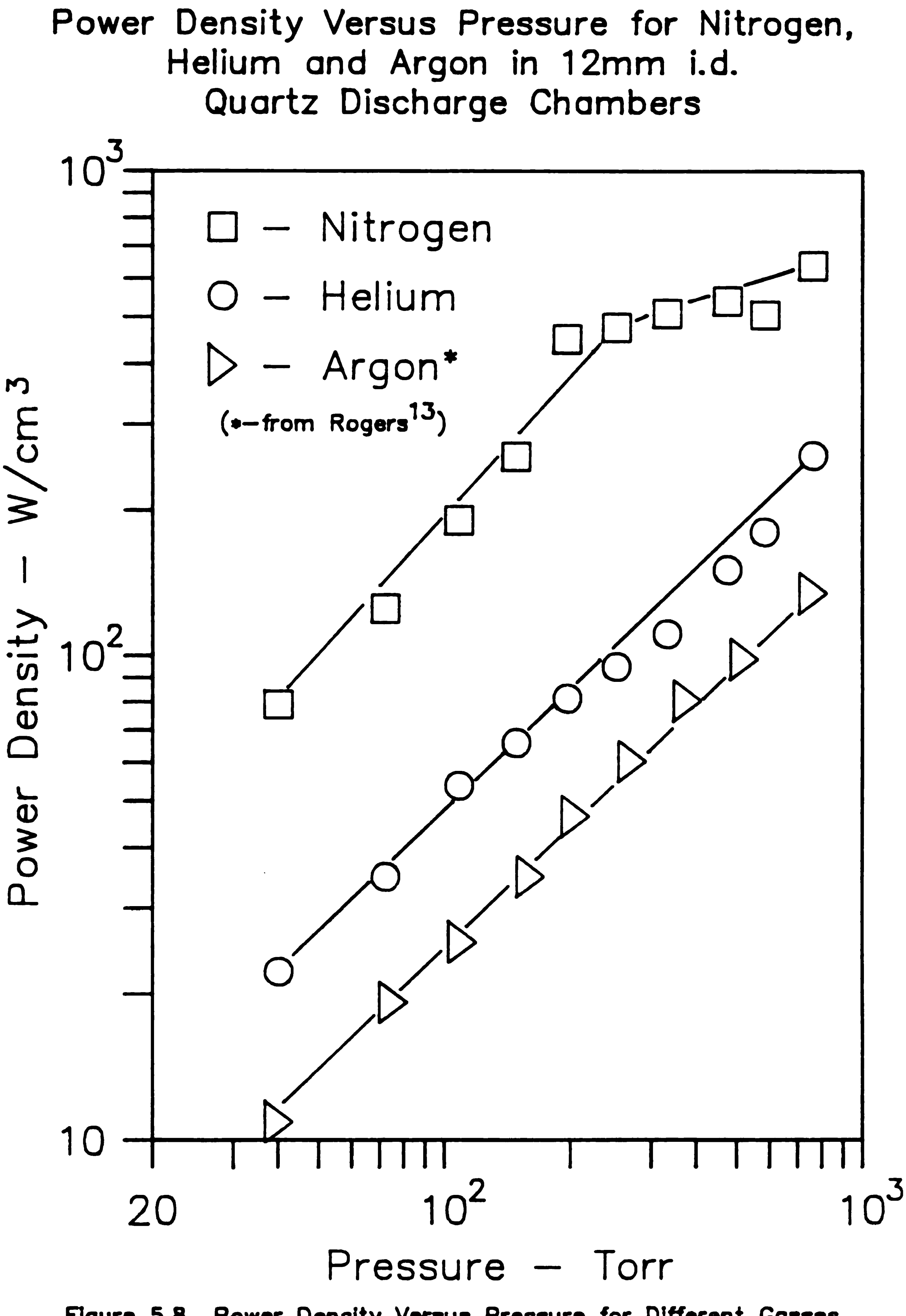

Figure 5.8 Power Density Versus Pressure for Different Gasses

Experiments were also conducted with O_2 to examine its properties. However, the oxygen that was used for the experiments was only 97% pure with most of the impurity being nitrogen. Figure 5.9 shows the results of these experiments for coupling efficiency vs. pressure and Figure 5.10 shows the cavity Q vs. pressure. Figure 5.11 shows the plasma density vs. pressure for these experiments. Maintaining the plasma discharge at pressures over 400 Torr proved difficult since the power source was limited to only 500 Watts. The oxygen formed a bright blue discharge in the center of the discharge chamber and contracted away from the walls at higher pressures. However at all pressures a second dim yellow discharge surrounded the blue discharge. It was possible that this was due to the presence of oxygen but no evidence was found for this. For conclusive result, the experiment should be redone with a high purity oxygen and the availability of more power.

All of the discharges in each of the different gases behaved the same as the pressure was increased, becoming constricted in the center of the discharge chamber away from the chamber walls. This occurred regardless of the size of the discharge chamber. Even though the microwave power was held constant, the discharge properties, such as power density, changed for a given pressure when the tube size was changed. This confirms the description of arc properties discussed in chapter 3. As the pressure is increased, recombination increases, constricting the discharge. Power coupling into the discharge is maximum at the center of the discharge chamber by design. Any movement off center, reduces energy coupling into the discharge and mismatches the coupling system.

Both of the diatomic gases, O_2 and N_2, showed consistent behavior

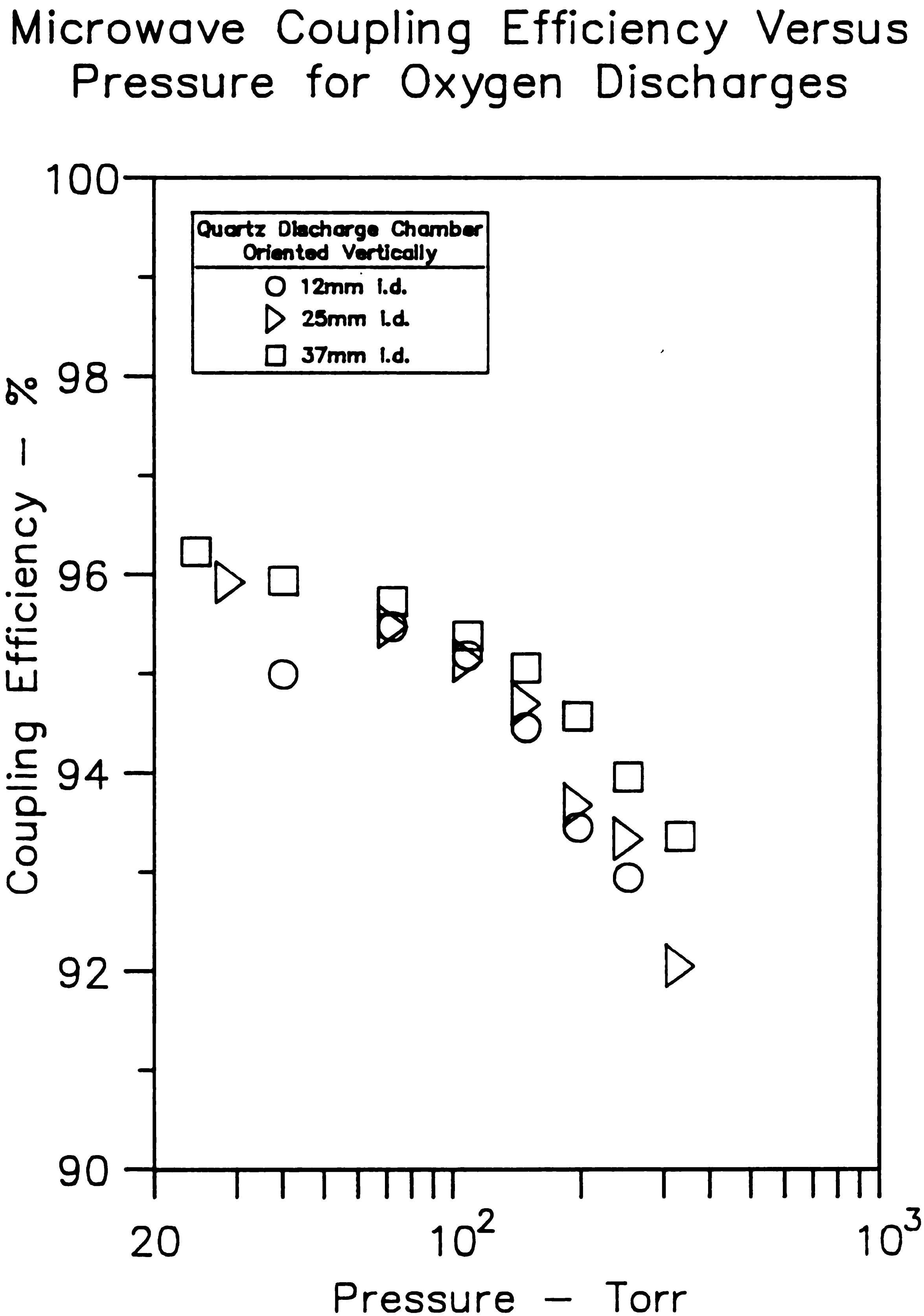

Figure 5.9 Microwave Coupling Efficiency for Oxygen

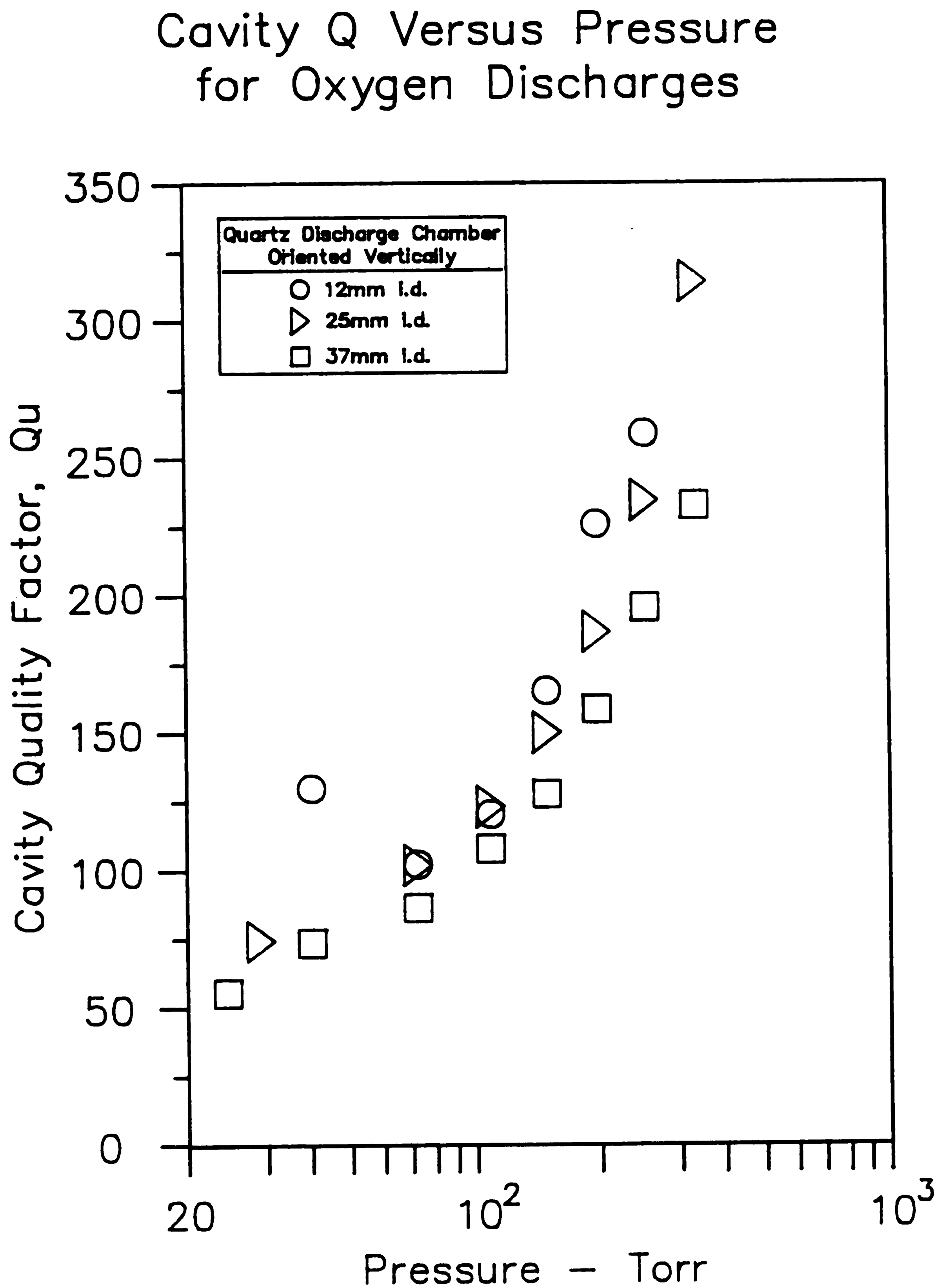

Figure 5.10 Cavity Q Versus Pressure for Oxygen Discharges

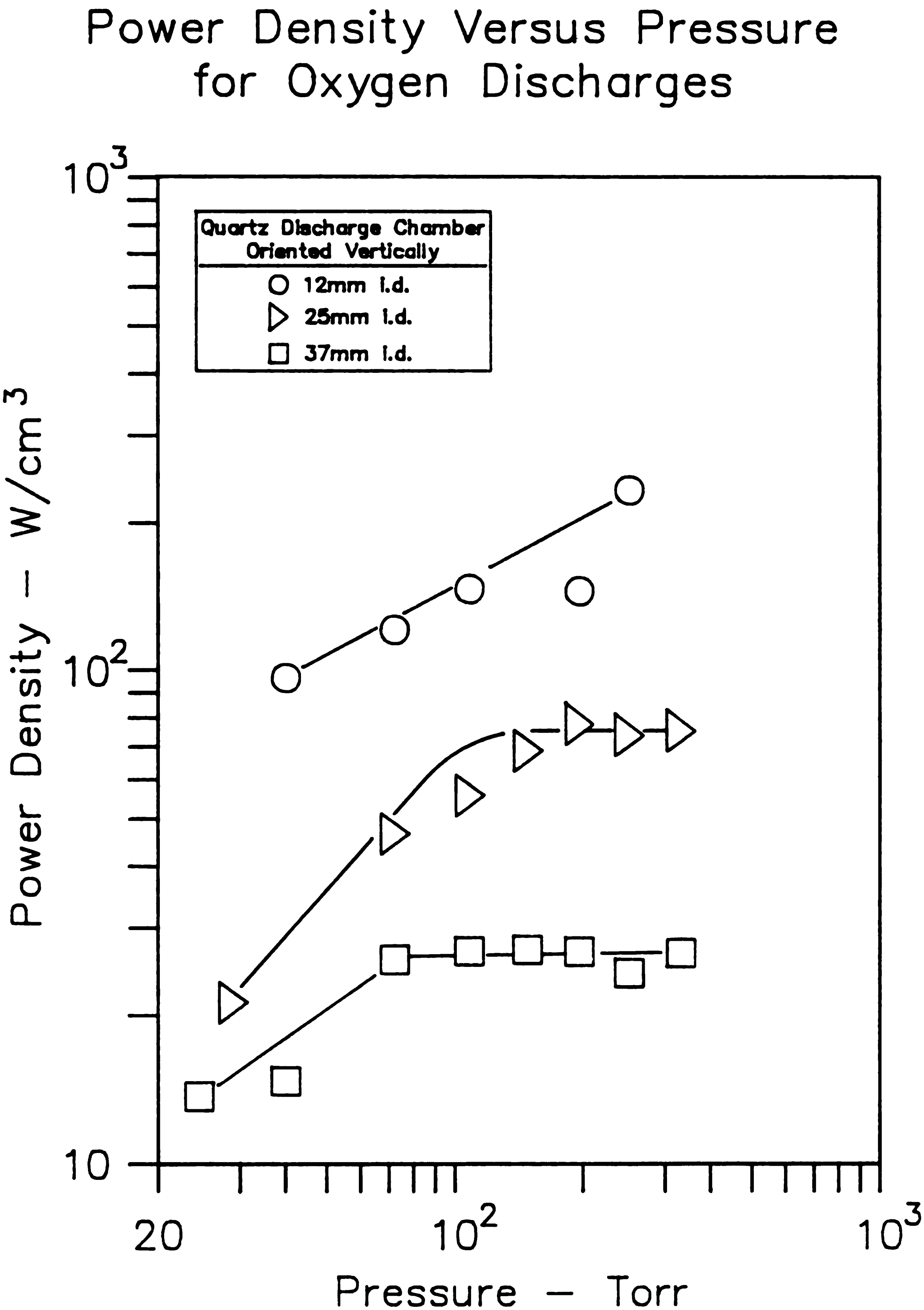

Figure 5.11 Power Density Versus Pressure for Oxygen Discharges

when compared to the monatomic gases Ar and He. Power densities were higher and cavity Q was higher for the diatomic gases indicating different loss processes than for monatomic gases.

5.4 SUMMARY

These experiments demonstrated the ability to generate non flowing helium, nitrogen and oxygen at pressures of 40 to 1000 Torr. Over 95% of the available microwave power was coupled into microwave discharge over the entire pressure range. This figure could easily be improved by the use of less lossy materials in the cavity walls and bettered designed microwave coupling circuits. As the pressure was increased the discharges contracted away from the discharge chamber wall forming small volume discharges. All of these results are desirable properties for an electrothermal thruster and serve to show that the concept is feasible.

CHAPTER VI

DEMONSTRATION OF A MICROWAVE ELECTROTHERMAL THRUSTER

6.1 INTRODUCTION

The design and testing of a microwave electrothermal thruster is described in this chapter. The results of these experiments were the first to demonstrate the feasibility of the microwave electrothermal thruster concept.[1] An experimental description of the thruster design used for these experiments is presented first, along with a description of how the experiment was conducted. Experimental measurements of thrust and specific impulse were taken using the direct thrust measurement system mentioned section 4.4.1. Efficiency, specific impulse and power to thrust ratio calculations were computed from these measurements and are presented in this chapter.

6.2 EXPERIMENTAL SYSTEM

A description of the experimental equipment and technique used to obtain the experimental data presented in this chapter is described in this section. The microwave electrothermal thruster is described first. Then a description of the experimental system used in measurements of the properties of this thruster is presented. The design and development iterations that produced the coaxial thruster are presented last.

6.2.1 PROTOTYPE ELECTROTHERMAL MICROWAVE THRUSTER

The prototype electrothermal microwave thruster, used to generate the results presented in this chapter, is shown in Figure 6.1. The design of this thruster was complicated. Because of this, the development of the thruster is detailed in section 6.2.3 showing the design iterations that led to the successful testing of this thruster. Figure 6.1 shows the entire thruster including the microwave coupling structure. Figure 6.2 shows an enlargement of the discharge chamber area of the thruster so details to fine to be shown in Figure 6.1 can be seen. Figure 6.2 continues the numbering system used in Figure 6.1 where applicable.

As shown in the figures the thruster consists of a coaxially fed microwave discharge located at the end of a 4.8 cm i.d. cylindrical, brass microwave coupling system. These figures show how the thrust discharge structure was incorporated onto the coaxial applicator. A teflon plug (6) with O-rings, seals the discharge zone from the external atmosphere air of the coaxial coupler (2), and provides a seal between the vacuum and the plasma discharge chamber (8). The plasma discharge chamber (8) is formed by a 23 mm i.d. quartz tube surrounding the discharge zone and narrowing to a 1 mm diameter nozzle downstream from the plasma and outside the electromagnetic excitation region. The cylindrical screen (9), which forms the outer waveguide conductor for the discharge chamber, is 6.5 cm in diameter and 9.5 cm long allowing only evanescent electromagnetic wave and slow wave coupling to the plasma discharges (3).

The input gas flow (7) is distributed around the teflon plug (6) by a distribution ring and enters the plasma discharge chamber (8)

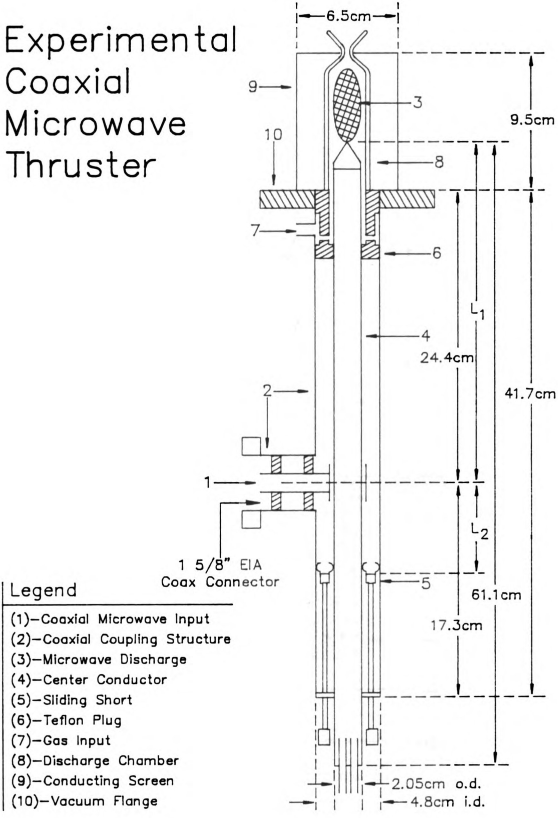

Figure 6.1 Experimental Coaxial Microwave Thruster

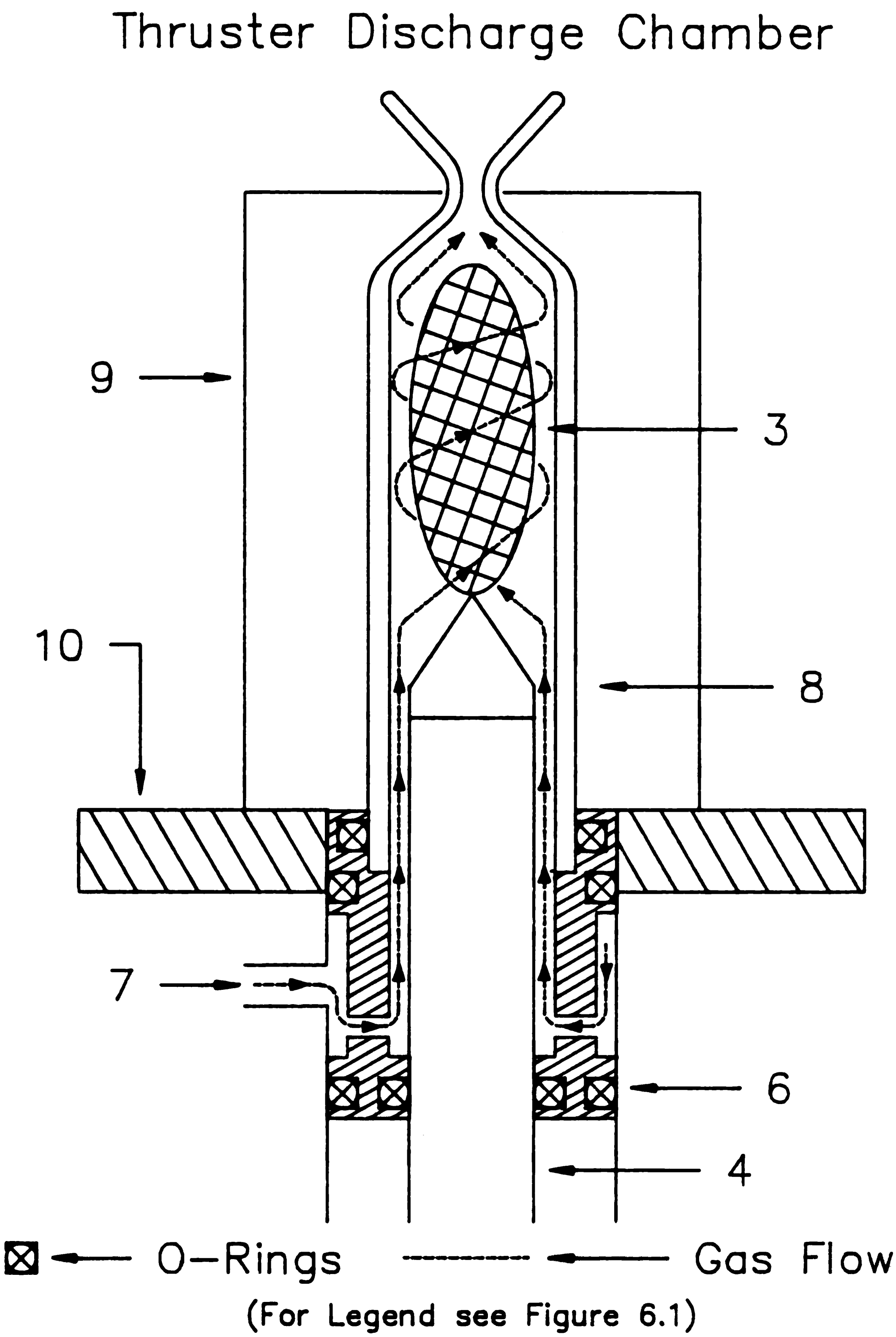

Figure 6.2 Enlargement of Thruster Discharge Chamber

through holes drilled at angles across the center axis of the plug. This produces a vortex flow in the chamber helping to stabilizing the discharge and causing a vortex flow through the discharge. Figure 6.2 shows the approximate gas flow pattern around the teflon plug and through the discharge chamber. At high pressures (>100 Torr) the flowing gas produces a stable discharge constricted away from the quartz walls of the discharge chamber, but attached to the end of the center conductor (4). The center conductor is water cooled to prevent melting of the inconel tip. A vacuum flange (10) is use to attach the thruster to a vacuum chamber. Figure 6.2 shows the O-rings used to seal the chamber in more detail.

6.2.2 MEASUREMENT SYSTEM AND EXPERIMENTAL PROCEDURE

The input microwave source was a continuously variable, 200-600 Watt, CW, 2.45 GHz magnetron oscillator. The input microwave system consisted of the same measurement system described earlier in section 4.2.2 and provided direct measurement of incident and reflected power. Microwave power is matched to the discharge by adjusting the sliding short, (5) in Figure 6.1, and by adjusting the center conductor, (4), for minimum reflected power. The important electrical lengths are shown in Figure 6.1 for this coaxial applicator. Lengths L_1 and L_2 indicate the center conductor and sliding short positions for a given experiment.

The experimental thrust test were performed at NASA Lewis Research Center's vacuum tank #8 using the experimental setup in Figure 6.3. As shown in this Figure the thruster was attached to the vacuum tank by 4" vacuum flange, (10) in Figure 6.1. This allowed the thruster to be

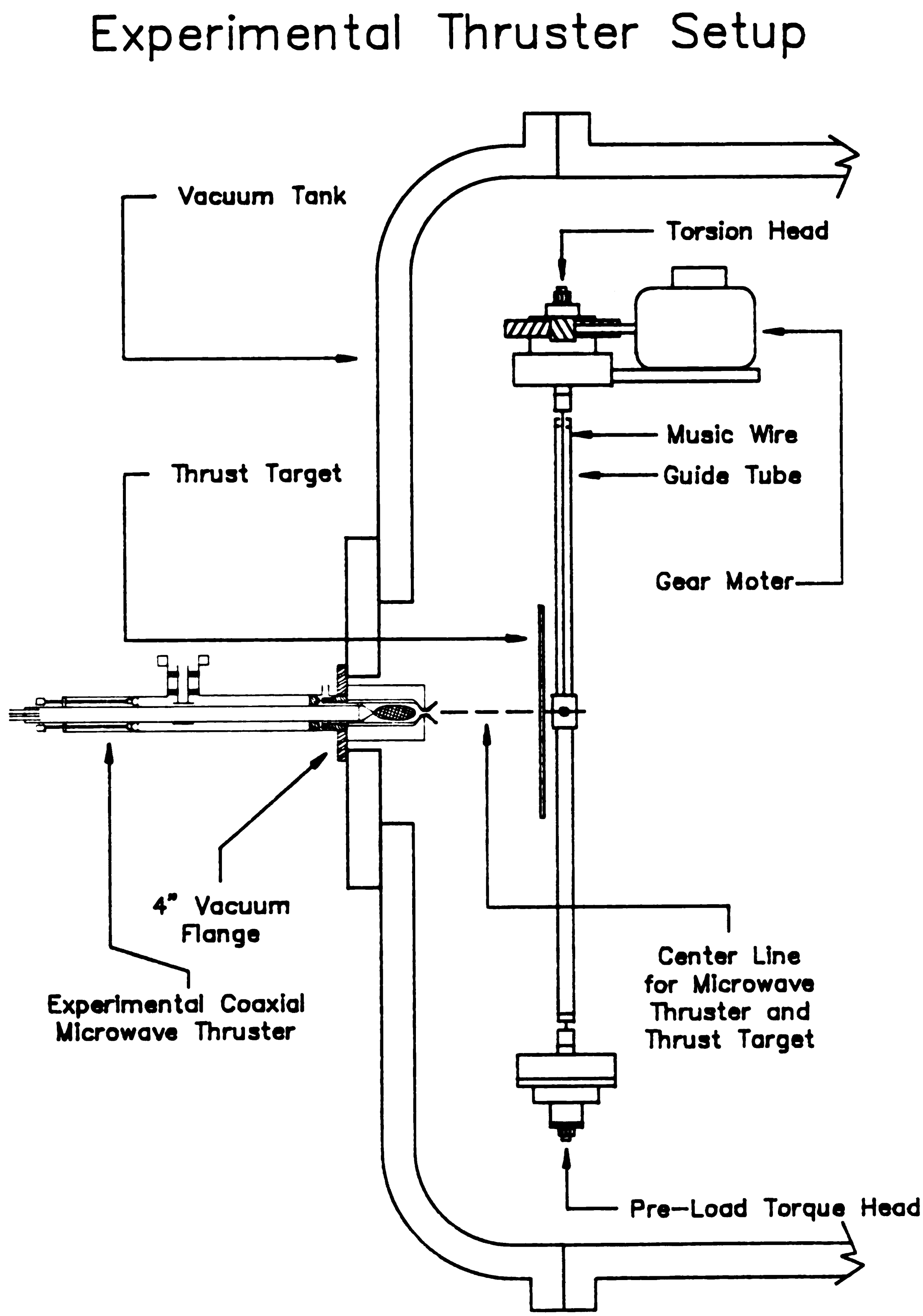

Figure 6.3 Experimental Setup of Microwave Thruster

exhausted into a vacuum environment held to below 10^{-4} Torr, assuring that a choked flow condition exists. Exhaust gas from the thruster impinges against a flat target of the direct thrust stand described in section 4.4.1. As shown in Figure 6.3, this thrust stand is mounted in the tank to allow the direct reading.

Experimental measurements were carried out using the experimental flow and pressure measurement system described is section 4.2.1. Nitrogen gas was tested at discharge pressures of 100 Torr to over one atmosphere and with flow rates in the range of 6.4×10^{-5} kg/s to 11.7×10^{-5} kg/s.

6.2.3 COAXIAL THRUSTER DEVELOPMENT

Figure 6.4a shows the initial applicator thruster design that was tested as a thruster concept. The applicator continues the numbering system used in Figure 6.1. The tests with this thruster in nitrogen gas were unsuccessful due an inability to keep the discharge on the tip of the center conductor (4). As the pressure was raised the discharge would form against the teflon plug (6) and melt it.

The thruster was redesigned and is shown in Figure 6.4b. The discharge chamber (8) was shortened and the teflon plug (6) was moved closer to the end of the torch. The thruster was set up and tested in a vacuum tank with a thrust stand to measure thrust. The thruster worked so well that even moderate levels of input power exceeded the thrust the thrust stand could measure. Some difficulty in tuning the thruster was encountered, so while the thrust stand was modified to measure greater thrust, the thruster was slightly changed to solve this.

The thruster was changed to the design shown in Figure 6.1. The

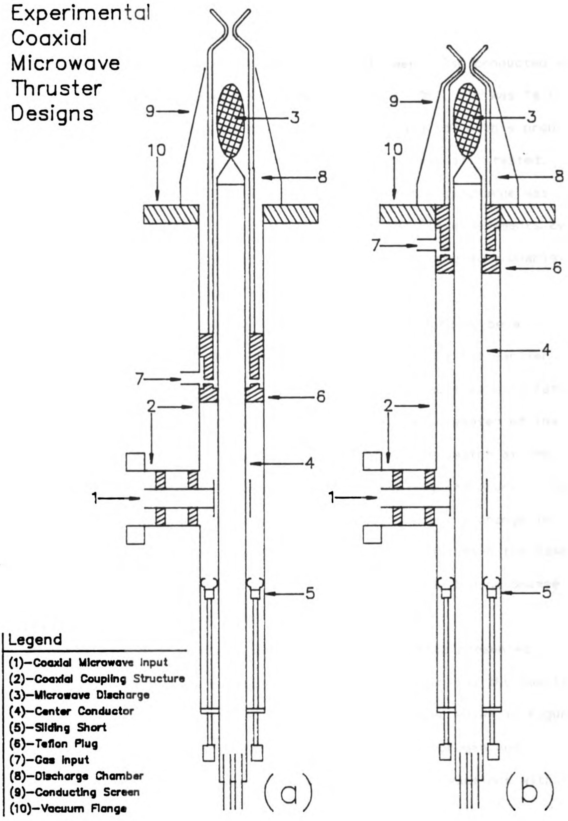

Figure 6.4 Experimental Microwave Thruster Design Variations

major change was to the shape of the screen outer conductor (9). Experiments with this thruster using nitrogen gas were very successful and are presented in this chapter. Experiments were also conducted with helium, but low efficiencies were observed (under 10%). It was felt that a discharge chamber with a smaller nozzle would solve this problem. A center conductor that could feed gas out the tip was also tested. It was felt that the efficiency could be improved if the discharge was moved off the tip by flowing gas through this tip. In experiments even the slightest gas flows would blow the discharge out and were unable to move it off the tip and still maintain it.

The tuning and matching of this thruster continued to be a problem. The best match that could be obtained was 85% but earlier experiments with the applicator shown in Figure 3.4 were able to match 95% or better into the applicator. The larger outer diameter of the screen (9) was felt to be causing a electromagnetic mismatch at the boundary with the outer conductor (2) of the coupling structure. The screen was modified and is shown in Figure 6.5a. With no change in diameter, the impedance to the discharge region would remain the same. However the efficiency of the thruster dropped and the tuning became more difficult and the modification was dropped.

Tests with hydrogen were desirable but the quartz presented difficulties. Chemical reactions between the hydrogen and the quartz would ruin the nozzle. A metal wall discharge chamber shown in Figure 6.5b was constructed. This thruster was tested in hydrogen and efficiencies of ~10% was observed. However hydrogen reactions with the teflon plug (6) severely damaged it and the tests were discontinued.

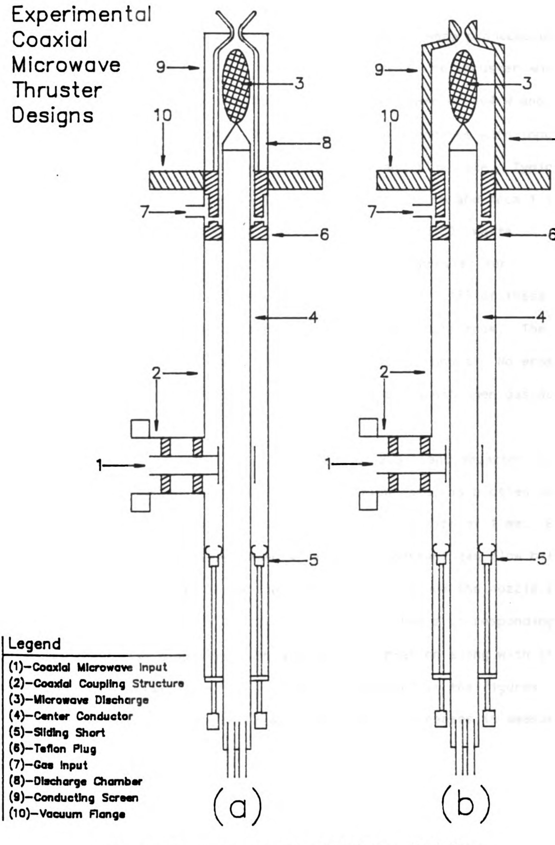

Figure 6.5 Microwave Thruster Design Variations

6.3 EXPERIMENTAL MEASUREMENTS

Experimental results presented in this chapter were produced with the thruster shown in Figure 6.1. Figure 6.6 shows the thruster working in vacuum tank #8. It is operating with a input power of 464 W and a flow rate of 11.7×10^{-5} kg/s. The discharge size increases with input power and decreases with increases in pressure and flow rate. Typical discharge lengths and diameters increase from 1 to 4 cm and from 1 to 1.8 cm respectively as power is increased from 200 to 600 Watts.

The measured experimental performance of the thruster for different nitrogen flow rates is shown in Figure 6.7. All of these results are for the thruster operating in a steady state mode. The thruster was operated at times for periods of over 3 hours. No erosion or melting was observed during this time while using nitrogen gas as a propellant.

The specific impulse, defined in section 2.3.1 and equation 2.1 as the ratio of thrust to the input propellant flow rate, is plotted versus measured thrust in Figure 6.7a for the fixed nozzle size of 1 mm. Each curve represents thrust measurements made with constant gas flow but increasing absorbed power from 200 to 600 Watts. Since the nozzle size was fixed, each level of propellant flow established a corresponding range of discharge pressures. This pressure variation along with the corresponding variation of input power is indicated in the figures legend. Increases in absorbed power resulted in increases in measured discharge pressure and thrust.

The cold specific impulse (specific impulse without a discharge) is shown in the lower left hand corner of each curve in Figure 6.7a, and is nearly independent of gas flow rate and agrees well with theoretical

Picture of Operating Microwave Thruster at Lewis Research Centers Tank #8

Mass Flow=10.6×10^{-5} kg/s Input Power=474 Watts

Discharge Pressure=800 Torr

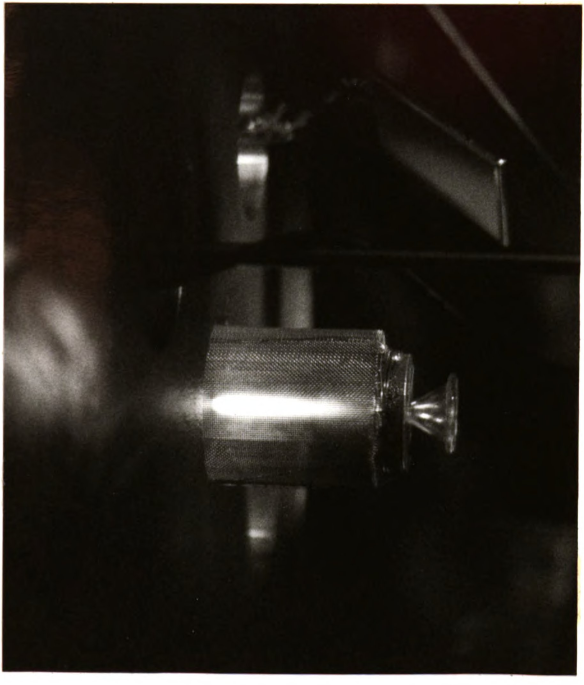

Figure 6.6 Picture of a Operating Microwave Electrothermal Thruster

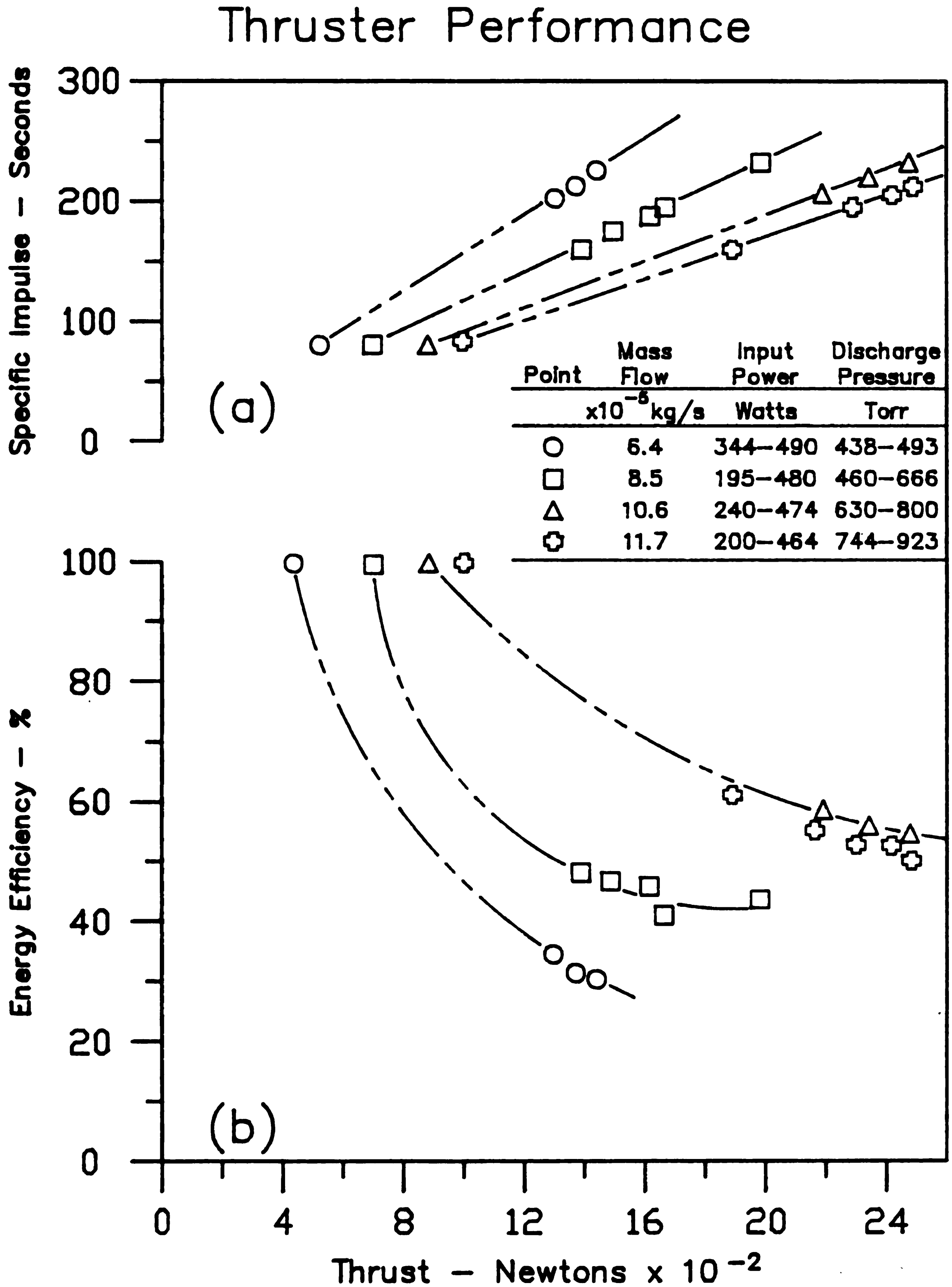

Figure 6.7 Coaxial Microwave Electrothermal Thruster Performance

calculations of room temperature gas. From its definition, equations 4.6 and 4.7, the specific impulse should have a straight line relationship versus thrust and a slope that varies as the reciprocal of the propellant flow rate. The experimental points in Figure 6.7a demonstrate this relationship. A straight line drawn through the "hot" data points is extrapolated to each corresponding cold flow point. Extrapolated extensions of these lines pass through the origin as expected.

The energy overall efficiencies are shown in Figure 6.7b. The efficiency is defined using the equation 4.9 in chapter 4 and the data from Figure 6.7a. As shown in Figure 6.7b, efficiency improved with propellant flow rate, reaching a maximum of about 60%. There is a large gap in points between cold and hot efficiencies since the microwave generator did not produce regulated power below about 200 Watts. Furthermore it is doubtful that the plasma discharge is stable at lower power levels. Over the absorbed power range of 200 to 600 Watts and at a constant flow rate, the efficiency decreased 10% or less with increasing power.

The power to thrust ratio plotted against specific impulse is shown in Figure 6.8. Lines of constant efficiency are shown, but they are terminated at the assumed cold specific impulse value of 80 seconds, because at that point all values of power to thrust ratio go to zero. It is interesting to note that although the power to force ratio is identically zero at unity efficiency when hot specific impulse is equal to the cold specific impulse, other values of hot specific impulse at near 100% efficiency result in a finite power to thrust ratio

Power to Thrust Ratio for the Microwave Electrothermal Thruster

Point	Mass Flow	Input Power	Discharge Pressure	L_1	L_2
	$\times 10^{-5}$ kg/s	Watts	Torr	mm	mm
○	6.4	344–490	438–493	275	37
□	8.5	195–480	460–666	269	38
△	10.6	240–474	630–800	275	37
✥	11.7	200–464	744–923	–	–

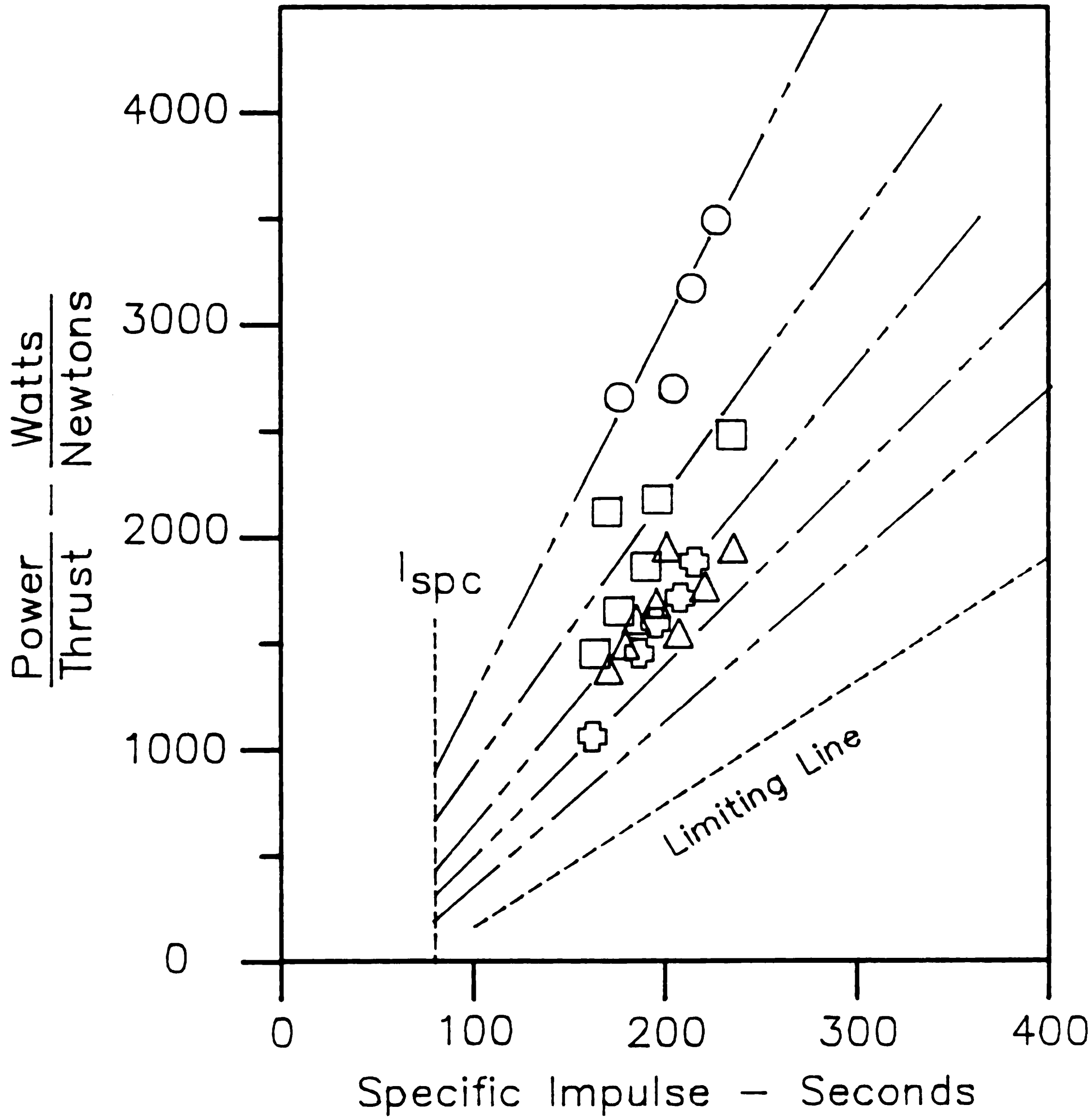

Figure 6.8 Power to Thrust Ratio for the Microwave Thruster

proportional to the quantity $I_{spH} - \frac{I_{spc}^2}{I_{spH}}$. When $I_{spH} \gg I_{spc}$, this quantity approached I_{spH}, such that the power to force ratio approaches $\frac{gI_{spH}}{2}$. Using the relationship $I_{spH} = \frac{v_H}{g}$, the power to thrust ratio then approaches $\frac{v_H}{2}$, which is also the time rate with which kinetic energy is imparted to the propellant exhaust divided by the thrust produced. Under the best of conditions the power to thrust ratio cannot be less than one half the exhaust velocity (in consistent units). At lower values of I_{spH}, the power to thrust ratios are calculated for efficiency equal to 100% and are drawn in Figure 6.8 as a broken line.

6.4 COMPARISON OF EXPERIMENTAL THRUSTERS

A performance comparison of the microwave electrothermal thruster against the data from two resistojets[20,21] and an arcjet[25] from chapter 2 is shown in Figure 6.9. The resistojets, designated A[20] and B[21], differ in heating approach and consequently in the dimensions of the propellant passages. The arcjet used in the comparison , C[25], was a 1 kW system.

The experimental results prove that a working microwave electrothermal thruster can be built. As shown in Figure 6.9 the performance of the microwave electrothermal thruster compares favorably with other electrothermal concepts operating in nitrogen gas. They also show that this type of a thruster can produce a significant increase in thrust over cold flow and that the efficiency of the input energy to output thrust can be as much as 60%. It should be pointed out that these results are only the most preliminary since this thruster was

Comparison of Several Electrothermal Thrusters with the Microwave Electrothermal Thruster

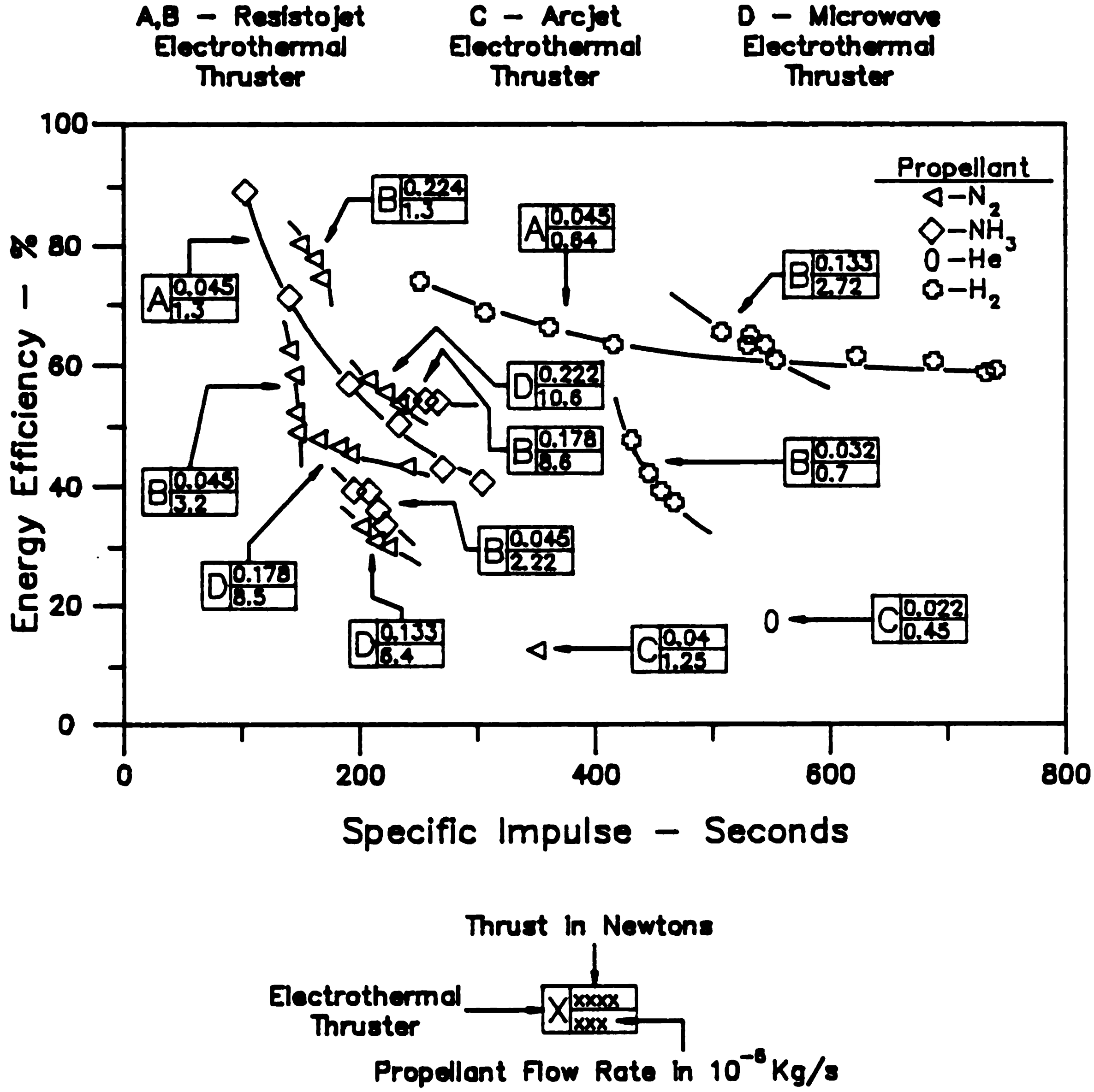

Figure 6.9 Electrothermal Thruster Comparison

built as a prototype and was not yet optimized to increase performance. Hopefully experiments with this thruster will continue and show greater improvements. It would be desirable to test H_2 and NH_3, and run tests at higher power and chamber pressure.

CHAPTER VII

CAVITY APPLICATOR THRUSTER RESULTS USING QUARTZ NOZZLES

7.1 INTRODUCTION

Experiments in Chapter 5 demonstrated the ability to generate and maintain a high pressure microwave discharge with a cavity applicator and with no gas flow. These experiments showed that microwave energy could be coupled into the discharge with a efficiency of greater then 98% and that power densities of greater then 100 W/cm^3 could be achieved. This chapter continues these experiments by applying the knowledge gained from chapter 5 to the development of a cavity applicator based microwave electrothermal thruster. While the prime emphasis of this chapter is on development of a thruster, the results presented and technique described can be extended to any microwave cavity applicator based discharge using a flowing gas. Indeed, while demonstrating a working thruster, this chapter also demonstrates the ability to generate and maintain high pressure microwave discharges in a flowing gas environment.

This chapter presents results of experiments using a thruster, incorporating a cavity type applicator for energy coupling. An experimental description of the thruster and the setup used to test it is presented first. Experimental measurements of thrust and specific impulse are presented next. Efficiency and power to thrust ratio are derived from the thrust measurements.

7.2 EXPERIMENTAL SYSTEM

An experimental thruster was built based on the design of the applicator shown in Figure 3.5. The thruster based on this applicator is shown in Figure 7.1. This figure continues the numbering system used in Figure 3.5 with the microcoax system omitted from the drawing to simplify it. The cavity applicator from Figure 3.5 has been modified to include a discharge chamber (6) with a nozzle (13) to convert the thermal energy into thrust and is shown as (D) in Figure 3.7. For all experiments presented in this chapter a cylindrical quartz discharge chamber was used with inside diameter of 23 mm or 28 mm and forced air cooling was added to prevent the chamber from melting. The nozzle was located at the exit of the cavity, as shown in Figure 7.1, for all the measurements of this thruster. Also a adjustable center body (14) has been added to help stabilize the discharge (4). The variable length input probe (8) and the sliding short (2) used the actuators described in section 3.4.1 (and shown as (B) and (C) in Figures 3.6 and 3.7) for more accuracy in the measurements.

The flow and pressure measurement system described in section 4.2.1 and shown in Figure 4.1 was used for the measurements in this chapter although only one gas was used at a time. The applicator was oriented in a vertical manner with the gas flow downward and out the nozzle at the bottom of the applicator. The small size of the vacuum system made it necessary to use a heat exchanger to cool the exhaust gas and prevent damage to the pumping system. These experiments were set up at Michigan State University and used a roughing pump to exhaust the

Cross Section of a Cavity Applicator Based Microwave Electrothermal Thruster

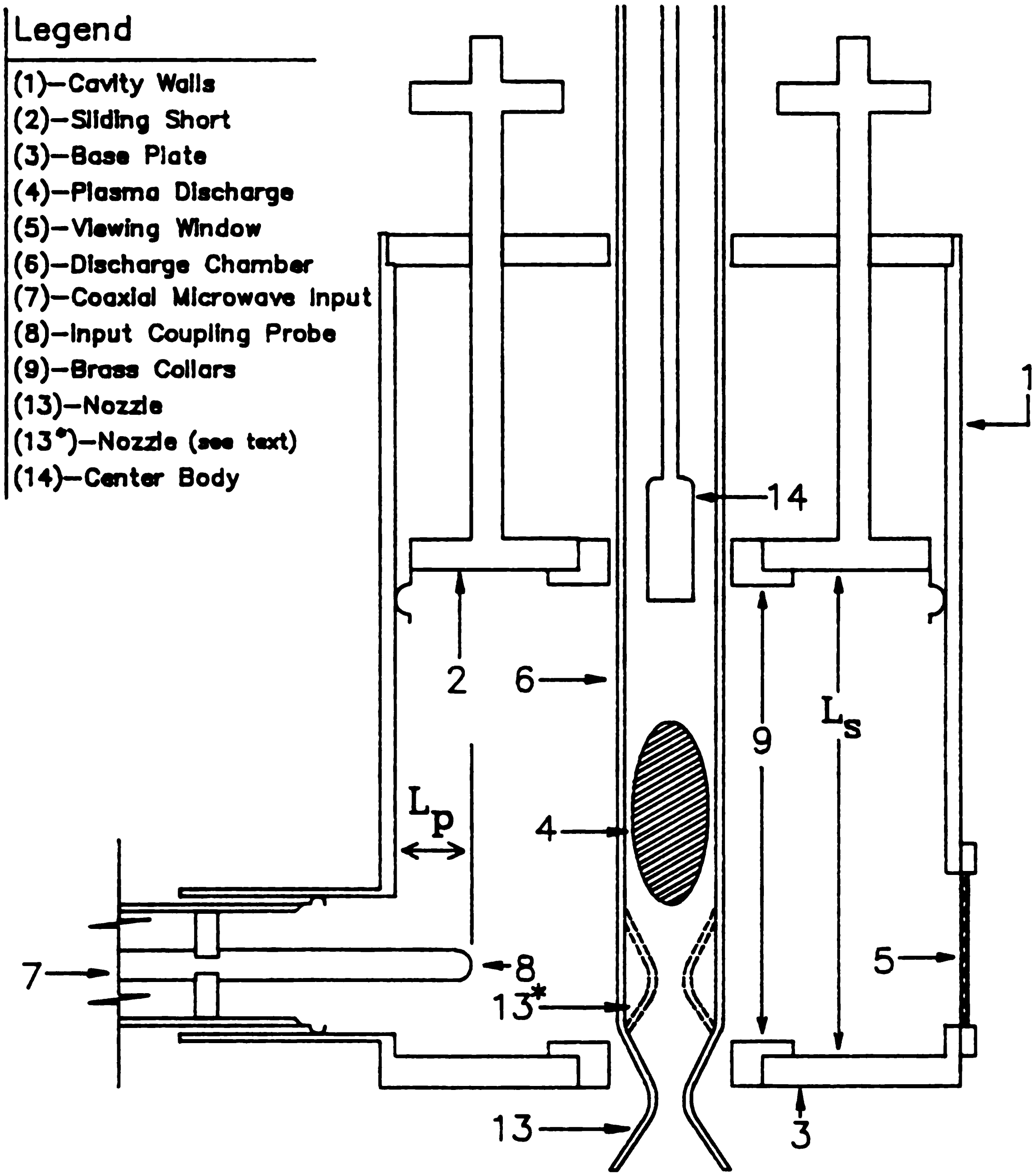

Figure 7.1 Cross Section of a Cavity Microwave Thruster

propellant. The microwave supply system of section 4.2.2 was used for measurement and control of microwave power. For these experiments a continuous wave, variable power, 0 to 2500 Watt microwave power source was used.

Experimental runs were performed by first establishing a desired propellant flow rate and holding this flow rate constant throughout the entire experimental run. Once the desired flow rate was achieved, the cold discharge pressure was measured. The discharge was then ignited and the input microwave power was adjusted to the desired level. The applicator input power, P_t, and the steady state discharge pressure p_H were measured for several operating points as the input power, P_t, was varied. After each experimental run, the discharge chamber was allowed to cool back to the initial conditions as a check against nozzle degradation.

The thrust force, specific impulse, energy efficiency and the power to force ratio were calculated from equations 2.1-2.5 and 4.8-4.9 with the thrust force being derived using the indirect thrust method described in section 4.4.3. As discussed in chapter 5, microwave coupling efficiency was very high, therefore P_t was assumed to be equal to P_a for these calculations. The input power P_t was increased until nozzle heating threatened to destroy the nozzle. Thus all experiments were limited by nozzle heating.

Results of experiments performed by S. Nakanishi[6] of NASA Lewis Research Center are also presented in this chapter. These experiments used an experimental setup and technique nearly identical to that described above. For these experiments a 0 to 600 Watt source was used with a cavity applicator identical to that described in Figure 7.1.

However in these experiments the position of the nozzle could be varied with respect to the position of the discharge. For the results of experiments presented, the nozzle was moved from (13) to inside the cavity (13*). A large vacuum tank with a diffusion pumping system was used to exhaust the propellant. The size of this system and its pumping speed made a heat exchanger, shown in Figure 4.1, unnecessary. This experiment was also oriented vertically, however in this experiment the gas flowed up through the applicator and the through the nozzle at the top. This orientation was felt to be beneficial since the gravitational gradient and buoyancy would increase the flow of heated propellant to the nozzle. Experiments were performed using this system without external forced air cooling of the discharge chamber.

7.3 EXPERIMENTAL MEASUREMENTS

Initial experiments were performed with nitrogen in a single applicator TM_{012} mode to develop a basic understanding and technique in thruster operation. The first section presents the results from these experiments. Further experiments were conducted with nitrogen in a TM_{011} mode to study the affect the mode has on the thruster operation. The next section presents the results of these experiments and the last section presents a review of these results.

7.3.1 EXPERIMENTS WITH NITROGEN IN DIFFERENT MODES

Initial experiments were performed with nitrogen in a TM_{012} mode using a 23 mm quartz discharge chamber with a nozzle diameter of 1.5 mm. The position of the discharge and the pattern of the electromagnetic fields are shown in Figure 3.8. The results of these experiments are shown in Figure 7.2 as energy efficiency versus input power for flow rates of 63×10^{-6} kg/s to 146×10^{-6} kg/s (3000 sccm to 7000 sccm) and the experimental range of conditions are described in Table 7.1 as point 1, 2 and 3. These data points proved difficult to maintain at higher input powers and at higher flow rates. The discharge would become unstable in position and sometimes be swept downstream from the intense microwave region and extinguished. However the thruster was operated for periods of greater than 1 hour with no nozzle melting or erosion, but had problems with the quartz discharge chamber deforming next to the discharge.

Further experiments were conducted using a discharge chamber with the stabilizing center body (14) shown in Figure 7.1. The data corresponding to these experiments is shown in Figure 7.2 and is described as points 4, 5 and 6 in Table 7.1. These experiments used a quartz discharge chamber with a inner diameter of 23 mm and nozzle diameter of 1.17 mm. The stabilizing center body served a dual purpose of forcing a boundary layer flow along the inner surface of the discharge chamber and of providing a wake or recirculation zone similar to a combustion stream flame holder. The center body worked as planed producing stable discharges. However, as the input power was increased the discharge extended to the nozzle and produced problems with nozzle melting. Thus the power levels were limited to < 2000 Watts to prevent the nozzle from overheating.

Additional experiments were conducted using nitrogen with the applicator operating in a TM_{011} mode using a 28 mm diameter discharge chamber with a nozzle diameter of 1.17 mm. The position of the discharge and the pattern of the electromagnetic fields are shown in

Table 7.1 Operating Conditions for Experiments with Nitrogen Propellant

Operating Conditions for Experiments with the Microwave Thruster of Figure 7.1 in Nitrogen Propellant

#	Point	Flow Rate (kg/sX10^{-6})	Discharge Pressure (Torr)	Cavity Mode	Nozzle Size	Center Body	L_s cm	L_p cm
1.	●	63.0	258–306	TM_{012}	1.5mm	no	14.55	1.95
2.	▼	104	440–486	TM_{012}	1.5mm	no	14.5	1.95
3.	●	146	562–624	TM_{012}	1.5mm	no	14.5	1.95
4.	●	63.0	503–525	TM_{012}	1.17mm	yes	14.5	1.95
5.	■	104	710–819	TM_{012}	1.17mm	yes	14.5	1.95
6.	▲	146	953–1021	TM_{012}	1.17mm	yes	14.5	1.95
7.	◄	36.5	380–440	TM_{011}	1.17mm	no	7.1	0.9
8.	◆	146	882–1000	TM_{011}	1.17mm	yes	7.1	0.8

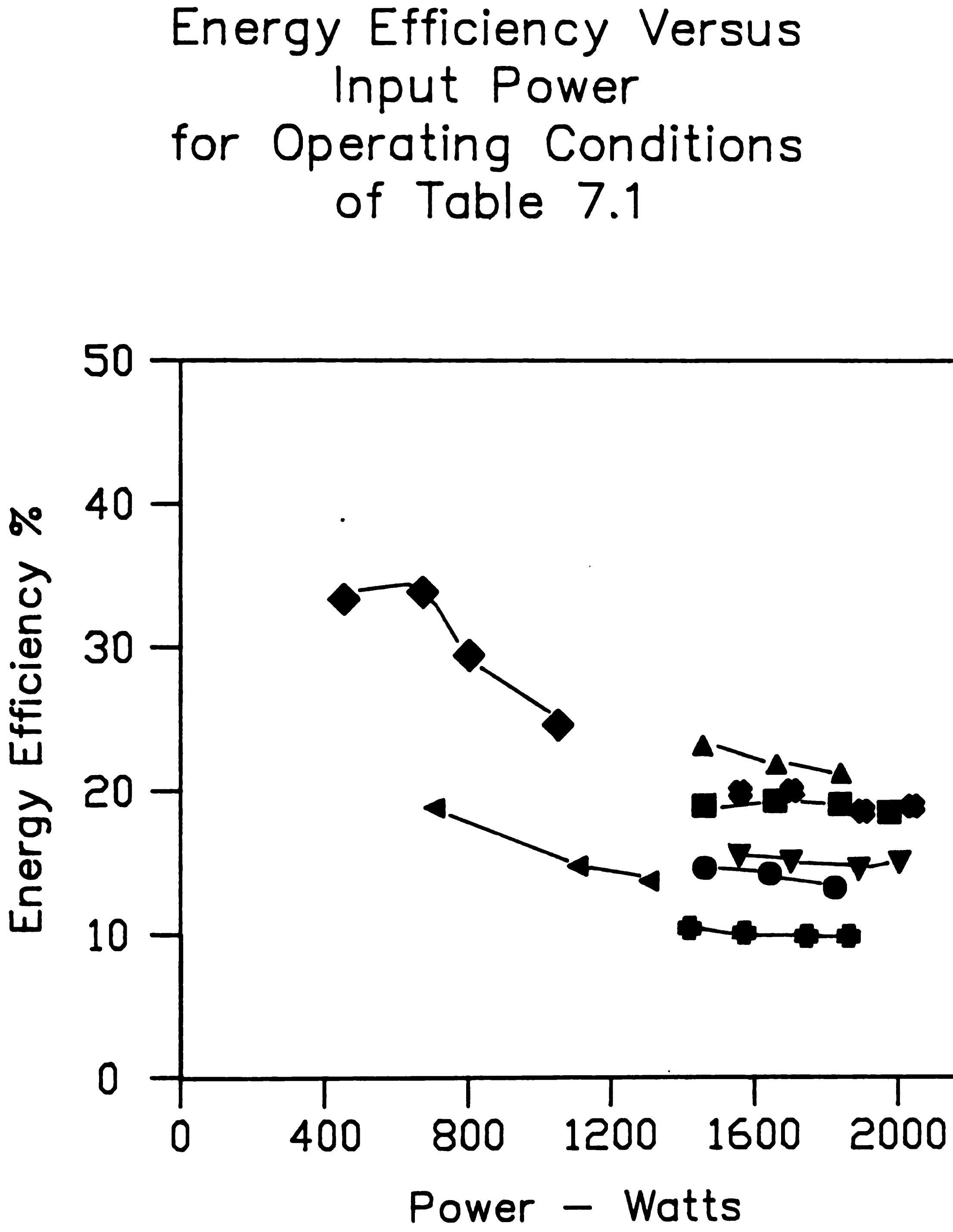

Figure 7.2 Energy Efficiency Versus Input Power for Nitrogen

Figure 3.8. The results of these experiments are shown in Figure 7.2 as solid points and are described as points 7 and 8 in Table 7.1. The discharge was next to but not quite touching the nozzle for both points using the TM_{011} mode. For data point 7 no flow stabilization was used, limiting the maximum flow that discharge could be sustained at. Even at the flow rate shown for point 7 there was still problems with the discharge similar to that in the TM_{012} mode with no stabilization, with the discharge being unstable and easily extinguished. Data point 8 used the same flow stabilization system described earlier. Stability was excellent at high flow rate, however the same nozzle melting problem mentioned earlier limited input power to less than 1 kW.

Figure 7.3 shows energy efficiency versus input power for experiments conducted by S. Nakanishi at Lewis Research Center. For these experiments a 29 mm i.d. quartz discharge chamber with a center body stabilization system was used with a 1.27 mm nozzle. The nozzle position in this system could be changed for different experiments, thus changing the distance from the discharge to the nozzle. Figure 7.3 shows the results for two different positions under identical condition of input power and propellant flow. It was observed that the best performance, i.e. energy efficiency and specific impulse, was obtained with the nozzle located inside the cavity from 3.6 to 3.0 cm from the fixed end plate. This distance is approximately one quarter electromagnetic wave length for the TM_{012} mode inside the cavity and is located at an axial electric field minimum. Thus the nozzle is located at the end of the plasma discharge core.

Specific impulse versus energy efficiency is presented in Figure 7.4 for all the points in Table 7.1 and the nozzle position

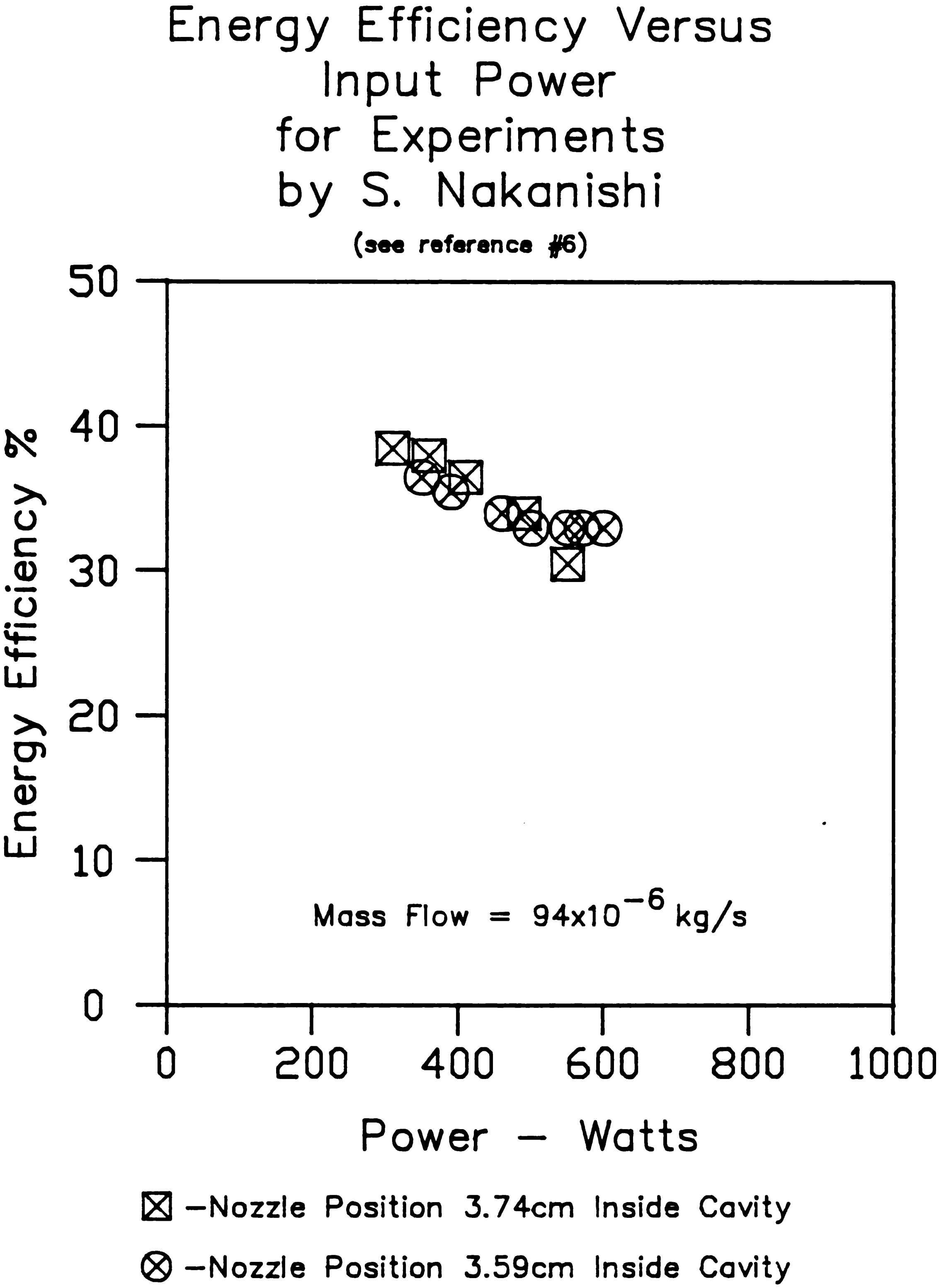

Figure 7.3 Results of Experiments by S. Nakanishi

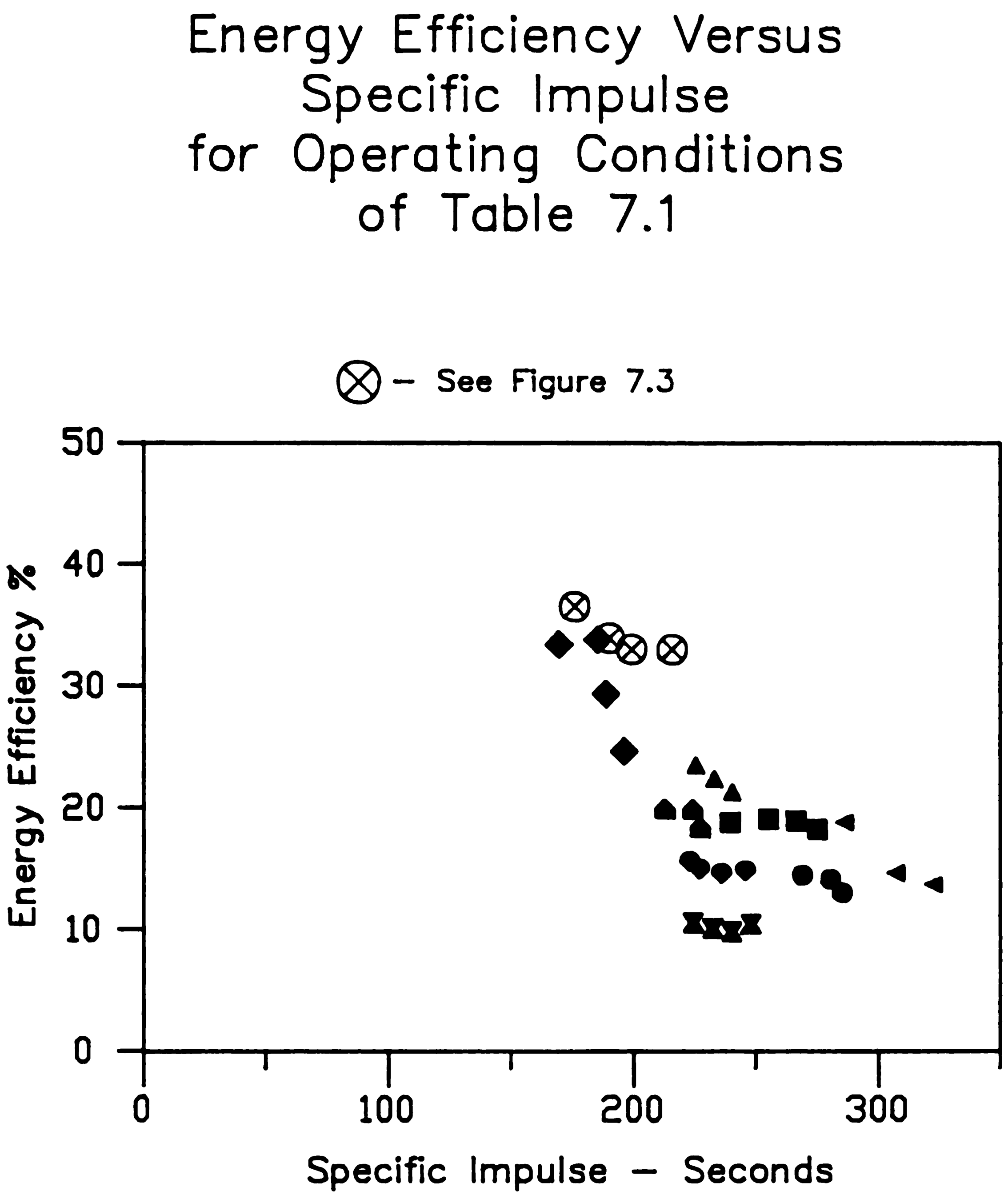

Figure 7.4 Energy Efficiency Versus Specific Impulse for Nitrogen

experiments of Figure 7.3. Maximum specific impulse was approximately 280 sec corresponding to a cold to hot discharge chamber pressure ratio increase of over three. The lower efficiencies for the points from Table 7.1, were due in part to forced air cooling, smaller chamber diameter and nonoptimum position of the nozzle.

7.3.2 EXPERIMENTS WITH HELIUM IN DIFFERENT MODES

The results in the previous section show that a cavity thruster using nitrogen propellant is a valid concept for electrothermal propulsion. However better performance was desirable along with operations using lighter propellants. This section presents the results of experiments using helium as propellant in the same cavity type thruster of the last section. Helium was tested using two different cavity modes, TM_{012} and TM_{011}. Figures 7.5 shows efficiency versus input power for the data point in Table 7.2. The legend in Table 7.2 details the different experimental configurations and operating conditions under which the experimental points were taken.

Discharge behavior in the TM_{012} mode was similar to that observed in the previous sections and is represented by data point 1 in Table 7.2. A 28 mm i.d. discharge chamber was used with a 1.17 mm nozzle and stabilization apparatus. No problems with stability were encountered but nozzle heating limited the maximum input power to less than 1.2 kW. Lower flow rates were also tested but produced severe nozzle heating and were discontinued.

Experiments with the TM_{011} mode with helium produced a discharge that was next to but not quite touching the nozzle as in nitrogen. Data points 2, 3, 4 and 5 from Table 7.2 used the same discharge chamber as

Table 7.2 Operating Conditions for Experiments with Helium Propellant

Operating Conditions for Experiments with the Microwave Thruster of Figure 7.1 in Helium Propellant

#	Point	Flow Rate ($kg/s \times 10^{-6}$)	Discharge Pressure (Torr)	Cavity Mode	Nozzle Size	Center Body	L_s cm	L_p cm
1.	○	26.7	280–328	TM_{012}	1.17mm	no	14.25	1.75
2.	□	8.9	170–196	TM_{011}	1.17mm	no	7.2	0.8
3.	△	14.8	260–320	TM_{011}	1.17mm	no	7.2	0.8
4.	◇	20.8	330–430	TM_{011}	1.17mm	no	7.2	0.8
5.	◁	26.7	402–546	TM_{011}	1.17mm	no	7.2	0.8
6.	○	8.9	567	TM_{011}	0.51mm	no	7.1	1.9
7.	▽	10.4	625	TM_{011}	0.51mm	no	7.1	1.9
8.	○	11.9	810	TM_{011}	0.51mm	no	7.1	1.9

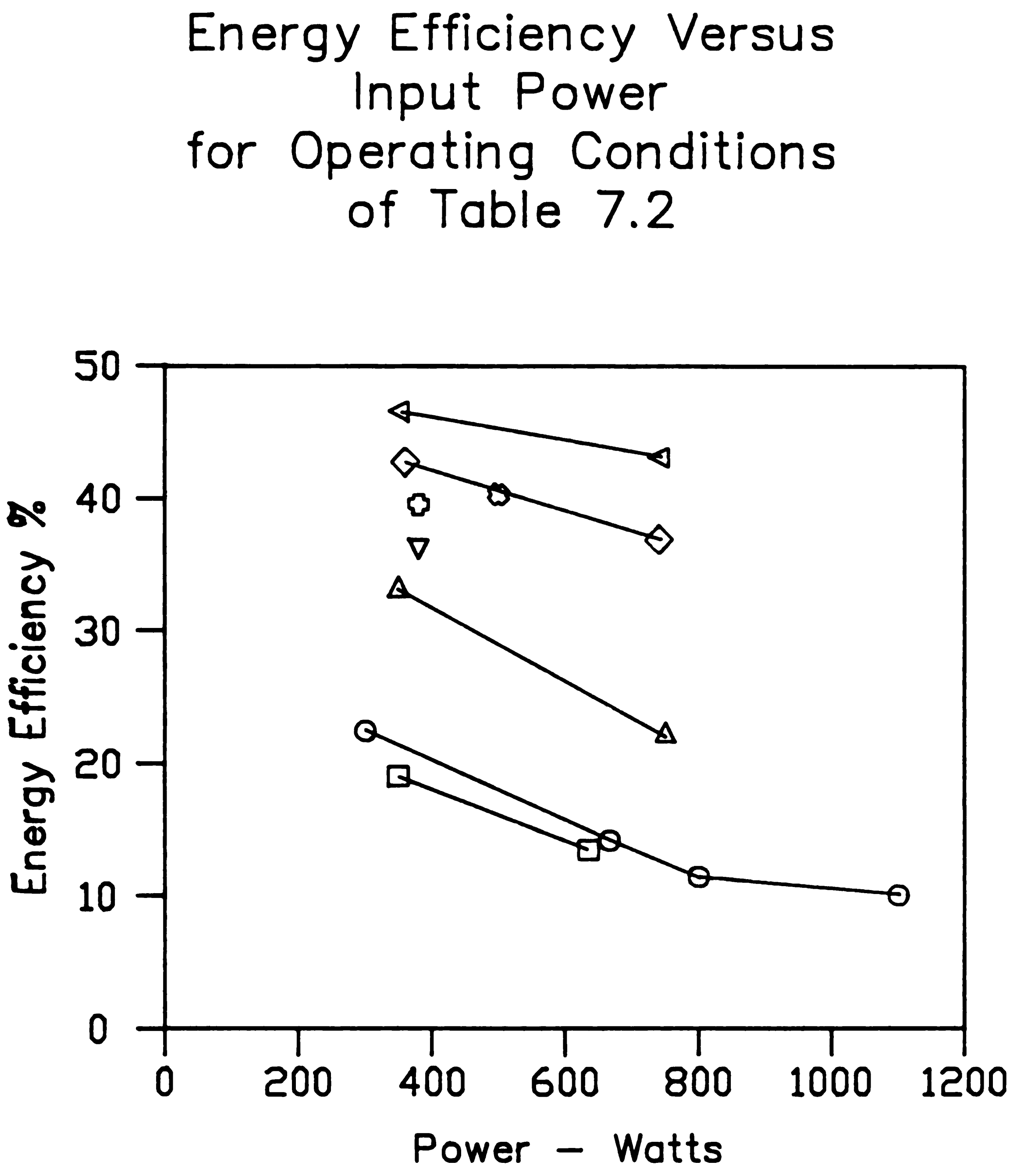

Figure 7.5 Energy Efficiency Versus Input Power for Helium

was used for point 1. No stabilization problem were encountered and the thruster was able to operate at several different flow rates. Nozzle heating was still a problem and input power was limited to below 800 W. As can be seen in Figure 7.5 efficiencies of up to 45% were achieved for input powers of up to 750 Watts.

Addition experiments were conducted with helium in a TM_{011} mode with a discharge chamber of 28 mm i.d. and a 0.51 mm nozzle. Data points 6, 7 and 8 from table 7.2 represent these experiments. No stabilization problem were encountered and the thruster was able to operate at several different low flow rates with good efficiencies. Nozzle heating was a severe problem and input power was limited to below 500 W. This also limited the number of data point since the minimum power required to sustain the discharge was near 500 W. As can be seen in Figure 7.5 efficiencies of up to 40% were achieved for input powers of up to 500 Watts. Figure 7.6 shows the energy efficiency versus specific impulse for all the points in Table 7.2. A maximum specific impulse of 600 sec at a efficiency of 40% was achieved.

7.3.3 DISCUSSION

Discharge behavior was similar to that observed in the coaxial thruster presented in chapter 6. For both modes the discharge lengths and diameters increased as input power increased, and decreased or constricted slightly as pressure or flow rate increased. A comparison between Figures 7.2 and 7.4, and the one for the coaxial thruster, Figures 6.7 and 6.8, indicate that the experimental trends for the two thruster geometers are similar except for the larger thrust output in the cavity thruster associated with its higher input powers.

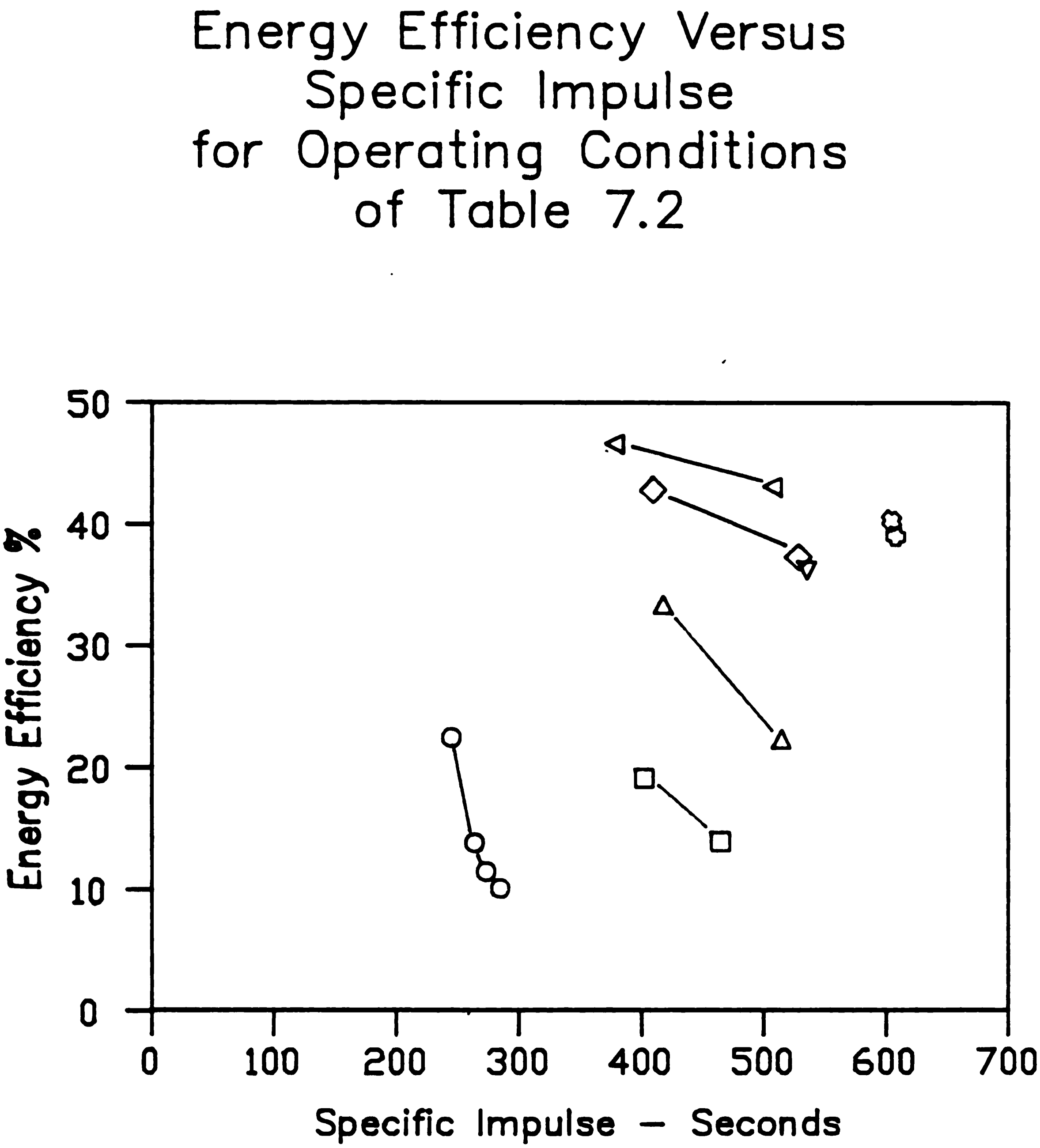

Figure 7.6 Energy Efficiency Versus Specific Impulse for Helium

In all the energy efficiency versus input power figures for a fixed experimental geometry and for constant flow rate, the energy efficiency decreased slightly as the absorbed power increased. Energy efficiency increased with increased flow and increased in the presence of a discharge stabilizing center body, while the thrust increased as input power increased. As expected, specific impulse increased as nitrogen gas mass flow rate decreased.

Figure 7.7 presents a comparison of specific impulse versus energy efficiency for several data point from Tables 7.1 and 7.2. As can be seen from the data, helium gas excited with the TM_{011} mode has higher energy efficiencies than in the TM_{012} mode. In nitrogen gas this was reversed and the TM_{012} mode had better efficiencies. Nitrogen gas had a maximum specific impulse of 280 sec and helium had a maximum specific impulse of up to 600 sec. Both of these result represent a increase of about 3 times over the cold specific impulse and the higher helium specific impulse can be attributed to its higher cold specific impulse.

Figure 7.8 presents a comparison of specific impulse versus thrust to power ratio for several data point from Tables 7.1 and 7.2. As can be seen from the data, helium gas excited with the TM_{011} mode has higher specific impulse than nitrogen gas in the TM_{012} mode. However the nitrogen has better power to thrust ratio. For all gases and modes the specific impulse drops as the thrust to power ratio increases as expected.

The results of these experiments show that a microwave electrothermal thruster based on a cavity is a valid concept. Optimum result were obtained in nitrogen in a TM_{012} mode while for helium the best result were obtained for a TM_{011} mode. From the standpoint of the

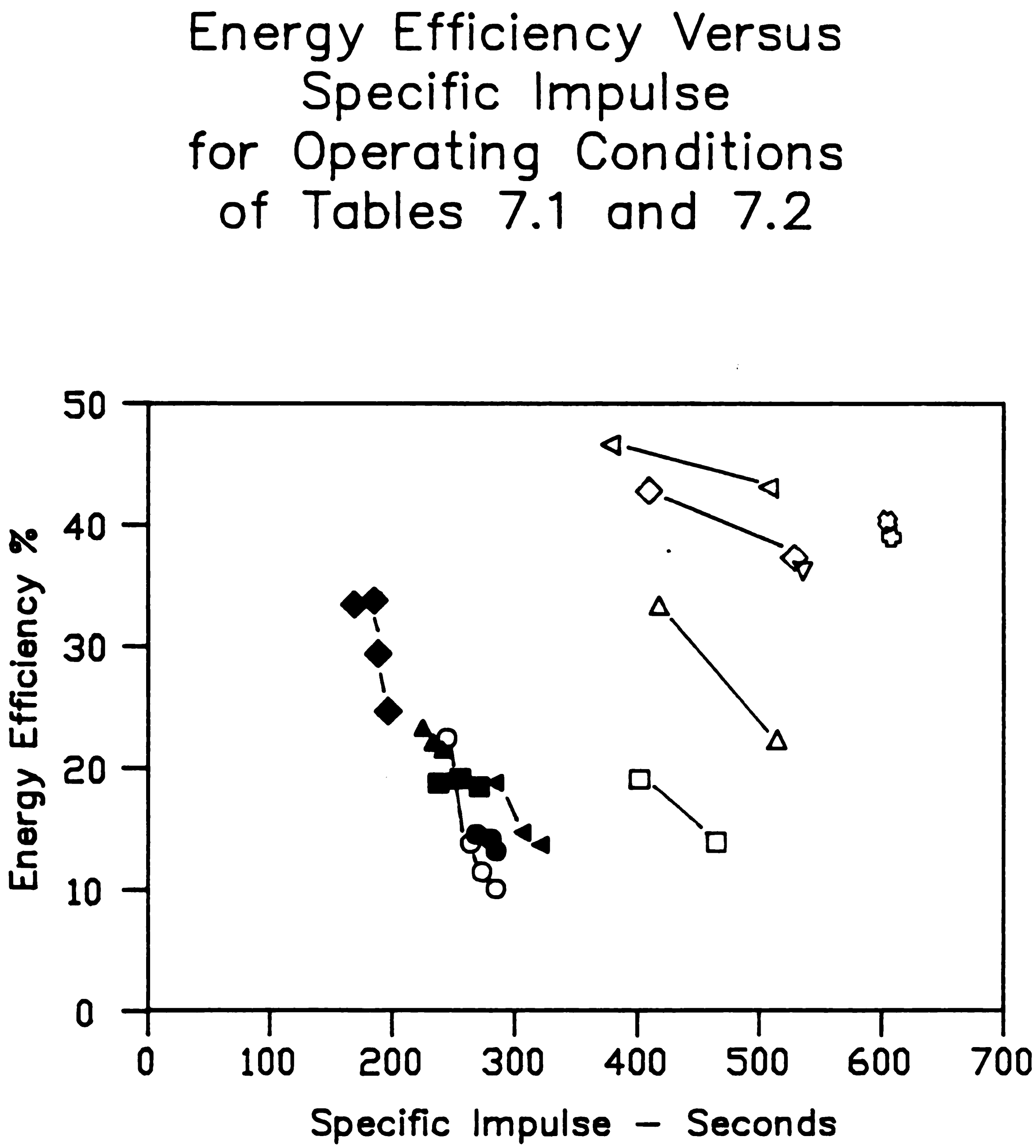

Figure 7.7 Energy Efficiency Versus Specific Impulse Comparison

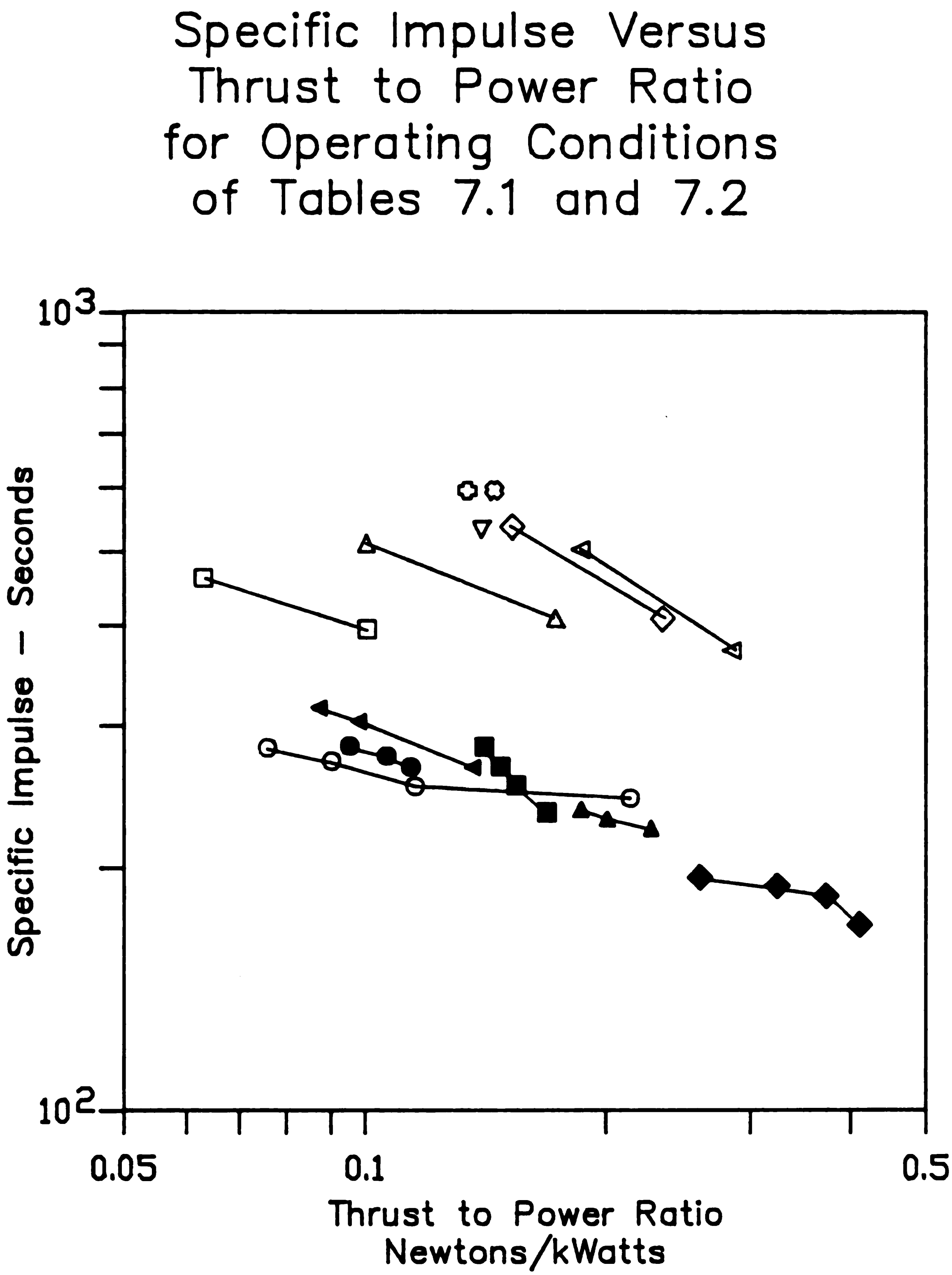

Figure 7.8 Specific Impulse Versus Thrust to Power Ratio Comparison

electromagnetic field pattern, the TM_{011} is half a TM_{012} mode. Further, from the discussion in section 3.5 on energy paths, the electromagnetic coupling into the discharge should be independent of the electromagnetic mode. The major difference between the two modes is the position of the discharge relative to the nozzle. This implies that the distance from the nozzle to the discharge is very important and the results of S. Nakanishi presented in Figures 7.3 and 7.4 confirm this. Further experiments need to be conducted that show what distance is optimal.

The experiments in nitrogen also showed the importance of gas flow paths around the discharge. The addition of a center body improved the operation and increased the performance of the thruster. Additional studies need to be done to determine the optimal flow path for the propellant. Nozzle melting limited all the experiments in the maximum power they could handle. Further experiments in helium with very small (0.51 mm) nozzles generated high specific impulse values but with very severe input power limitations. Nozzle designs that allow for very small nozzles for potential use with hydrogen are desirable. These nozzles need to be designed to withstand greater temperatures and chemical reaction problems associated with gases such as hydrogen.

CHAPTER VIII

EXPERIMENTS WITH METAL NOZZLE THRUSTERS

8.1 INTRODUCTION

The design and initial test of a revised version of the cavity thruster is described in this chapter. Specific revisions are; (1) the use of stainless steel nozzles, (2) quartz discharge chamber redesign, and (3) operation over a wider range of discharge pressure. The experimental measurements of thrust, specific impulse and energy efficiency for different gas flow rates in nitrogen and helium gas are presented. Measured performance is compared to the earlier cavity applicator based microwave electrothermal thrusters presented in Chapter 7. The experimental results in this chapter are described as initial because at the time this thesis is being written, these are the results that have been obtained. Further research with this thruster is planed at Michigan State University, and will be the subject of future papers.

8.2 EXPERIMENTAL SYSTEM

First the development of the applicator used in these tests is described. Next the basic experimental system used for these tests is described.

8.2.1 MICROWAVE APPLICATOR

The quartz nozzle of the thruster shown in Figure 7.1 limited the maximum specific impulse that could be obtained. A new design was built and tested using a metal nozzle and is shown in Figure 8.1. The numbering system of Figure 7.1 is continued with the changes noted. The shorting plate (3) is still fixed in position during operation but is designed so that it is removable, allowing different base plate, nozzle, flow and discharge chamber configurations to be tested. The discharge (4), which could be viewed through a brass screened window (5) is formed inside a quartz discharge chamber (6), in the center of the cavity. A combination base plate and advanced discharge chamber is showed attached to the base of the applicator. Gases enter through the base plate and distributed evenly by a gas flow system that helps to cool the nozzle and preheat the input gas. The nozzle itself has removable inserts allowing different high temperature materials to be placed in its throat.

Figure 8.2 shows the base plate system of the thruster shown in Figure 8.1 and continues the numbering system of this figure. Gases enter through the gas input port (16) and distributed evenly by a gas flow system (17) that helps to cool the nozzle and preheat the input gas. The gas is injected into the discharge chamber via a circle of small holes (18) and exits via the nozzle (13) and nozzle insert (15) after passing through the discharge zone (4). A large vacuum plate (21) attaches the applicator to the vacuum system. The vacuum plate is sealed to the discharge chamber by an O-ring (19) and the plate is kept cool by a water cooling channel (20).

The gas flow pattern is shown by the arrows in Figure 8.2. The

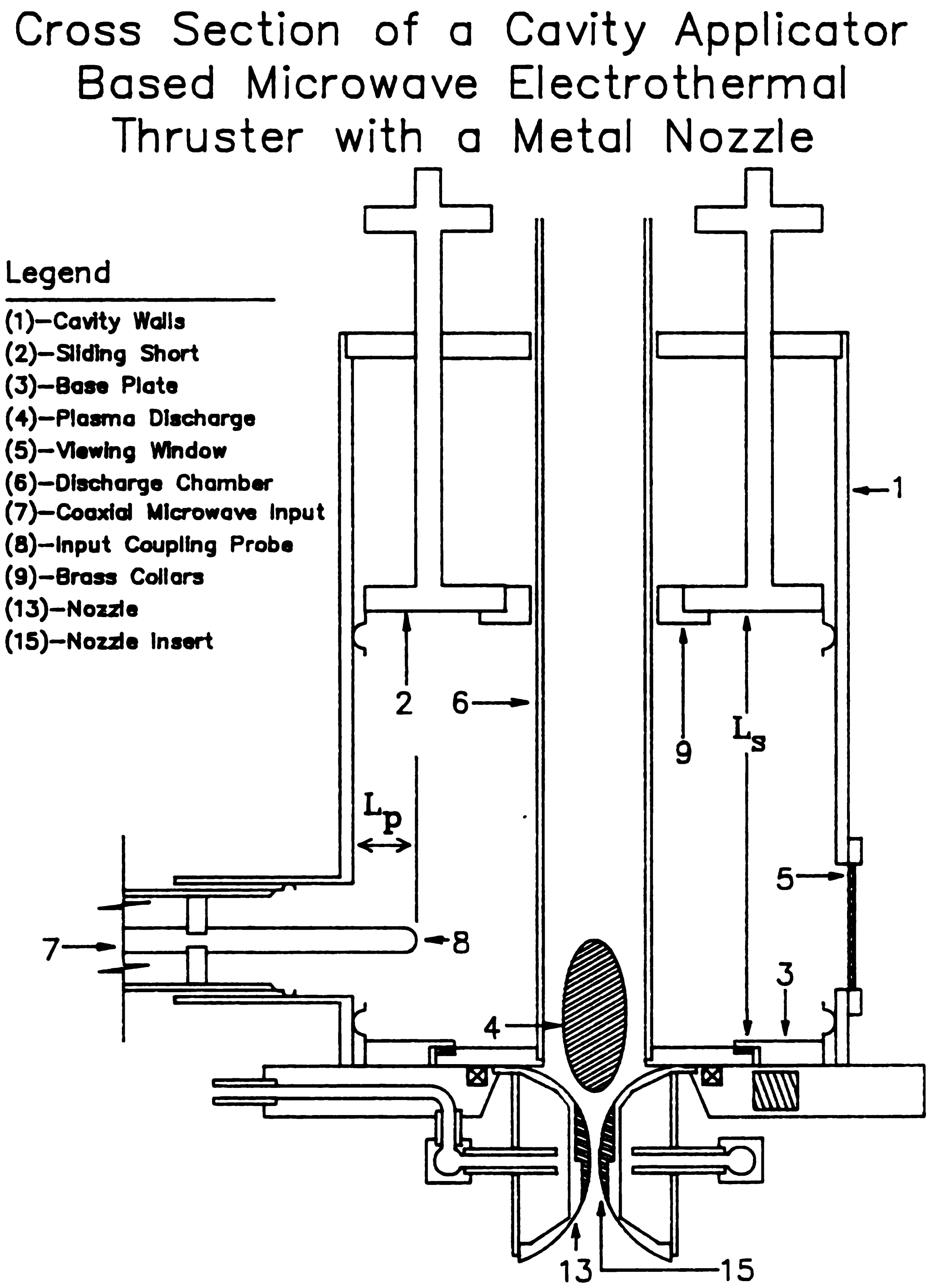

Figure 8.1 Cross Section of a Microwave Thruster with a Metal Nozzle

Cross Section of a Cavity Applicator Base Plate

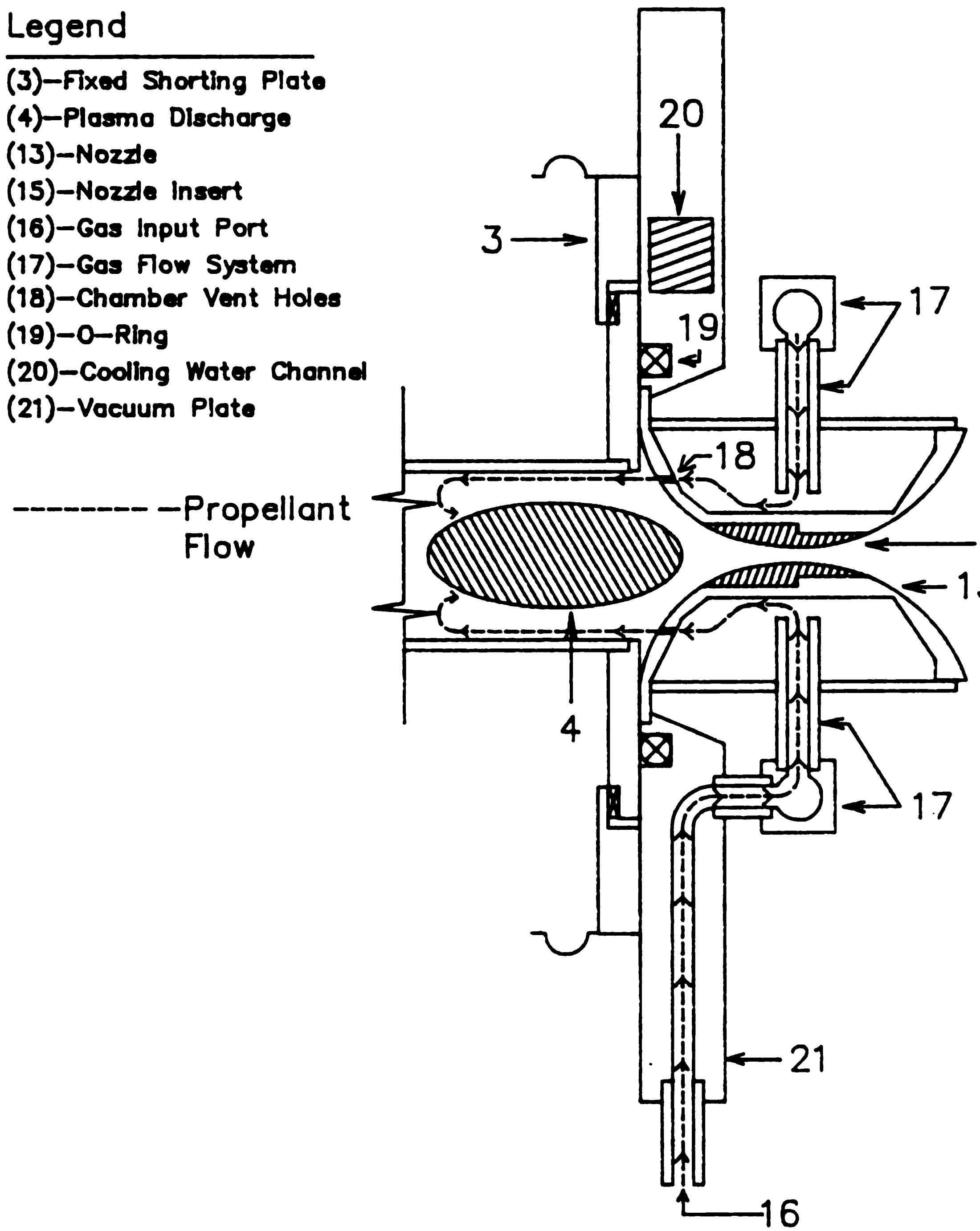

Figure 8.2 Enlargement of Cavity Base Plate

propellant passes through the flow system in the base plate of the applicator, and as shown the input gas flows over the outside of the nozzle to help keep the it cool. It then enters the discharge chamber through a ring of small holes at the base of the discharge chamber. The propellant then flows between the discharge and the chamber wall cooling the wall and also keeping the discharge from contacting the wall. The propellant then flows back, partially through the discharge and partially around it. The heated propellant is then exhausted through the nozzle which is pointed in an upward direction.

The discharge chamber (4) of the thruster shown in Figure 8.1 was constructed by epoxying a 25 mm i.d. cylindrical quartz tube onto a brass base plate. In low power test experiments, with the incident power limited to 500 Watts, the epoxy would melt limiting operation of the thruster. The discharge chamber in Figure 8.1 was replaced with the chamber (4) shown in Figure 8.3. This chamber was shaped like half a sphere and was of fused quartz construction.

Experiments with the thruster of Figure 8.3 were conducted with power levels of up to 1.5 kW in helium and nitrogen. However stability problems with the discharge formation gave very poor performance results. The discharge would not form in the center of the chamber as shown in Figure 8.3. Instead it formed near the walls and would move around the chamber in a random fashion. The discharge chamber configuration shown in Figure 8.4 was tested because of this problem with discharge stability. This discharge chamber was also a quartz hemisphere but it has a 25 mm i.d. cylindrical quartz tube extending from the top of the hemisphere. A 18 mm i.d. cylindrical quartz tube was added down the center to help stabilize the discharge. In addition

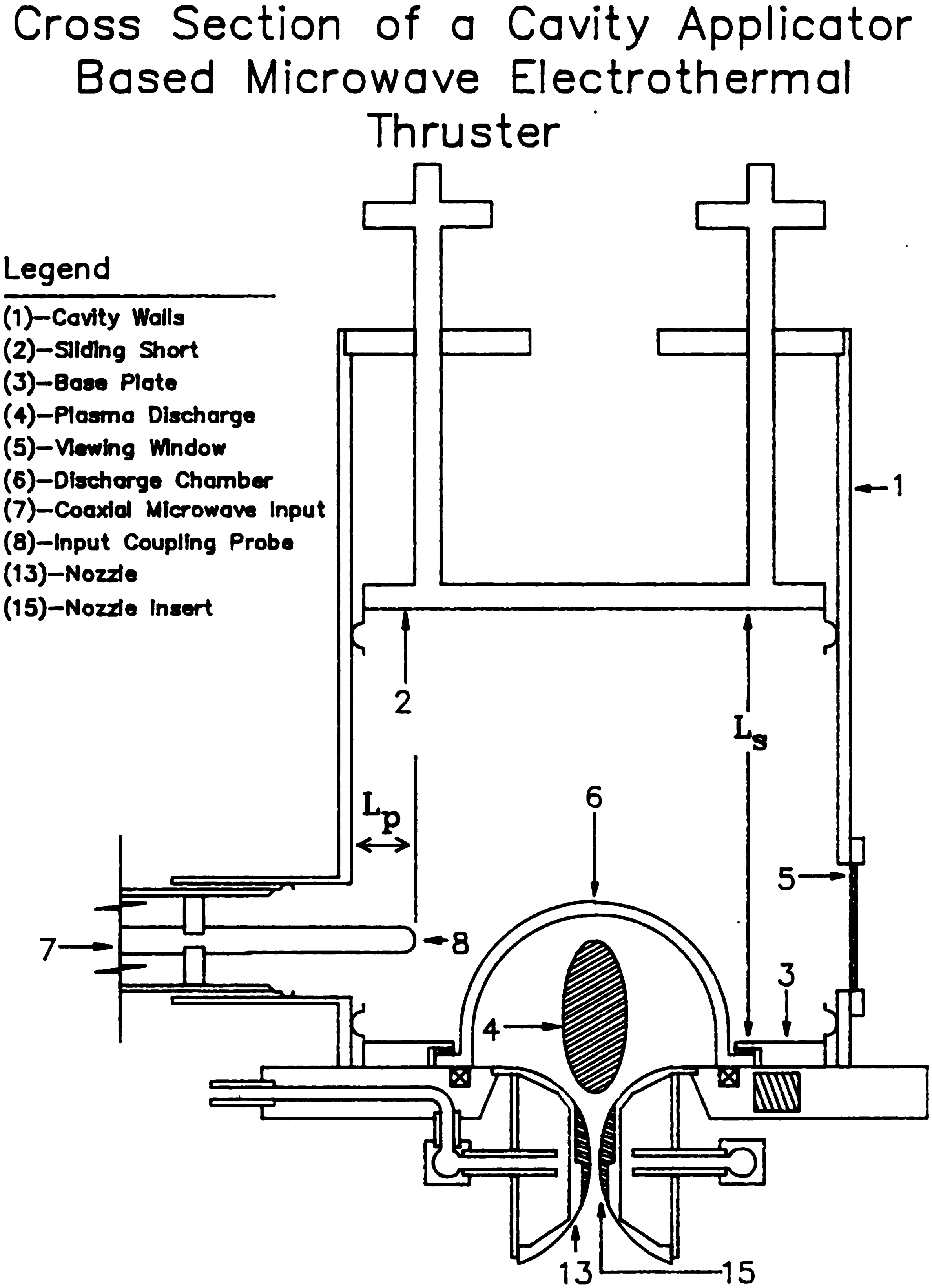

Figure 8.3 Microwave Thruster with a Spherical Discharge Chamber

Cross Section of a Cavity Applicator Based Microwave Electrothermal Thruster used in Experiments

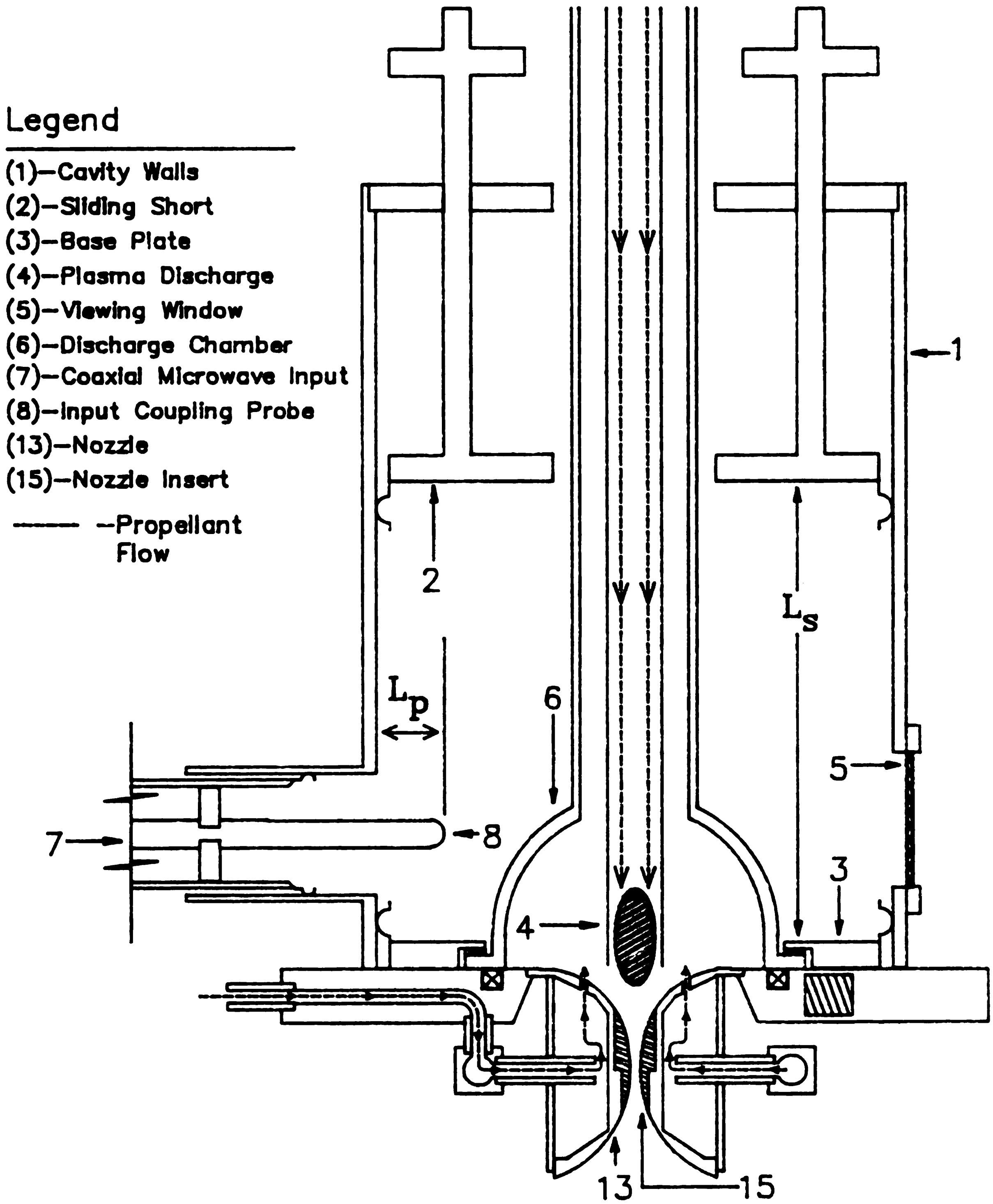

Figure 8.4 Microwave Thruster used for the Experiments in this Chapter

to the gas flow path through the base plate, there was gas flow down the center of the second quartz tube. This configuration produced excellent results using nitrogen but still had some stability problems in helium. Results for both gases are presented in section 8.3.

8.2.2 EXPERIMENTAL APPARATUS

The basic microwave power and measurement system used for these experiments was described in Chapter 4. The thruster measurements were performed with a continuous wave 2.45 GHz variable power (from 0 to 2500 Watts) microwave system. Experimental measurements were performed using nitrogen and helium gas as propellant, with flow rates of up to 31.3×10^{-6} kg/s.

The base of the energy absorption chamber was attached to a vacuum chamber that included a heat exchanger to cool the exhausted propellant. The pressure and gas flow rates were measured using the measurement system of Chapter 4. The measurements were performed with the applicator in a vertical position as shown in Figure 8.5. As shown in this figure the nozzle of the thruster was above the discharge. As mentioned in Chapter 7 for the experiments by S Nakanishi, it was felt that this orientation helped the operation of the thruster.

Measurement of hot and cold discharge chamber pressure for constant propellant flow rates were performed for different levels of input power, different propellant flow rates and variations in discharge chamber configuration. Using the rational of the indirect thrust measurement described in section 4.4.3, energy efficiency, specific impulse, thrust and thrust to power ratio were calculated using equations 2.1-2.5 and 4.6-4.9.

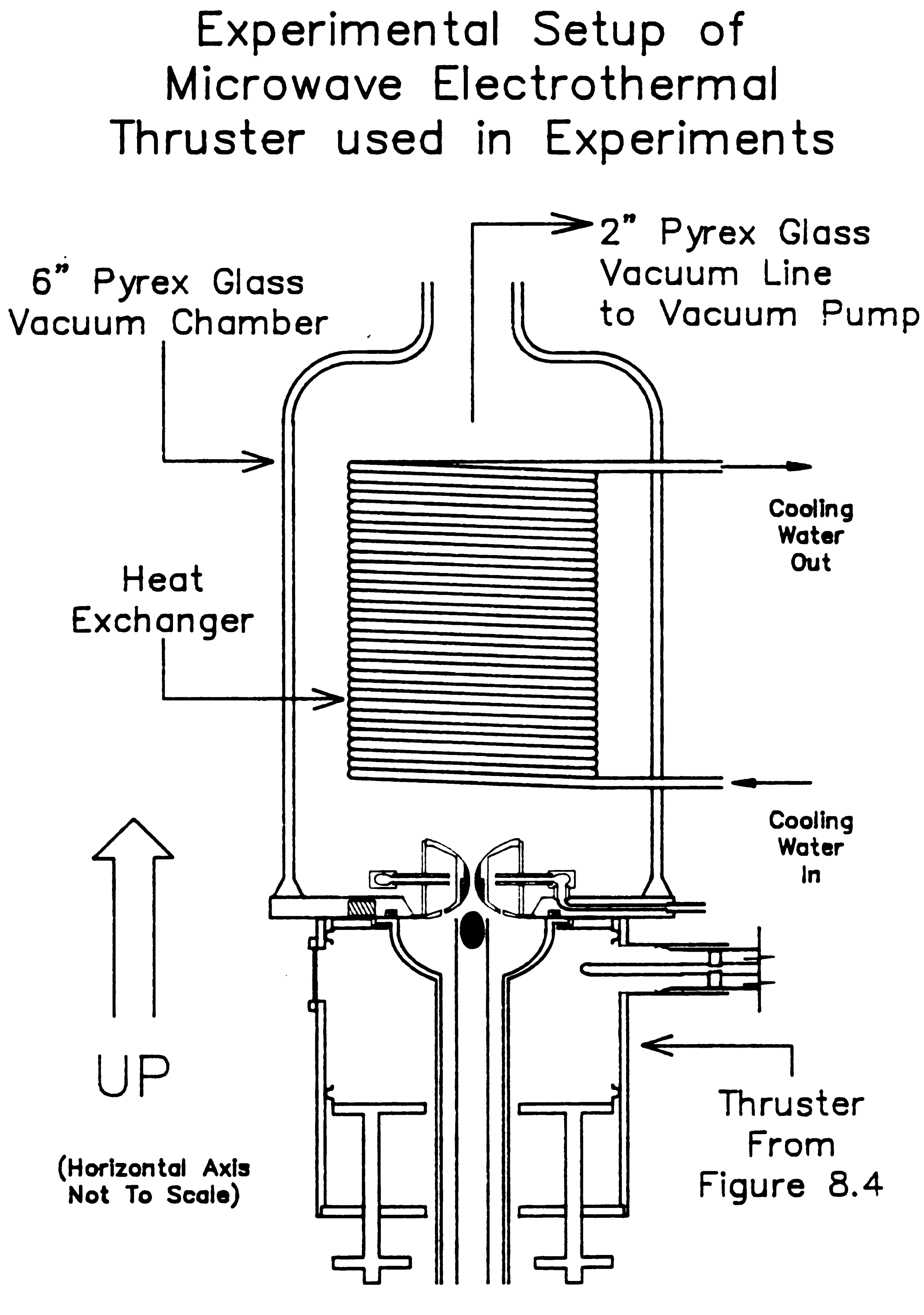

Figure 8.5 Experimental Setup of Microwave Thruster

8.3 EXPERIMENTAL RESULTS

Experimental runs were performed by first establishing a desired propellant flow rate and holding this flow rate constant throughout the entire run. The cold discharge chamber pressure, p_c, was measured. The discharge was started and the input microwave power was adjusted, and the applicator input power, P_t, and the steady state "hot" discharge pressure p_H were measured. After each experimental run, the discharge chamber was allowed to cool back to "cold" conditions as a check against significant nozzle erosion. As discussed in Chapter 5, microwave coupling efficiency is very high, thus P_t is approximately equal to the microwave power absorbed by the discharge, P_a, and thus the energy efficiency, the thrust to power ratio and the specific impulse can be calculated. Figures 8.6-8.8 summarize the experimental results where the legend in Table 8.1 details the different experimental configurations and operating points.

Figures 8.9-8.11 show these results compared to earlier results with quartz nozzles. The nozzle used in this test was very small and designed mainly for use with helium. This limited the maximum flow rate that nitrogen could be tested at to 31.1×10^{-6} kg/s since higher flow rates produced a discharge chamber pressure that was to great. As can be seen in the figures the results for nitrogen are very good if the low gas flow is taken into account. Results for helium are not as good as earlier result with the quartz nozzles. This is due to the instability of the helium discharge inside the discharge chamber. Nozzle erosion or melting was not observed during the $\geq$1 hr. of experimental operation.

Table 8.1 Operating Conditions for Experiments Presented in Chapter 8

Operating Conditions for Experiments with the Microwave Thruster of Figure 8.4

#	Point	Flow Rate (kg/sX10^{-6})	Discharge Pressure (Torr)	Cavity Mode	Nozzle Size	Dual Flow	L_s cm	L_p cm
1.	⧗	10.4	212–247	TM_{011}	0.35mm	yes	6.85	1.1
2.	●	20.8	645–690	TM_{011}	0.35mm	yes	7.25	1.8
3.	▲	31.3	1115–1147	TM_{011}	0.35mm	yes	7.25	1.8
4.	⧖	8.9	382–465	TM_{011}	0.35mm	yes	7.0	1.85
5.	○	14.8	787–872	TM_{011}	0.35mm	yes	6.9	1.92
6.	△	17.8	1040–1080	TM_{011}	0.35mm	yes	6.9	1.92

Solid Points – Nitrogen Propellant

Open Points – Helium Propellant

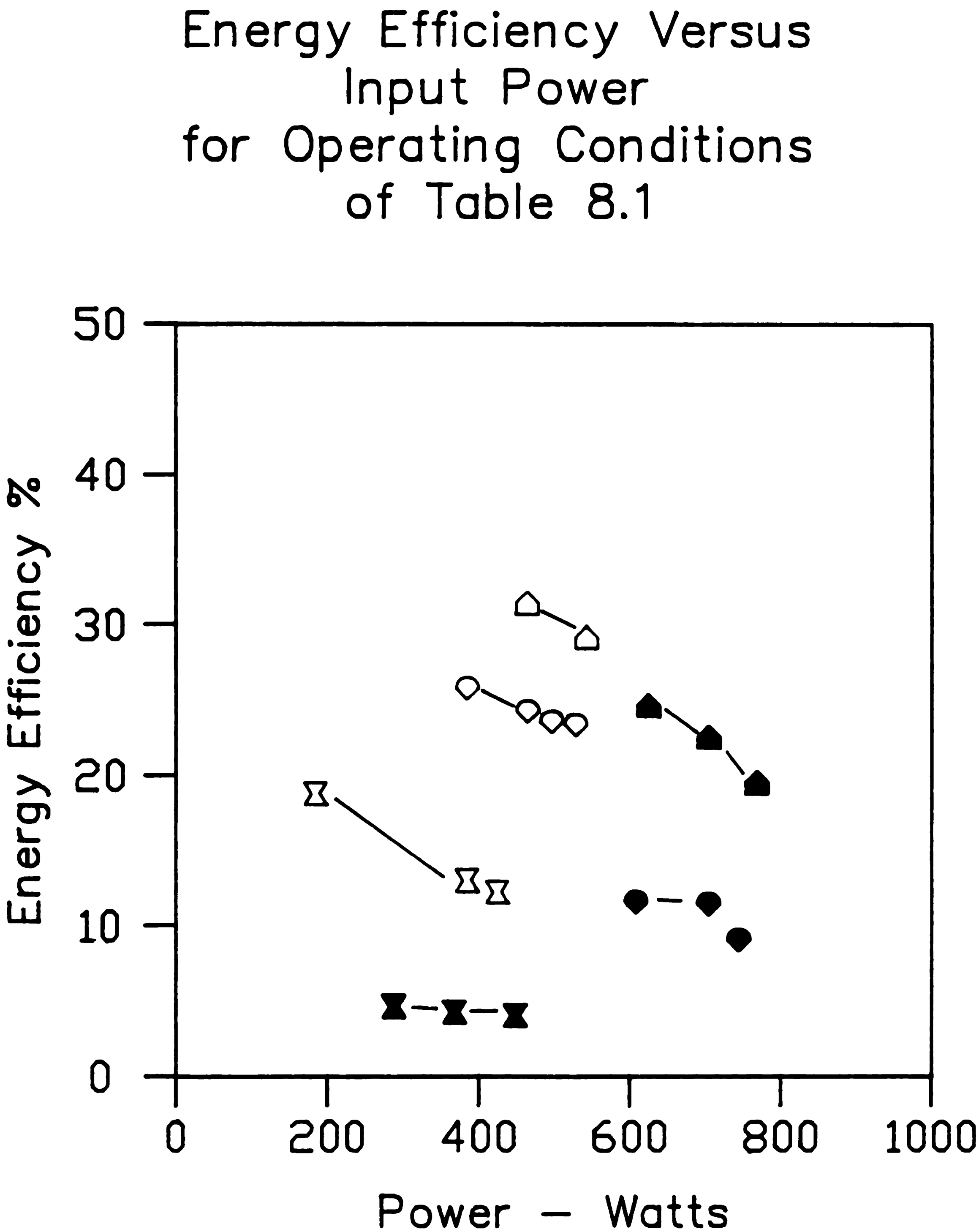

Figure 8.6 Input Power Versus Specific Impulse

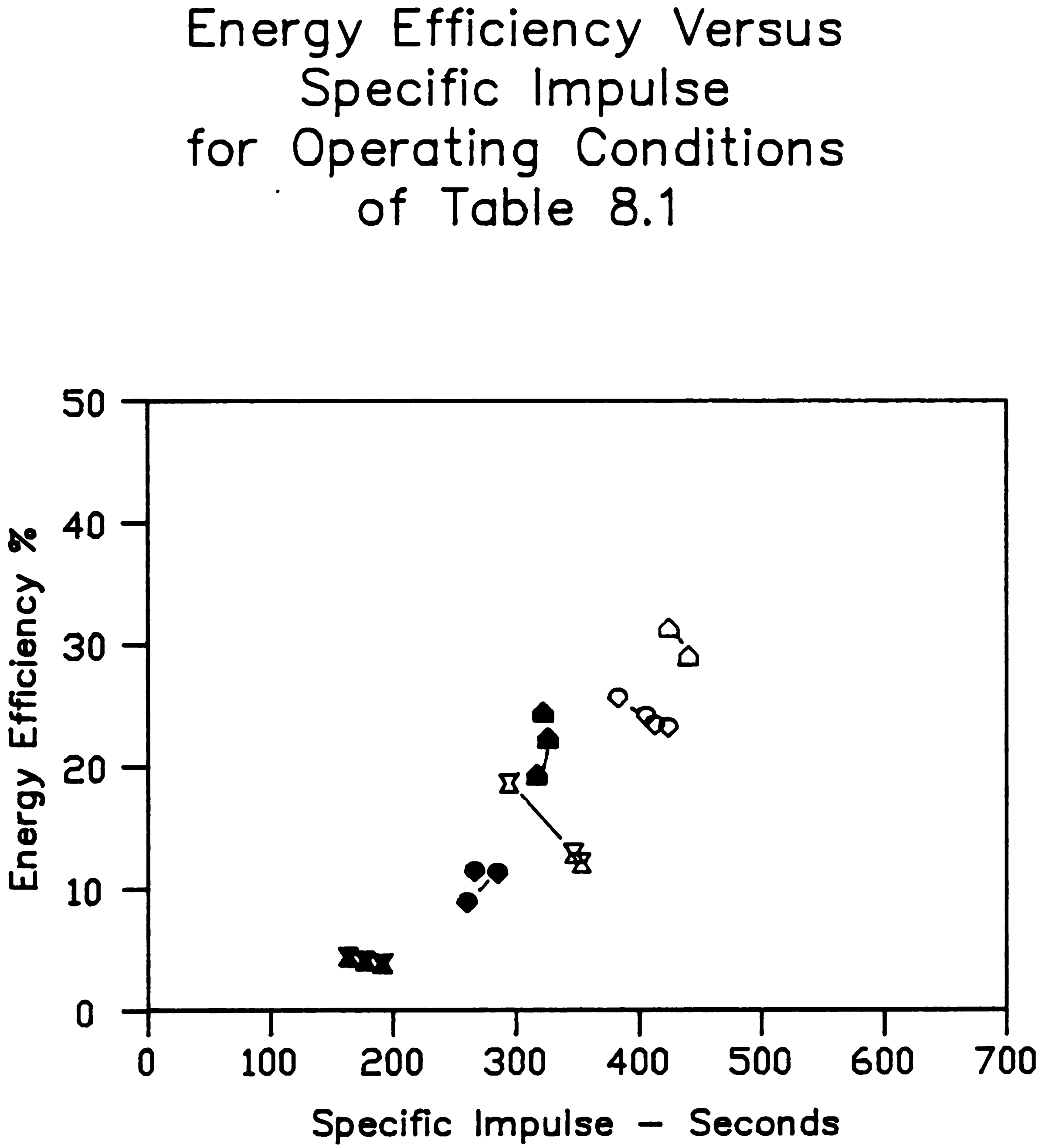

Figure 8.7 Energy Efficiency Versus Specific Impulse

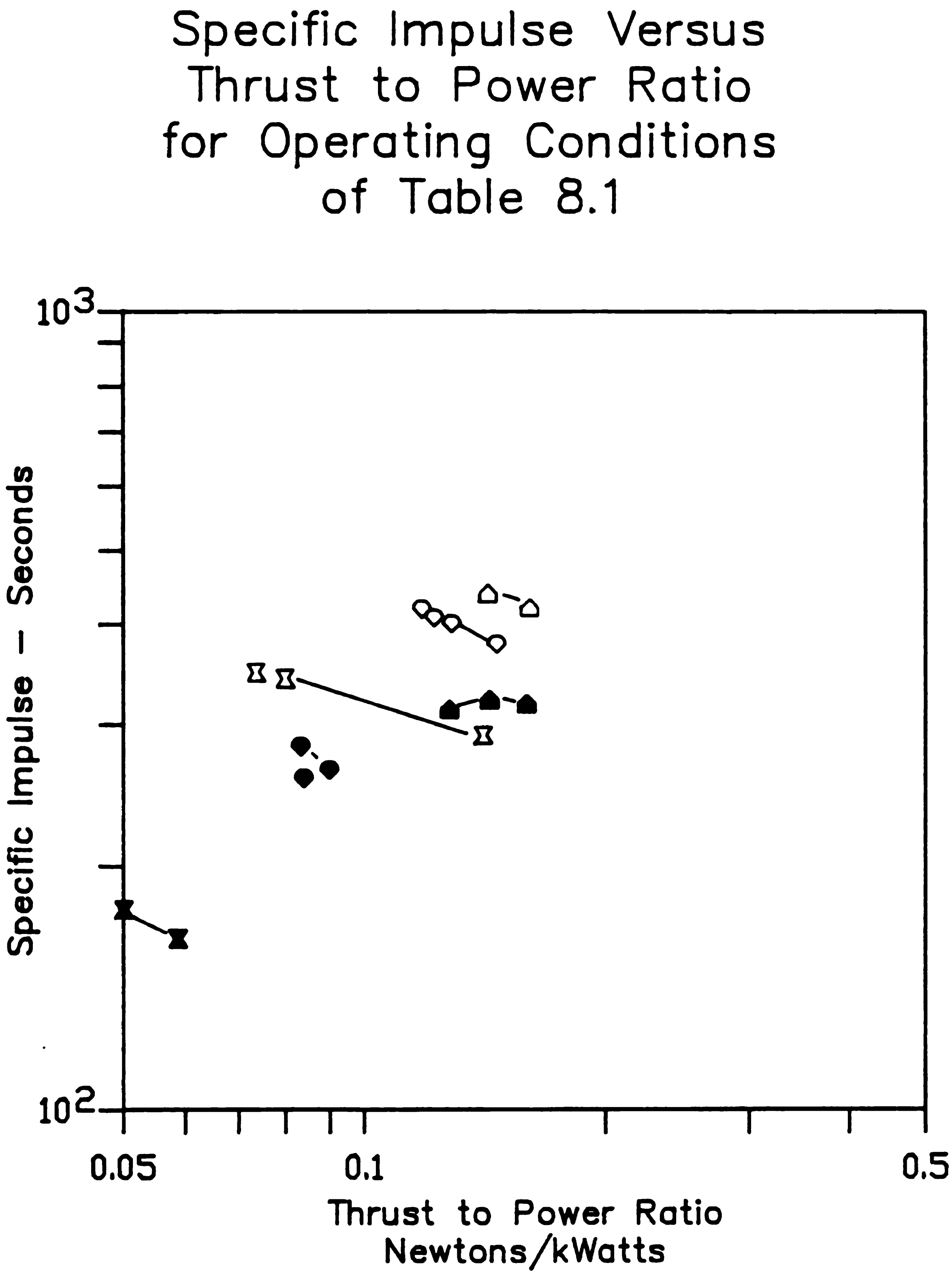

Figure 8.8 Specific Impulse Versus Thrust to Power Ratio

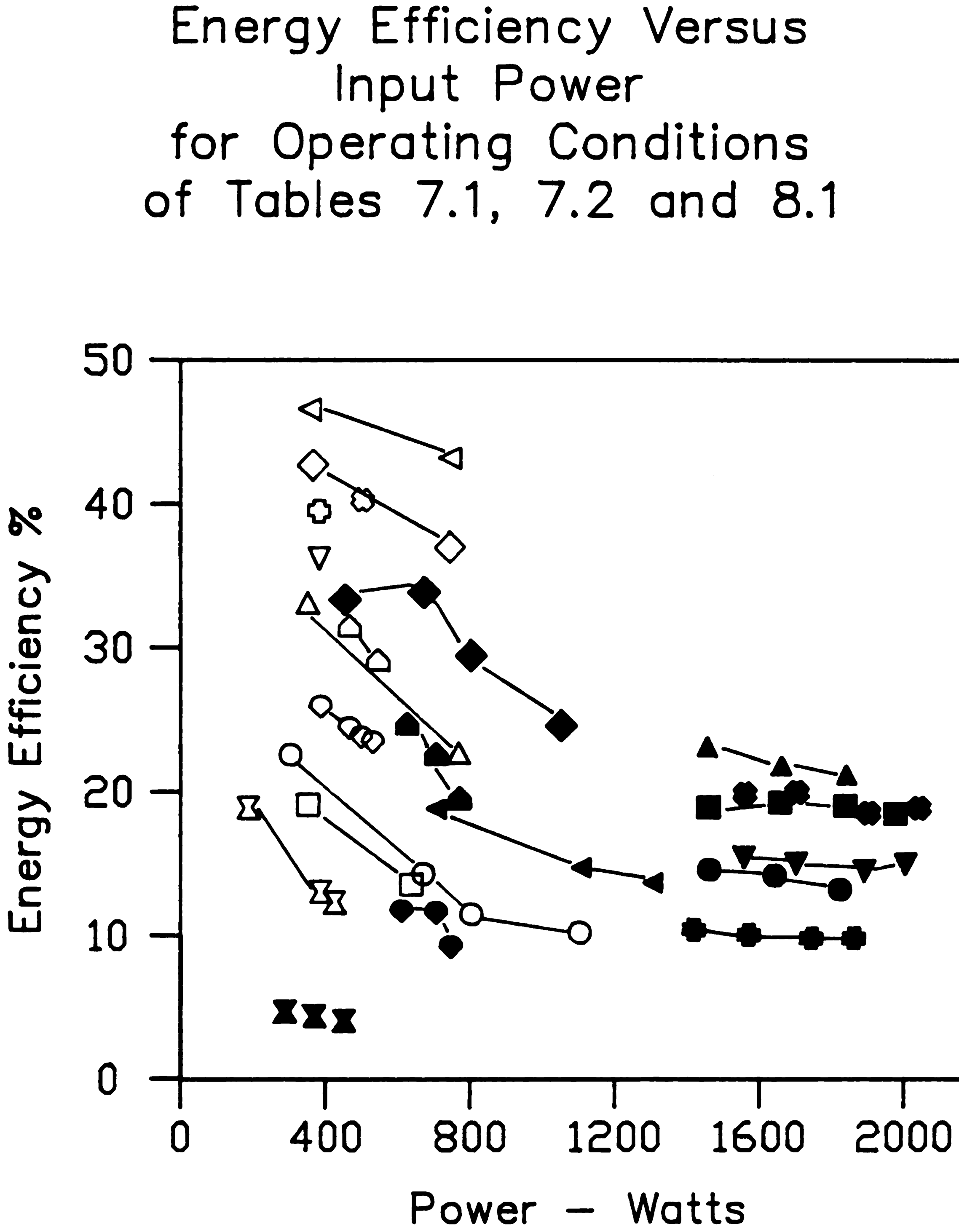

Figure 8.9 Energy Efficiency Versus Input Power Comparison

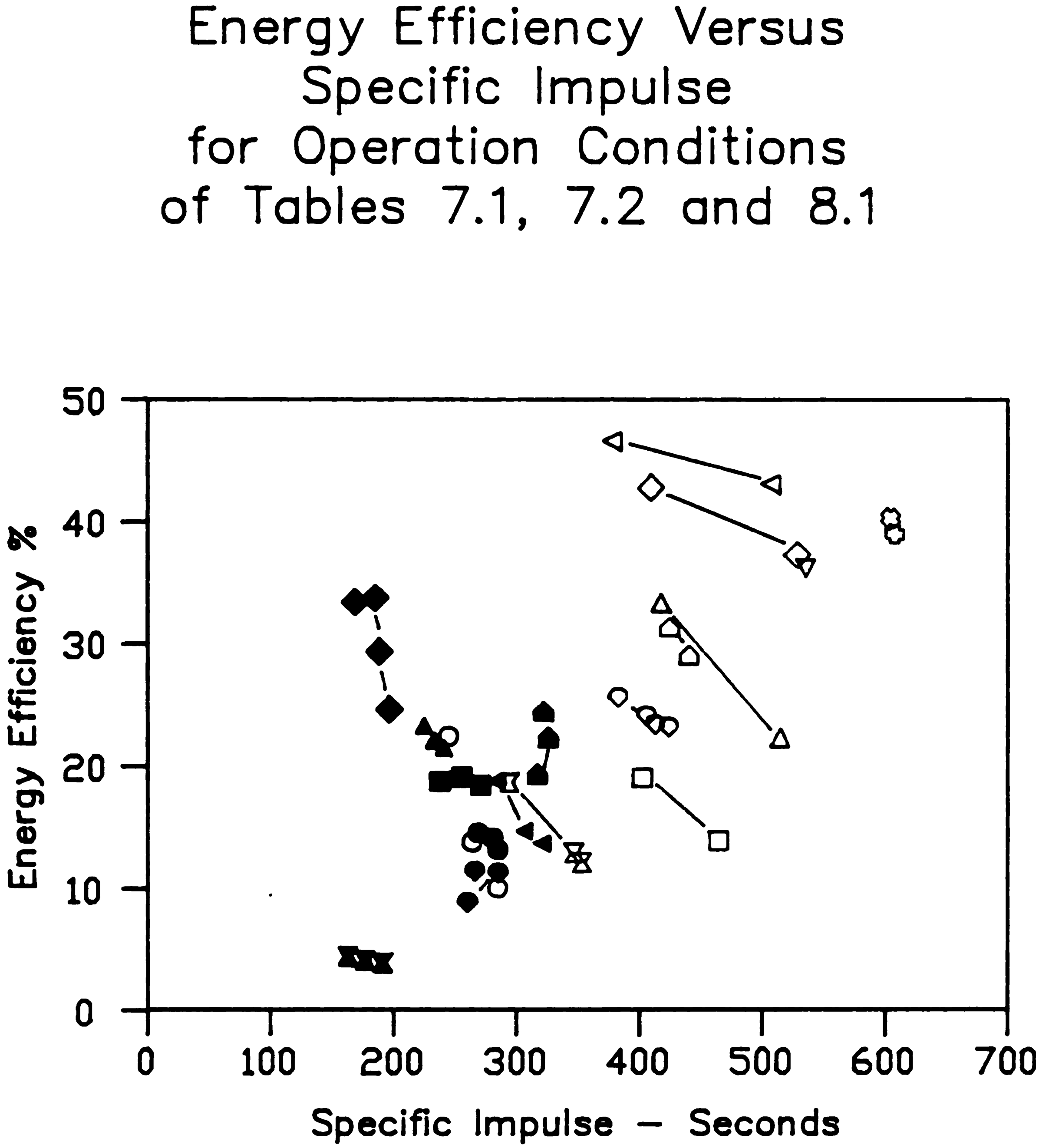

Figure 8.10 Energy Efficiency Versus Specific Impulse Comparison

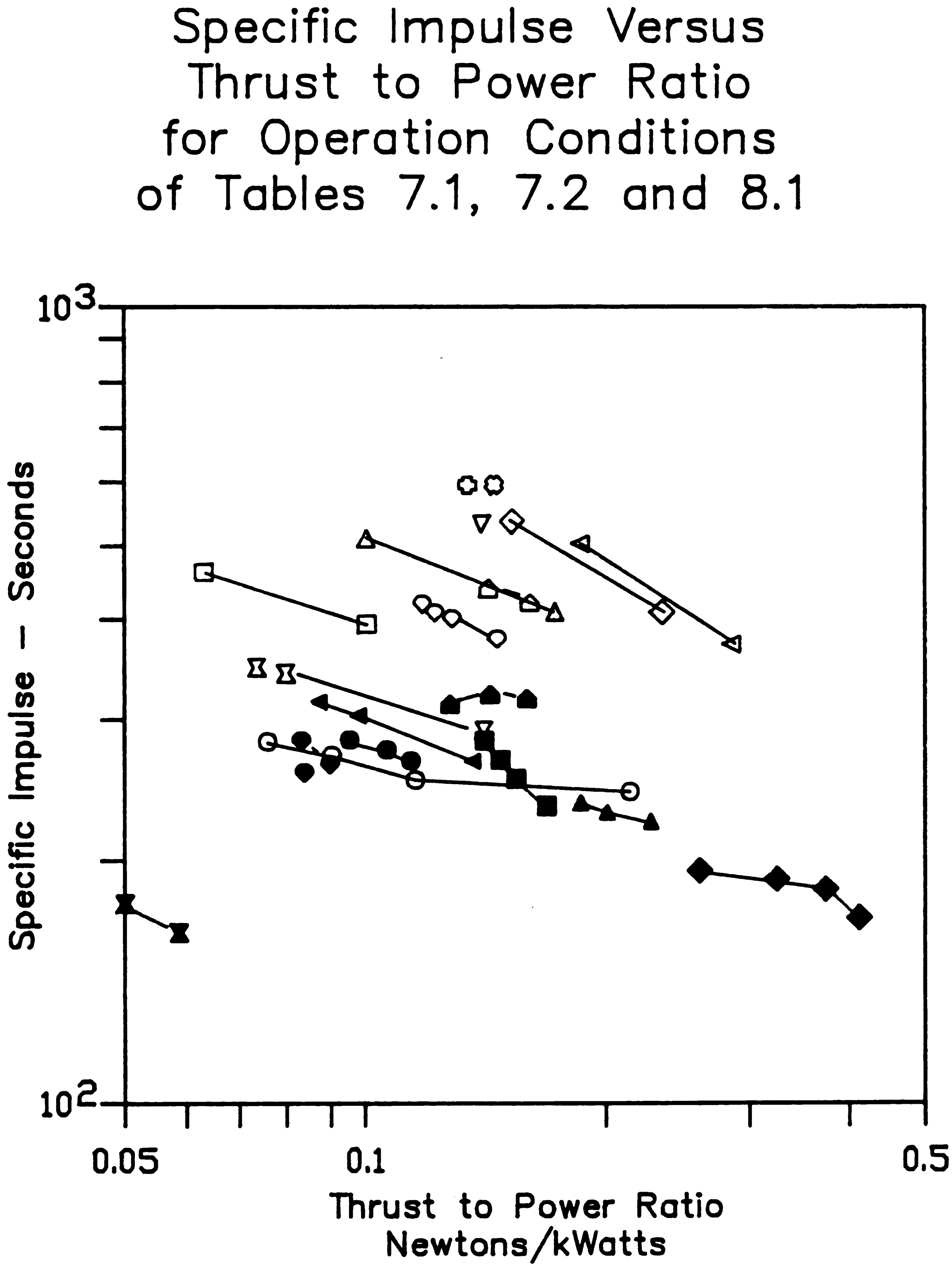

Figure 8.11 Specific Impulse Versus Thrust to Power Ratio Comparison

8.4 DISCUSSION OF RESULTS

The thruster had excellent results in nitrogen at very low flow rates compared to earlier experiments with nitrogen at higher flow rates using quartz nozzles. Further, unlike earlier experiments with nitrogen in a TM_{011} mode using a quartz nozzle, there was no observed nozzle melting. The use of the metal nozzle eliminated all problems with nozzle erosion for these initial experiments.

The results with helium were not so good. While the nozzle melting problem was solved by the use of metal nozzles, the helium discharges could not be formed in the optimal position for the best energy transfer to the propellant gas. Further experiments are needed to study this and to design a new internal flow system and discharge chamber that can control the position of the discharge for optimum energy transfer to the propellant.

CHAPTER IX

CONCLUSIONS

9.1 SUMMARY OF RESULTS

Initial experiments demonstrated the ability to generate microwave discharges at atmospheric pressure in He, N_2 and O_2 gases. These discharges were stable from 40 to 1000 Torr in pressure with a input microwave power of 500 Watts. Coupling efficiency of microwave power into the discharge was measured to be in excess of 95% over a pressure range of 40 to 760 Torr. As pressure increased, the discharges were observed to contract from the chamber walls forming intense small volume discharges with high power densities. Different diameter discharge chambers were tested to check their effect on discharge properties. Chamber wall-discharge interactions were found to have a great effect on discharge properties. The experiments demonstrated the basic components necessary to produce a working microwave electrothermal thruster.

The experiments have demonstrated a working microwave electrothermal thruster thus proving that the concept works. Two different microwave design concepts were employed to produce a working electrothermal thruster. The first of these devices utilized a coaxial microwave discharge to heat the propellant. This device operated at a microwave frequency of 2.45 GHz in a TEM mode and was tested in a power range from 200 to 600 Watts. Experimental measurement of thrust, specific impulse and energy efficiency were taken for nitrogen gas with flow rates up to 10.6×10^{-6} kg/s. Measured thruster energy efficiency varied between 30% to 60%.

The second of these devices employed a cylindrical cavity microwave discharge to heat the propellant. This device operated at a microwave frequency of 2.45 GHz in a TM_{012} cylindrical cavity mode in power ranges from 1400 to 2000 W. Experimental measurement of thrust, specific impulse and energy efficiency were taken for nitrogen gas with flow rates of up to 146×10^{-6} kg/s resulting in measured thruster energy efficiencies between 10 to 25% and specific impulse of up to 280 sec. Experiments with helium gas operating in the TM_{011} mode resulted in energy efficiencies of up to 50% and specific impulse of 200-600 sec.

These measured energy efficiencies and specific impulses compared favorably with other electrothermal thrusters such as the resistojet and arcjet. However, both of these devices were designed to demonstrate the basic concept of a microwave electrothermal thruster and were, therefore, kept simple in design and were not optimized. For example, the quartz nozzle used in all of these experiments limited the maximum specific impulse due to melting failure of the quartz. Forced air cooling of the discharge chamber was also employed during all experiments resulting in reduced efficiencies due to increased energy losses.

A new cavity applicator configuration was designed and tested. This new design incorporated a metal nozzle with regenerative cooling in a removable base plate. Experiments with this new thruster design produced very good results in nitrogen although discharge stability problems limited results in helium. The stainless steel nozzle showed no signs of erosion or melting. If the problems with discharge stability can be solved, it is expected the performance will improve over the results of earlier designs.

9.2 CONCLUSIONS

These experiments demonstrated how to generate a high pressure microwave discharge under flow and no flow conditions without melting the enclosing walls. Experiments with no gas flow demonstrated that the coupling of microwave power into the discharge is a very efficient process. Plasma volume was measured during these experiments and the discharge power density was determined versus pressure for He, N_2 and O_2.

This experimental work demonstrated that the microwave electrothermal concept is technically feasible and the measured performance compares favorably with other electrothermal propulsion concepts. However, many questions remain about its use in a real space application, but no major problem were discovered during this research.

9.3 RECOMMENDATIONS

In experiments in this thesis measurements with hydrogen as a propellant were never tried for safety reasons. Most electrothermal thrusters are tested in hydrogen since it has the highest cold specific impulse of any gas. The experiments with the cylindrical cavity and coaxial applicators presented in this thesis, should be repeated using hydrogen gas. The values of energy efficiency and specific impulse can be then be compared to other electrothermal thrusters using hydrogen. Further, these experiments will have the benefit of demonstrating and improving the understanding of hydrogen gas discharges at microwave works and would provide some direction in the development of new thrusters. If developed well enough, a working model of the thruster could be developed and the maximum performance that could be obtained could be calculated.

To help develop these models measurements of fundamental microwave discharge properties need to be conducted. Spectroscopic measurements would give the values of electron temperature and gas temperature inside the discharge. Identification of the constituent species present in the discharge would also be of value along with their distribution in the discharge. Energy balance measurements would serve would serve to develop a understanding of energy paths that exist in the discharge.

The total microwave thruster system needs to be studied. This includes not just the microwave electrothermal thruster, but all the other system components that are required for it to operate a thruster such as the microwave supply system and the propellant supply system. Factors such as total system cost, weight, lifetime, etc. need to be studied. For any real space applications these factors need to be compared to those of other thruster concepts to get a good understanding of which concept is best.

APPENDIX A

APPENDIX A

MICROWAVE FREQUENCY COMBUSTION FLAME INTERACTION

A.1 INTRODUCTION

A review of previous experiments studying the interaction between a high frequency electromagnetic field and a combustion flame is presented in section A.2 of this appendix. Experiments studying the interaction between a combustion flame and the electromagnetic field of a microwave cavity operated in a single mode, are presented in section A.3.

Combustion flames are of great importance to world energy production. Almost all transportation and energy production in the world derives its energy from combustion flames. In chemical production, combustion flames directly produce chemicals or produce the energy required for their production. In homes combustion flames provide energy for heating and cooking, and in industry combustion flames are used in processes such as welding, heat treating, etc..

Because combustion flames are used so extensively, any method to improve their performance is desirable. It is possible that by adding a high frequency electromagnetic field to a combustion flame, its operation could be improved in a beneficial manner. If the efficiency could be increased, the pollution be reduced or other useful benefits be found from these interactions, this research would prove to be of great value.

As an example of one potential benefit, the use of microwaves to assist combustion in an internal combustion engine is detailed by Ward[82] and, Ward and Wu[83]. In order to reduce pollution in an internal combustion engine a leaner fuel/air mixture can be used. However, this results in a lower flame speed which results in lower efficiency. It is suggested in the first paper that microwave energy could be used to increase the flame speed, thereby increasing efficiency. The second paper presents a theoretical model that indicates this may be possible. One factor in favor of this conclusion is the greater number of electrons present in a hydrocarbon flame a microwave field could interact with. An electron density of 10^{11} electrons/cm^3 is stated in the paper for lean hydrocarbon flames while for H_2 and CO a figure of 10^6 electrons/cm^3 is given.

The exact definition of a flame is rather vague, but for this appendix a flame can be considered a highly exothermic reaction between gases. It is also useful to define some other terms.[84,85]

Diffusion flames: In a diffusion flame the flame occurs at the boundary between the two gases. The rate and manner in which they diffuse together controls the direction and rate of propagation of the flame front. This is shown in Figure A.1a.

Premixed flames: In a premixed flame the two gases are mixed before being burned. A term called flame velocity can be defined as the rate the flames moves through the premixed gases. This is shown in Figure A.1b.

Flame Plasma: The flame plasma is the plasma or region of peak ion/electron interaction that exists in the reaction zone of a flame.

As shown in Figure A.2, a flame can be divided into several zones.

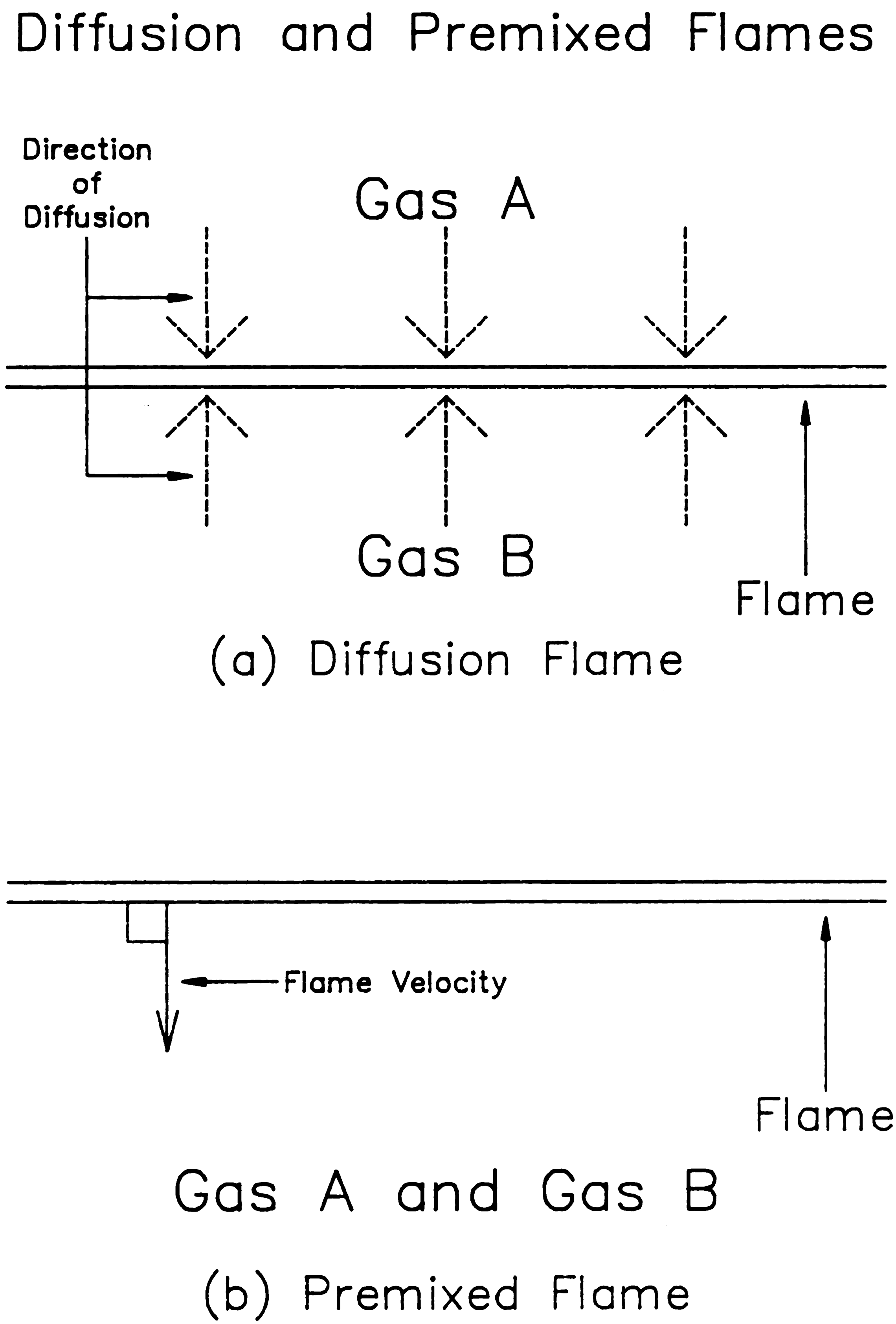

Figure A.1 Diffusion and Premixed Flames

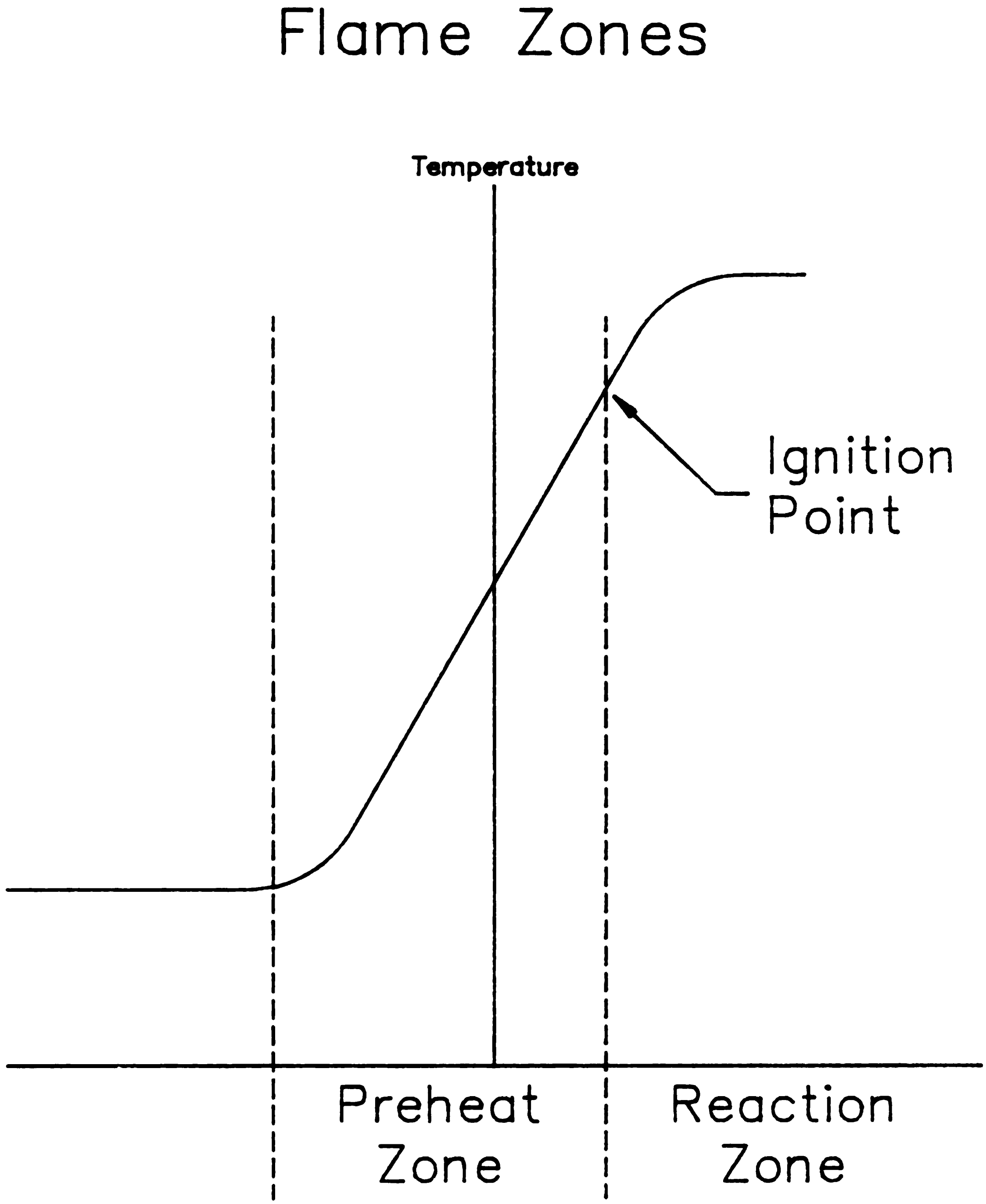

Figure A.2 Flame Zones

In the preheat zone heat from the chemical reaction heats the gases entering into the region in which the chemical reaction is taking place. The ignition point is the point where the combustion starts. The reaction zone is the region in which most of the combustion takes place. Many radicals, ions and electrons are present here.

For example, in a hydrogen-oxygen flame above 600 C some of the radical reactions present in the reaction zone are:[86]

$$H + OH + M > H_2O + M$$

$$H + H + M <> H_2 + M$$

$$O + O + M <> O_2 + M$$

A.2 EXPERIMENTAL REVIEW

Figure A.3 shows an experimental set up used by Jaggers and Von Engel.[87] As shown it consisted of a vertical convection free tube which was evacuated, then filled with premixed gases. A flame was ignited at the top of the column and allowed to propagate down the column. Two diodes placed a known distance apart were used to measure the time it takes for the flame to travel between the diodes. The flame velocity was then calculated from this data. A transverse electric field could be set up by applying a voltage between the two 90 cm long aluminum rods fitted to the inside wall of the tube. These remained in position throughout the experiment to retain the uniformity whether or not the electric field was used.

Initially town gas (55% H_2, 20% CO, 20% methane and 5% N_2) was used as fuel and mixed with air. No measurable change in flame velocity was observed when an electric field of up to 1kV/cm in a dc or 50 Hz

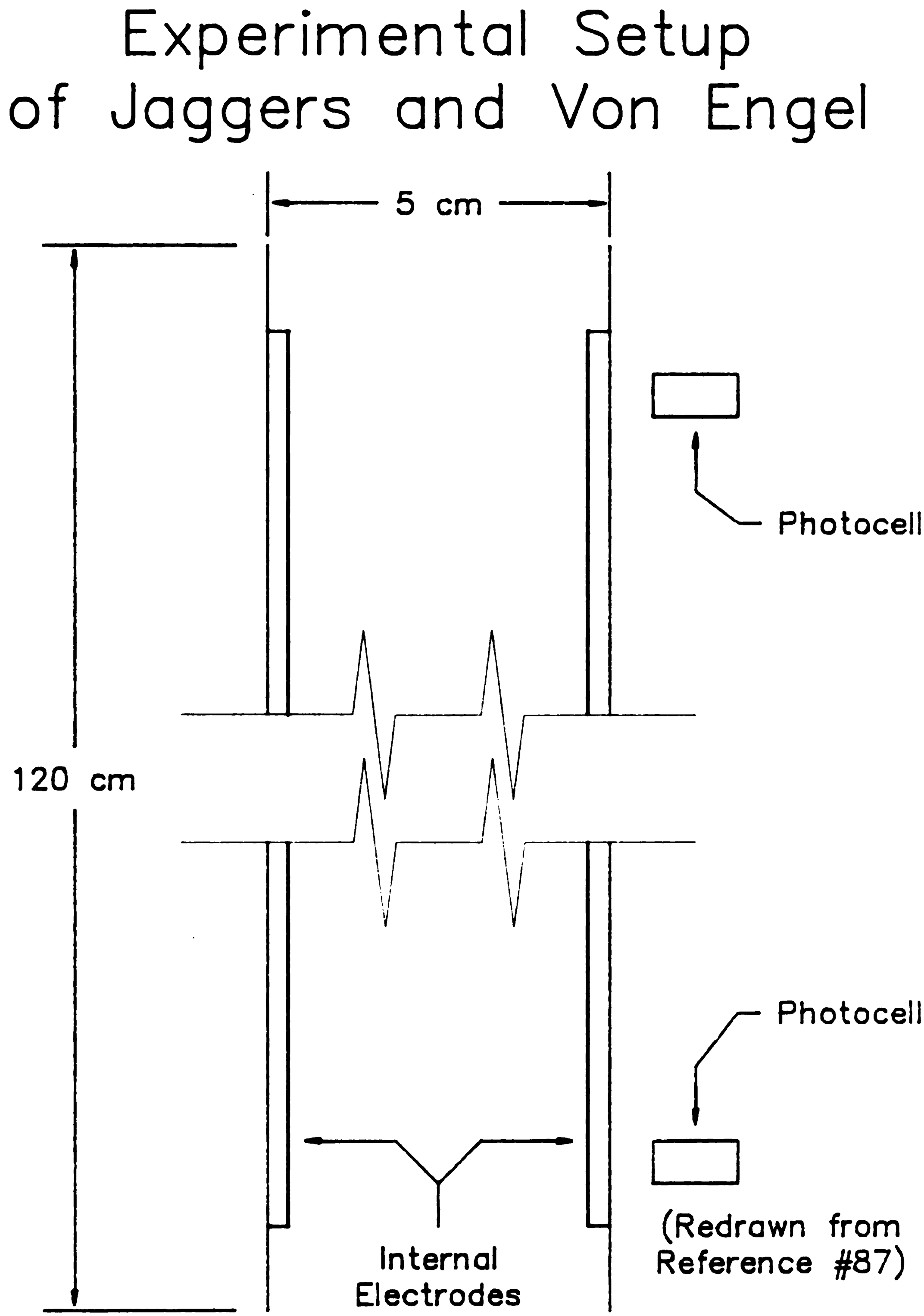

Figure A.3 Experimental Setup of Jaggers and Von Engel electric field was applied. Several reasons were given for the lack increase in flame speed. Two of these were non-uniform mixing and lack of hydrocarbons present in the mixture.

For hydrocarbon flames the results were better. For a 10% methane-air mixture in an electric field of 440 V/cm at 5 MHz, a 10 cm/s increase in flame velocity was observed over the no field case. A definite increase was observed for methane-air mixtures of 7.5% to 11.5%. For a 5% ethylene-air mixture in a electric field of 440 V/cm at 5 MHz an increase of 50 cm/s was observed over the no field case. For ethylene/air mixtures between 4.2% and 5.4% a large increase in flame speed was observed and for mixtures up to 6.5% a smaller increase was still observed.

Figure A.4 shows a second experimental setup that was tested using a floating flame. A long 5 cm diameter tube served as the flame apparatus. A premixed gas flow was passed up through the Pyrex tube. By adjusting the velocity of the gas the flame could be held stationary in the glass tube.

When the electric field was added the flame would move down an amount z. For both methane and ethylene there was a measurable change in z in the presence of an electric field. This change reached a maximum of 1 mm for methane with an electric field strength of 800 V/cm rms at 7 MHz.

Jaggers and Von Engel felt that the main effect the electric field had on the flame was to change the properties of the electrons in the flame front. Assuming all the current flows through the flame reaction zone, the electron density can be determined by the current flow assuming the flame front is uniform. This gives a electron density of

Floating Flame Apparatus of Jaggers and Von Engel

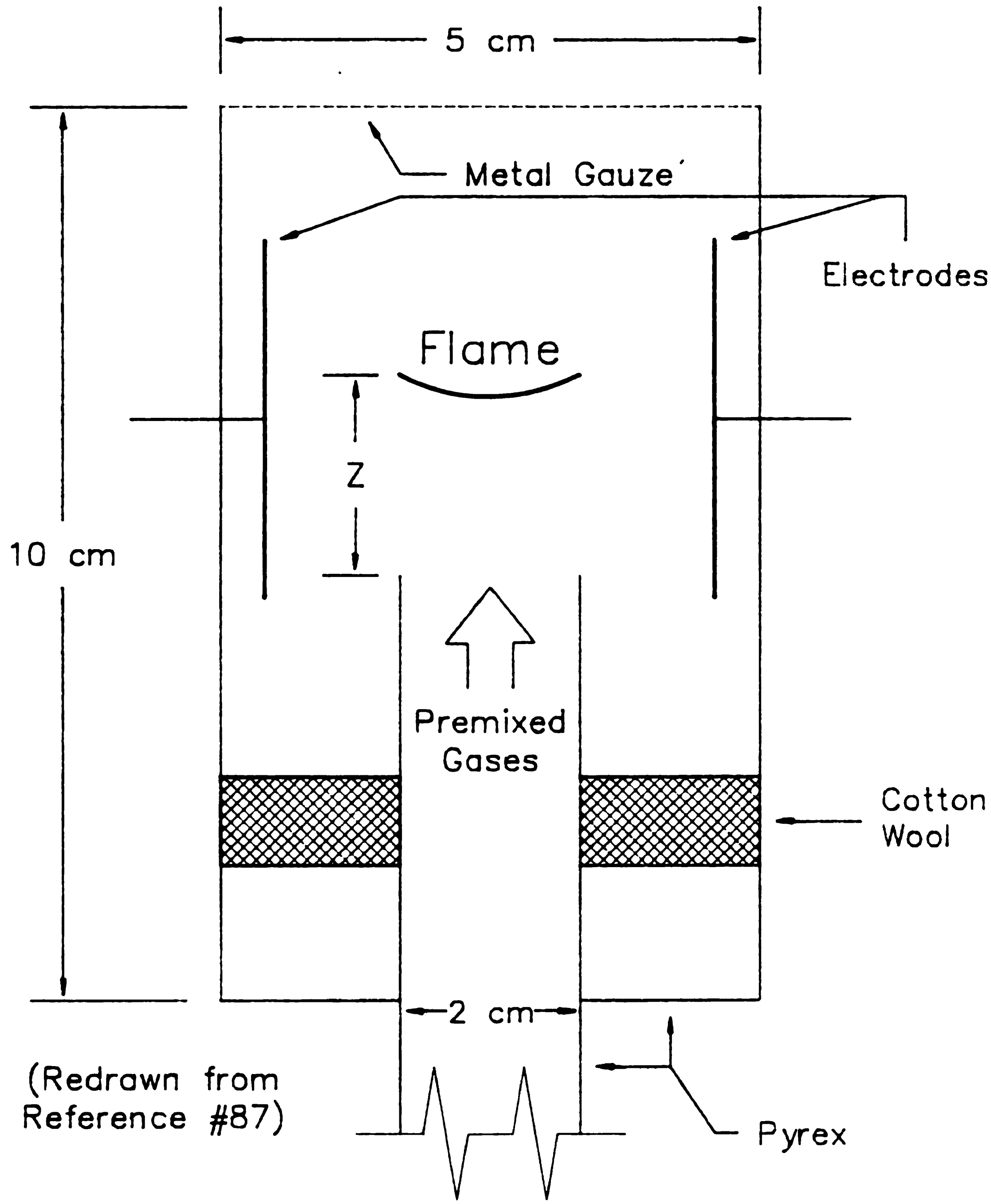

Figure A.4 Floating Flame Apparatus of Jaggers and Von Engel

$10^{11}/cm^3$ for ethylene and $5x10^{10}/cm^3$ for methane.

Jaggers and Von Engel give a value of 10,000 Watts for the energy of the chemical reaction. Since the electrical field generated a current of less than 0.5 mA the energy coupled by the field into the electrons is under 1 Watt. If this were dissipated in the ion or neutral gas this would produce an increase in temperature of only 4 K, but if it were dissipated in the electrons it would produce an increase of 4000 K in the electron gas temperature. The authors felt this increase in temperature is responsible for the observe experimental results.

Figure A.5 shows an experimental setup used by Tewari and Wilson.[88] The flame chamber is first evacuated then filled with the desired air/fuel mixture. A laser then ignites the mixture and a high speed camera takes pictures that are used to determine the flame speed. Two electrodes placed in the top and bottom of the flame chamber introduce RF into the flame.

The authors tested methane/air mixtures, methane/oxygen/argon mixtures and hydrogen/air mixtures. Using an electric field of 1.67 kV rms at 6MHz and a electrode separation of 2.2 cm, results for methane/air give an increase of as much as 100% for flame velocity under some conditions. The methane/oxygen/air mixture had less RF influence than the methane/air mixture. This was contrary to what the authors thought would happen. They felt that neutral argon gas would absorb less energy from the electrons than neutral nitrogen gas so the flame velocity would be larger. For a 10% hydrogen/air mixture there was a very slight increase in flame velocity.

Figure A.6 shows an experimental setup used by MacLatchy, Clements

Experimental Setup of Tewari and Wilson

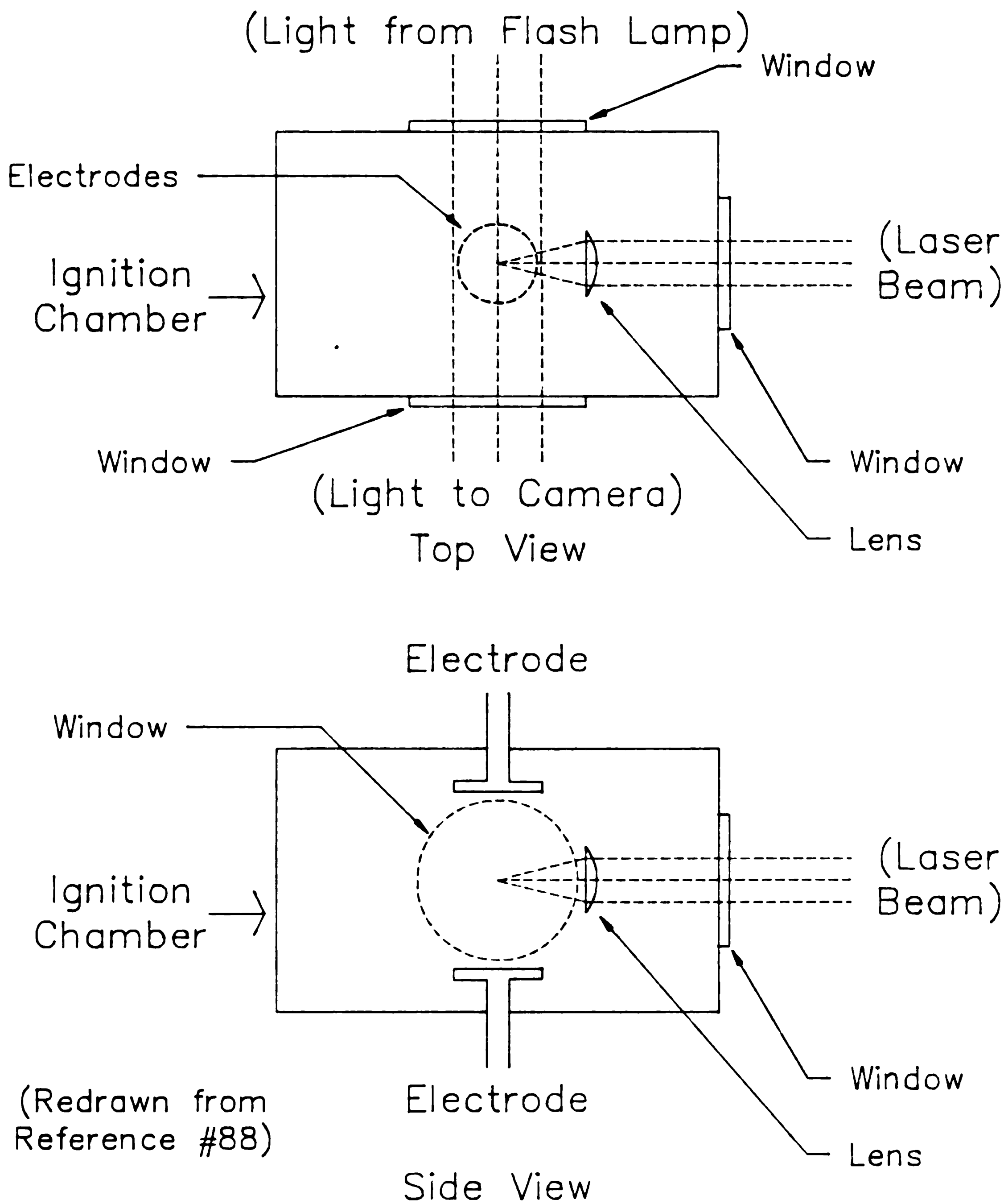

Figure A.5 Experimental Setup of Tewari and Wilson

Experimental Setup of MacLatchy, Clements and Smy

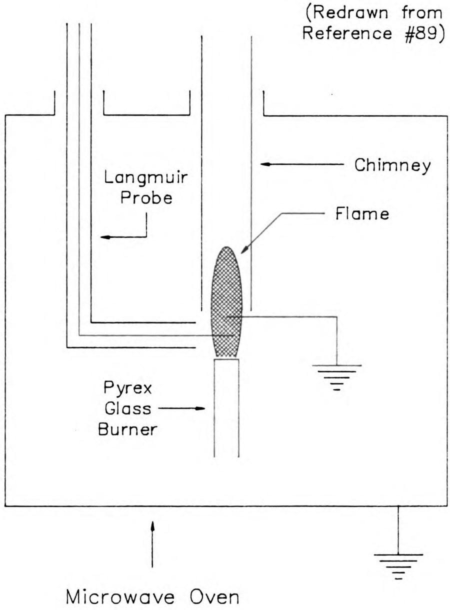

Figure A.6 Experimental Setup of MacLatchy, Clements and Smy and Smy.[89] The experiment was performed in a commercially available microwave oven. The oven operated at 2.45 GHz and generated 500 Watts, although the magnetron operated on only half cycle of the electrical alternating current supply. A Meker style burner made entirely of pyrex glass was used and propane was used as a fuel. The burner was placed in an experimentally determined point of high electric field. The flame was started the top of a chimney attached to the burner, outside the microwave oven. Then the gas flow was turned off and the flame would propagate down the chimney, into the microwave oven and the flame speed could be measured.

A Langmuir probe was used to measure electron temperature and ionization density in the flame front. Results of the probe gives an increase in electron temperature of 4000 K in the presence of microwaves compared to 300 K for no microwaves. However, no increase in flame speed was observed.

Figure A.7 shows the experimental setup of Clements, Smith and Smy.[90] As shown in the figure the experimental set up consisted of a magnetron tube connected directly to a cylindrical cavity. The cavity was tuned with a quartz rod to a resonant frequency of 2.448 GHz when loaded with the flame and was excited in a TM_{010} mode when empty with a power level of 1800V/cm rms at the center. A 22 mm i.d. cylindrical quartz tube ran axially through the cavity. The premixed gases were fed up through the tube and the flame was started at the top. The gas flow was shut off and the flame was allowed to propagate down the tube through the cavity. Two photo diodes at the ends of the tube were used to measure flame speed.

Results were given for propane/air, ethylene/air and acetylene/air

Experimental Setup of Clements, Smith and Smy

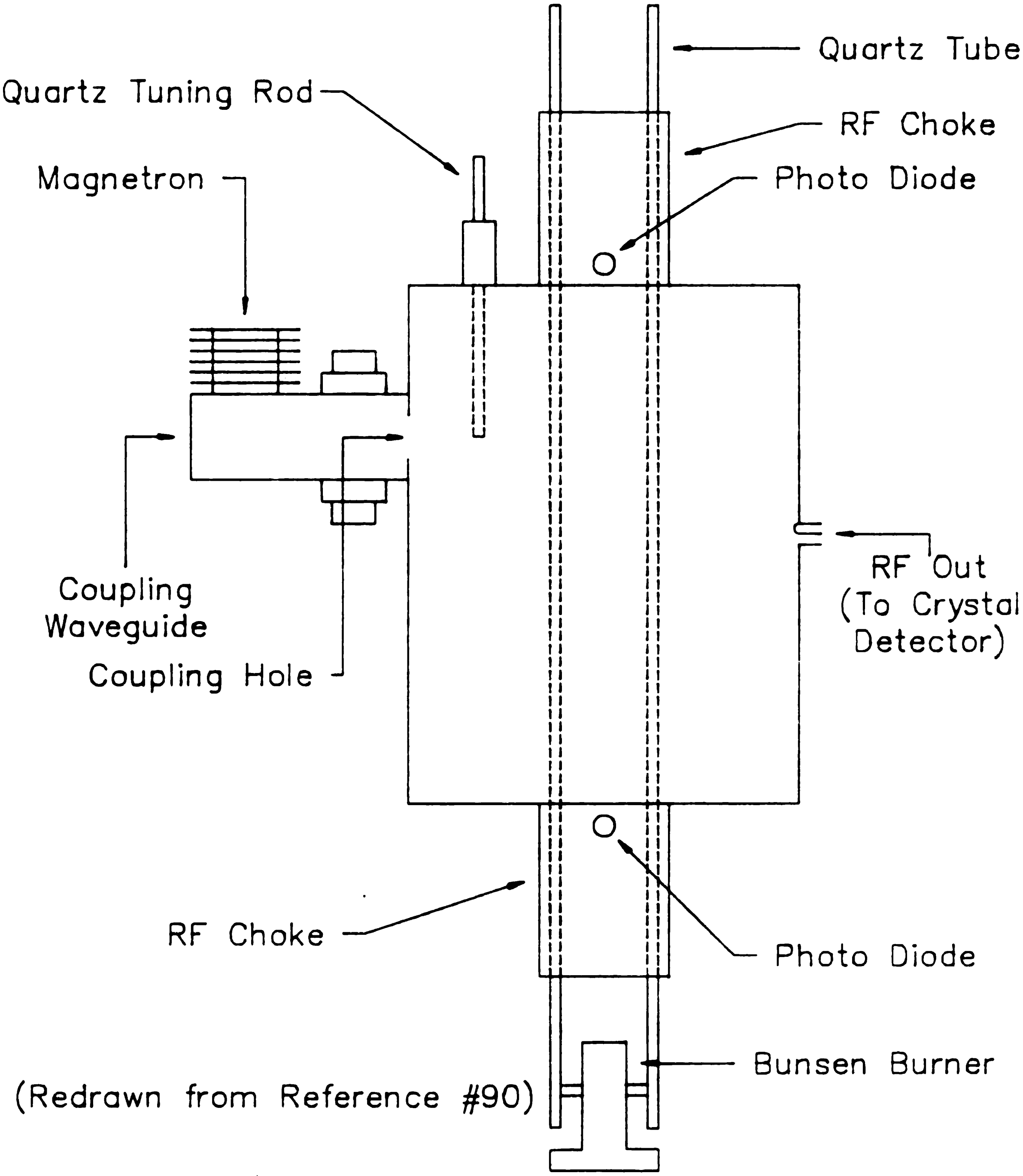

Figure A.7 Experimental Setup of Clements, Smith and Smy mixtures. The flame speed was found to be strongly dependent on the temperature of the quartz tube so the temperature of the quartz tube was held constant using forced air cooling. The experiment showed small but significant enhancement of flame speed under conditions with no gas breakdown by the microwave field. This ranged from a maximum increase of 20% to a decrease of 5%. With a gas breakdown, increases of up to 40% were observed.

The experimental setup shown in Figure A.8 was used in experiments by Ward.[91,92] As shown in the figure the experiment used a cylindrical bomb. This device is basically a cylinder filled with premixed gases, then the mixture is ignited and the mixture burns very rapidly inside the cylinder. In this experiment the cylinder was designed to operate as a TM_{010} mode cavity at 2.45 GHz. The cavity was evacuated and then filled with a propane/air mixture. The mixture was then ignited and measurements were taken using a RF probe, a Langmuir probe and a pressure transducer. A increase of up to 2 times is reported for the flame speed with the addition of the microwave field.

A.3 MICROWAVE-COMBUSTION FLAME RESEARCH

Initial flame experiments were conducted using the setup shown in Figure A.9. The microwave cavity is described in section 3.4 of this thesis. A candle was positioned so that its flame was at the center of a TM_{012} cavity mode. Input power was supplied be a 100 Watt continuous wave microwave source. The cavity was set off resonance and the microwave power would be turned on. The candle was lit and placed in the center of the cavity. Then the cavity would slowly be tuned to resonance. As the cavity was adjusted to resonance the flame would

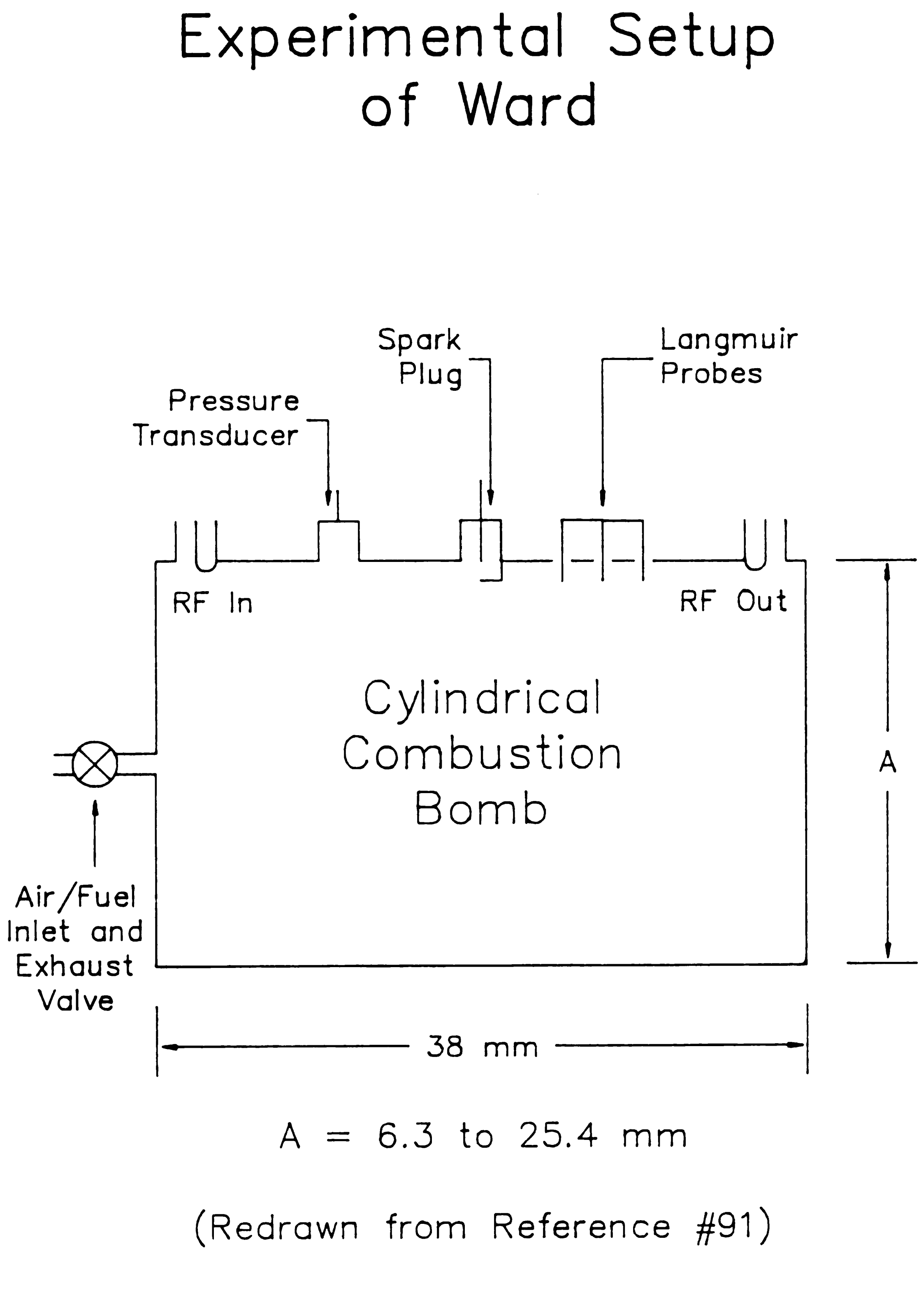

Figure A.8 Experimental Setup of Ward

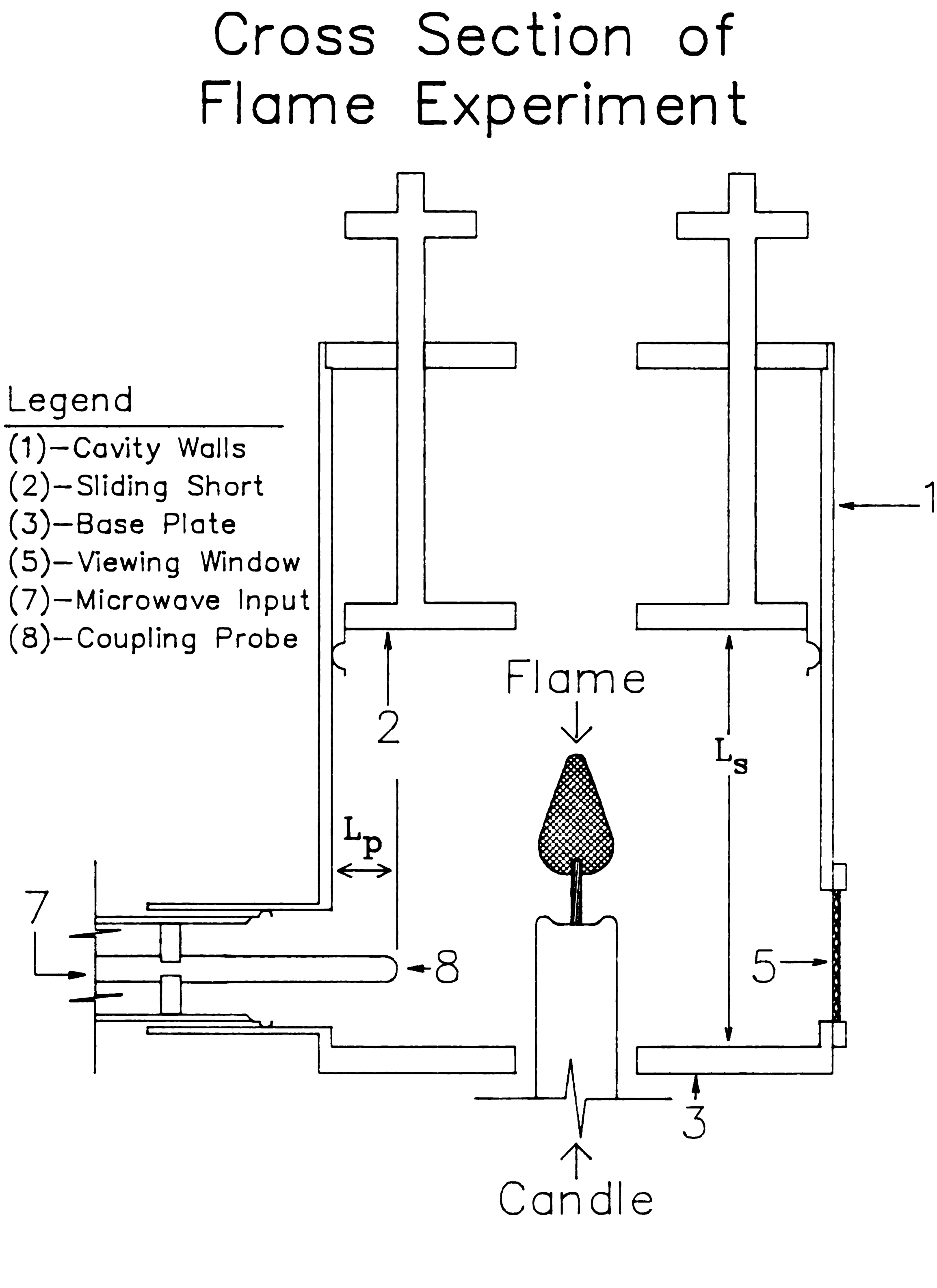

Figure A.9 Cross Section of Flame Experiment suddenly increase in length until it was about 10 cm long. It would stay like this for about 15 second and then go out. The combustion products of the flame were found to be contaminating the walls of the cavity so the experiments were discontinued. The cause of the observed effects was difficult to ascertain. It was possible that the microwaves were directly coupling into the flame. However, it is also possible that the microwaves were being coupled into the candle wax and heating it, thereby providing more fuel to the flame.

A advanced experimental setup was constructed and is shown in Figure A.10. The same microwave cavity was used but a quartz tube was added to keep the flame combustion products off the cavity. The flame source was a Bunsen burner using propane. The cavity was tuned to a TM_{012} mode (shown in Figure 3.8) and a piece of screen was placed across the bottom opening to increase the field strength in the flame. A microwave sweep system, shown in Figure A.11, was used for the input power to the cavity. The cavity was tuned for a center frequency of 2.45 GHz with a bandwidth of 6 Mhz and a input power level of 25 Watts from a traveling wave tube.

Figure A.12 shows the sweep results for propane input pressure of 6 lbs/in^2 to the bunsen burner and Figure A.13 shows the results for a input pressure of 7 lbs/in^2. With the addition of a flame to the cavity, a frequency shift of 0.2 Mhz and a slight drop in Q is observed. This indicates that the presence of the flame is affecting the microwave field inside the cavity, thus changing the cavity resonance. There are two possible reasons for this change in field pattern. First, the microwave field may be coupling into the flame, affecting the field pattern. Second, the hot flame may be affecting the dielectric constant

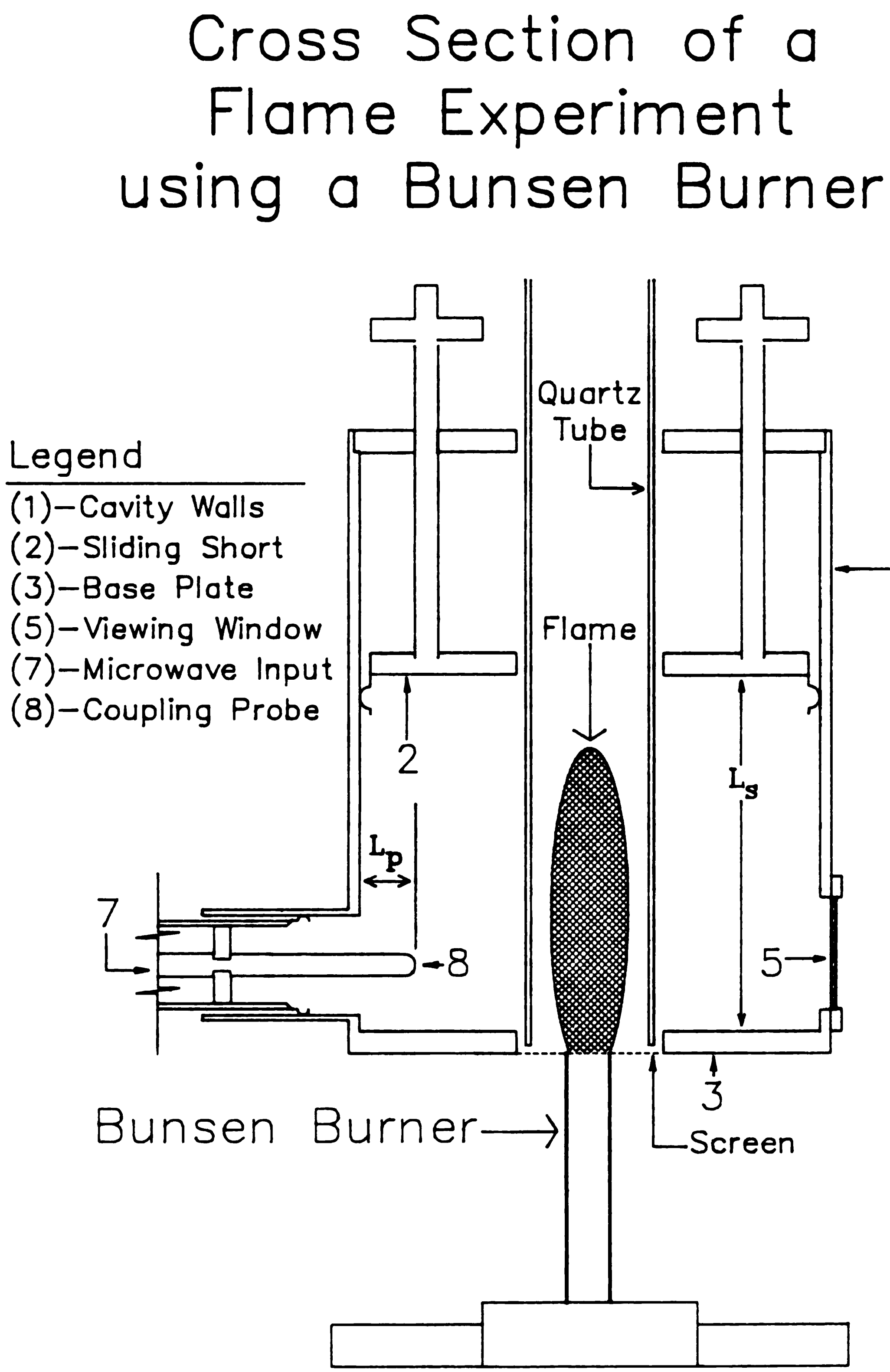

Figure A.10 Cross Section of a Flame Experiment with a Bunsen Burner

Experimental Microwave Sweep System

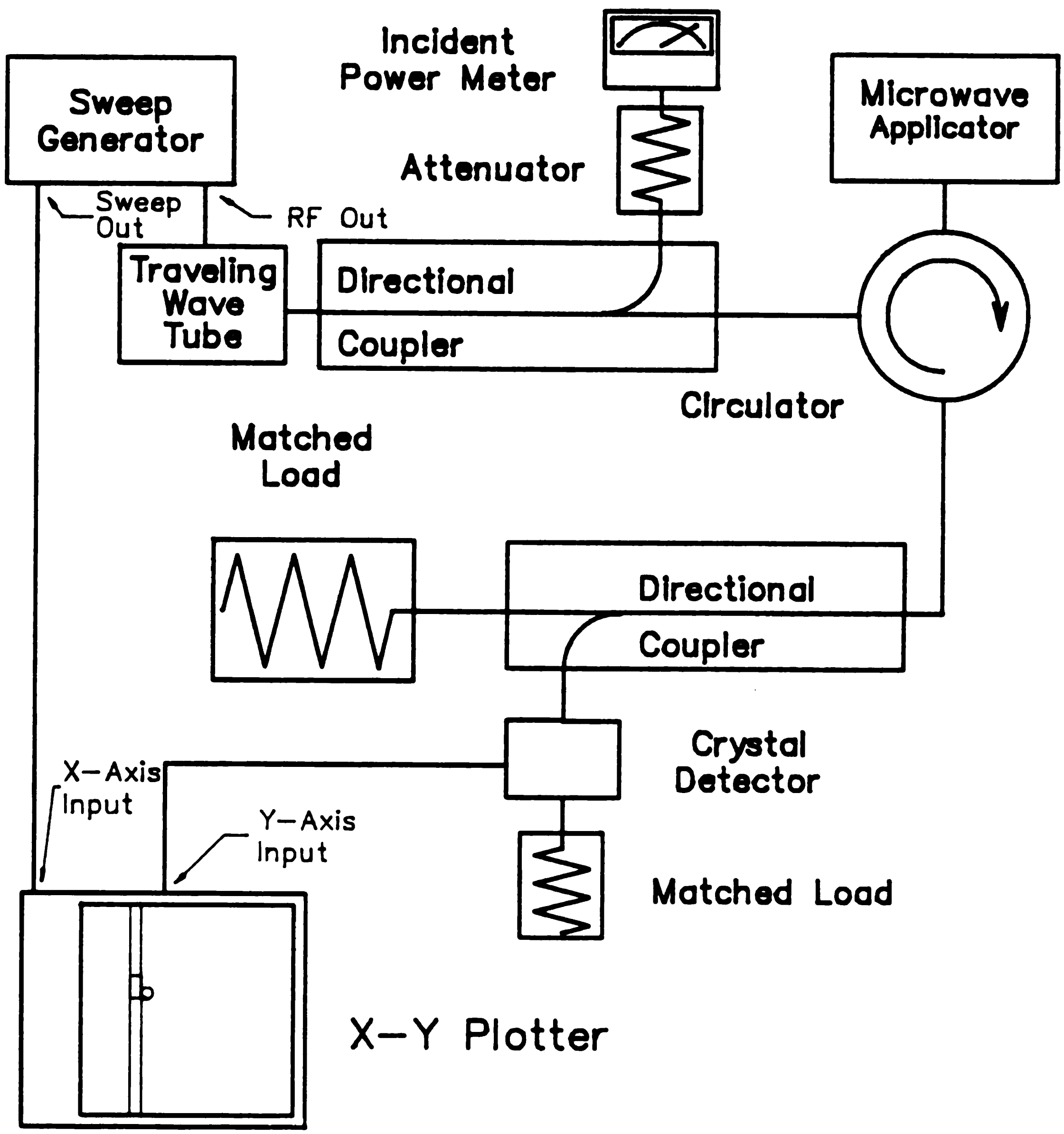

Figure A.11 Experimental Microwave Sweep System

Experimental Results

Reflected Power Versus Frequency

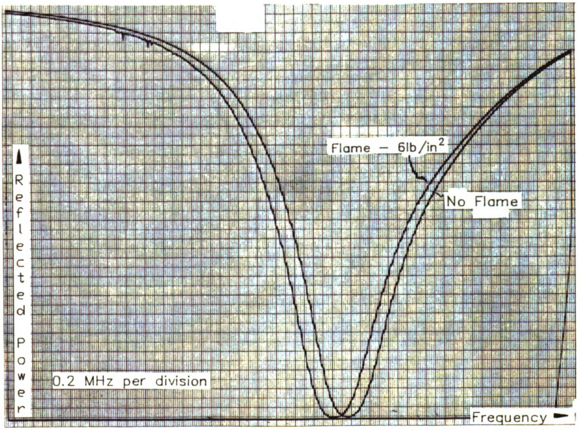

Figure A.12 Experimental Results

Experimental Results

Reflected Power Versus Frequency

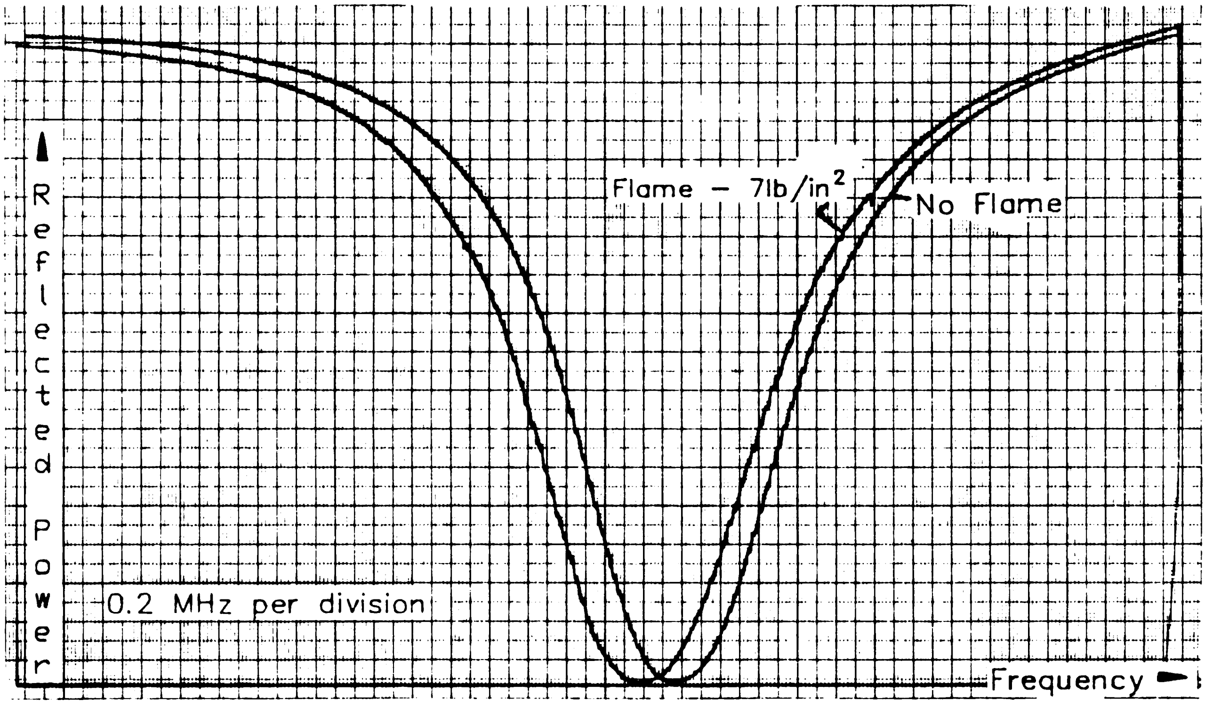

Figure A.13 Experimental Results

of the air present in the cavity causing a change in the resonant frequency.

The interaction may seem small but it should remember that the chemical power of the flame is >1000 Watts and only 25 Watts of microwave power was available. In addition it should be remembered that the region of the plasma in the flame is very small and may not be oriented in the most ideal manner for microwave coupling.

A.4 CONCLUSIONS

The result of the experiments were inconclusive. However, they demonstrated important methods and experimental setups that with further refinement could demonstrate microwave interaction with a flame. Earlier results presented in the literature review support that this is possible and should be studied. Additional experiments need to conducted that study the chemistry and energy changes that occur with the addition of a microwave field. Studies of the basic microwave-flame interaction would also be beneficial to the understanding to combustion flames and microwave discharges.

LIST OF REFERENCES

LIST OF REFERENCES

1. Whitehair, S., Asmussen, J., and Nakanishi, S., "Demonstration of a New Electrothermal Thruster Concept," Applied Physics Letters, vol. 44, p. 1014-1016, 1984.

2. Whitehair, S., Asmussen, J., and Nakanishi, S., "Microwave Electrothermal Thruster Performance in Helium Gas," accepted for publication in Journal of Propulsion and Power.

3. Whitehair, S. and Asmussen, J., "The Generation and Maintenance of Stable High Pressure Microwave Arcs," presented at the Fifth Topical Conference on Radio Plasma Heating ,February 21-23, 1983, Madison, WI, also published in the conference proceedings, Proceedings of the Fifth Topical Conference in Radio Frequency Plasma Heating, p. 296-299.

4. Asmussen, J. and Whitehair, S., "Measurement of the Electromagnetic Field Pattern Surrounding Atmospheric Microwave Discharges," presented at the 1983 IEEE International Conference on Plasma Science, San Diego, CA, May 23-25, 1983.

5. Asmussen, J. and Whitehair, S., "Performance Measurements on a Microwave Electrothermal Engine," presented at the 1984 IEEE International Conference on Plasma Science, St. Louis, MO, May 14-16, 1984.

6. Asmussen, J., Whitehair, S., and Nakanishi, S., "Experiments with a Microwave Electrothermal Thruster Concept," AIAA/JSASS/DGLR 17th International Electric Propulsion Conference, IEPC 84-74, May 1984, Tokyo, Japan.

7. Whitehair, S., Asmussen, J. and Nakanishi, S., "Recent Experiments with Microwave Electrothermal Thrusters," presented at the AIAA/DGLR/JSASS 18th International Electrical Propulsion Conference, Alexandria, VA, AIAA-85-2051, Sept. 30-Oct. 2, 1985.

8. Whitehair, S., Frasch, L. and Asmussen, J., "Experimental Investigation of Microwave Electrothermal Thruster Configurations," presented at the 13th IEEE International Conference on Plasma Science, Saskatoon, Saskatchewan, Canada.

9. Whitehair, S. and Asmussen, J., "An Electrodeless Microwave Plasmatron," disclosure to Michigan State University, April 18, 1983.

10. Whitehair, S., Asmussen, J., Nakanishi, S. and Malinkey J., "Microwave Electrothermal Thruster," disclosure to NASA Lewis Research Center, Oct. 25, 1983.

11. Fredericks, R., " An Experimental and Theoretical Study of a Resonantly Sustained Plasma in Microwave Cavities," Ph.D. Dissertation, Michigan State University, 1971.

12. Mallavarpu, R., "An Investigation of the Electromagnetic Behavior of a Microwave Plasma Source Over a Wide Range of Pressures and Flow Rates," Ph.D. Dissertation, Michigan State University, 1976.

13. Rogers, J.,"Properties of Steady-State, High Pressure Argon Discharges," Ph.D. Dissertation, Michigan State University, 1982.

14. Sutton, G.P., Rocket Propulsion Elements, John Wiley & Sons, New York, 1976.

15. Garrison, P.W., "Advanced Propulsion for Future Planetary Spacecraft," Journal of Spacecraft and Rockets, vol. 19, p. 534-538, 1982.

16. Hawkins, C.E. and Nakanishi, S.," Free Radical Propulsion Concept," NASA TM 81770, 1981.

17. Chapman, R., Filpus, J., Morin T., Snellenberger, R., Asmussen J., Hawley M. and Kerber R., "Microwave Plasma Generation of Hydrogen Atoms for Rocket Propulsion," Journal of Spacecraft and Rockets, vol. 19, p. 579, Nov.-Dec. 1982.

18. Jahn, R.G., Physics of Electric Propulsion, McGraw-Hill, New York, 1968.

19. Page, R.J., Halbach, C.R. and Short, R.A., "3-kW Concentric Tubular Resistojet Performance," Journal of Spacecraft and Rockets, vol. 11, p. 1669-1674, 1966.

20. Page, R.R. and Stoner, W.A., "The Design and Technology Development for a 150 MLB Resistojet for H_2 or NH_3," AIAA/JSASS/DGLR 16th International Electric Propulsion Conference AIAA-82-1949, November 17-19, 1982.

21. Zafran, S., and Jackson, B.,"Electrothermal Thruster Diagnostics," Vol. I and II., TRW Space Technology Group, NASA CR 168174, May, 1983.

22. Jackson, F.A., et al, "An Operational Electrothermal Propulsion System for Spacecraft Reaction Control," AIAA Paper 66-213, 1966.

23. Schoeck, P.A., "Physical Phenomena and Technical Problems of Arcjet Engines," Journal of the British Interplanetary Society, vol. 19, p. 337-349, 1963-64.

24. John, R.R., Bennett, S. and Connors, J.F., "Arcjet Engine Performance: Experiment and Theory," AIAA Journal, vol. 1, p. 2517, 1963.

25. McCaughey, O.J., "Development of a Plasmajet Rocket Engine for Attitude and Orbit Control," Report No. FR-112-651, Plasmadyne Corp., June 1964.

26. Wallner, L.E. and Czika, J., "Arc-Jet Thruster for Space Propulsion," NASA TN D-2868, June 1965.

27. Ducati, A.C., Giannini, G.M. and Muehlberger, E, "Experimental Results in High Specific Impulse Thermo-Ionic Acceleration," AIAA Journal, vol. 2, p. 1454, 1964.

28. Kantrowitz, A., "Propulsion to Orbit by Ground-Based Lasers," Astronautics and Aeronautics, vol. 10, p. 74-76, 1972.

29. Glumb, R.J. and Krier, H., "Concepts and Status of Laser-Supported Rocket Propulsion," Journal of Spacecraft and Rockets, vol. 21, p. 70-79, 1984.

30. Franzer, D.L., "Continuous Laser-Sustained Plasmas," Journal of Applied Physics, vol. 49, p. 1727-1731, 1973.

31. Gulati, A. and Merkle, C.L., "Absorption of Electromagnetic Radiation in an Advanced Propulsion System," Journal of Spacecraft and Rockets, vol. 21, p. 101-107, 1984.

32. Jackson, J.P. and Nielson, P.E., "Role of Radiative Transport in the Propagation of LSC Waves," AIAA Journal, vol. 12, p. 1498-1501, 1974.

33. Reed, T.B., "Induction-Coupled Plasma Torch," Journal of Applied Physics, vol. 32, p. 821-824, 1961.

34. Eckert, H.V., and Pridmore-Brown, D.C., "Temperature Profiles in Argon Induction Plasmas: Theory and Experiment," Journal of Applied Physics, vol. 42, p. 5051, 1971.

35. Reed, T.B., "Growth of Refractory Crystals Using the Induction Plasma Torch," Journal of Applied Physics, vol. 32, 1961.

36. Jones, R.M., "Comparison of Potential Electric Propulsion Systems for Orbit Transfer," Journal of Spacecraft and Rockets, vol. 16, p. 88-95, 1984.

37. Petrash, D.A., "Station Keeping Will Eat Energy On a New Scale," Astronautics and Aeronautics, vol. 21, p. 64-65, 1983.

38. Kaufman, H.R. and Robinson, R.S., "Electric Thruster Performance for Orbit Raising and Maneuvering," Journal of Spacecraft and Rockets, vol. 21, p. 180-186, 1984.

39. Berkopec, F.D. and Stone, J.R., "NASA Electric Propulsion Technology," AIAA paper 85-1999, 1985.

40. Gilmour, A.S., Microwave Tubes, Artech House, 1986.

41. McMillan, R.W., "Near-Millimeter-Wave Sources of Radiation," Proceedings of the IEEE, vol. 73, p. 86-107, 1985.

42. Crapuchettes, P.W., "Magnetrons as Generators of Microwave Power," Microwave Power Engineering, vol. 1, p. 18-42, Academic Press, New York, 1968.

43. Brown, W.C., "The Amplitron," Microwave Power Engineering, vol. 1, p. 84, Academic Press, New York, 1968.

44. Neugebauer, W., and Mihran, T., "A Ten State Electrostatic Depressed Collector for Improving Klystron Efficiency," IEEE Transactions on Electron Devices, vol. 19, 1972.

45. M/A-COM Microwave Power Devices, Inc., "Update: RF/Microwave Power".

46. Nalos, E. J., "New Developments in Electromagnetic Energy Beaming," Proceedings of the IEEE, vol. 66, p. 276-289, 1978.

47. Frasch, L. and Asmussen, J., "Electrothermal Propulsion of Spacecraft with Time-Varing Electromagnetic Energy," AIAA 18th International Electric Propulsion Conference, Alexandria VA, Sept. 30 to Oct. 2, 1985.

48. Asmussen, J. and Rogers, J., "An Assessment of the Potential Application of Microwave Discharges to Electric Propulsion Engines," MSU/NASA Lewis Research Center Conference on Advanced Propulsion Concepts Using Time Varying EM Fields, Michigan State University, Feb. 23-25, 1982.

49. Babat, G.I., Electrodeless Discharges and Some Allied Problems," Journal of the Institute of Electrical Engineers, London, vol. 94, p. 27-37, 1947.

50. Asmussen, J., Mallavarpu, R., Hamann, J.R., and Park, H.C., "The Design of a Microwave Plasma Cavity," Proceedings of the IEEE, vol. 62(1), p. 109-117, January, 1974.

51. Fredericks, R.M. and Asmussen, J., "High-density Resonantly Sustained Plasma in a Variable-Length Cylindrical Cavity," Applied Physics Letters, vol. 19, p. 508-510, 1971.

52. Halverson, S.L. and Hatch, A.J., "Frequency-Shifting Method of Exciting a Plasma in a Resonant Cavity," Applied Physics Letters, vol. 14, p. 79, 1969.

53. Moisan, M., Beaudry, C. and Leprince, P., "A Small Microwave Plasma Source for Long Column Production Without Magnetic File," IEEE Transactions on Plasma Science, vol. 3, p. 55, 1975.

54. Fritz, R. and Asmussen, J., "Experimental Characteristics of RF Surface Wave Generated Plasma Sources," IEEE International Conference on Plasma Science, Montreal, Canada, June 1979.

55. Cobine, J.D. and Wilbur, D.A., "The Electric Torch and Related High Frequency Phenomena," Journal of Applied Physics, vol. 22, p. 835-841, 1951.

56. Moriarty, J.J. and Brown, V.M., "Toroidal Microwave Discharge Heating of Gas," Journal of Microwave Power, vol. 3, p. 180-186, 1968.

57. Rogers, J. and Asmussen, J., "The Experimental Production of Microwave Plasma Filaments and Discharges at High Pressure," proceedings 1981 IEEE International Conference on Plasma Science, May 18-20, 1981.

58. Miyake, S., Takeuchi, S. and Arata, T., "The Experimental Investigation of Coaxial Microwave Plasmatron in Nitrogen Gas," Japanese Journal of Applied Physics, vol. 13, p. 296-305, 1974.

59. Mallavarpu, R., Asmussen, J., and Hawley, M.C., "Behavior of a Microwave Cavity Discharge over a Wide Range of Pressures and Flow Rates," IEEE Transactions on Plasma Science, vol. PS-6(4), p. 341-354, December, 1978.

60. Asmussen, J. and Root, J., "Characteristics of a Microwave Plasma Disk Ion Source," Applied Physics Letters, Vol. 44, p. 396-398, 1984.

61. Asmussen, J. and Root, J., "Ion Generating Apparatus and Method for the Use There Of," U.S. Patent. No. 4 507 588, Mar. 26, 1985.

62. Root, J. and Asmussen, J., "Experimental Performance of a Microwave Cavity Plasma Disk Ion Source," Review of Scientific Instruments, vol. 56, p. 1511-1519, 1985.

63. Ramo, S., Whinnery, J.R., and Van Duzer, T., Fields and Waves in Communications Electronics, 1st ed., J. Wiley and Sons, New York, 1972.

64. Fredericks, R.M., and Asmussen, J.,"Retuning and Hysteresis Effects of a rf Plasma in a Variable Size Microwave Cavity," Journal of Applied Physics, vol. 42, p. 3647-3649, 1971.

65. MacDonald, A.D. and Tetenbaum, S.J., "High Frequency and Microwave Discharges," Gaseous Electronics, Hirsch, M.N. and Oskam, H.J. editors, vol. 1, Academic Press, New York, 1978.

66. Marec, J., Bloyet, E., Chaker, M., Leprince, P. and Nghiem P., "Microwave Discharges," Electrical Breakdown and Discharges in Gases, Kunhart, E.E. and Luessen H.L. editors, Part B, Plenum Publishing Corp., 1983.

67. Pfender, E., "Electric Arcs and Arc Gas Heaters," Gaseous Electronics, Hirsch, M.N. and Oskam, H.J. editors, vol. 1, Academic Press, New York, 1978.

68. Chapman, R., Morin, T., Finzel, M. and Hawley, M.C., "Measurement of Energy Distribution in Flowing Hydrogen Microwave Plasmas," Journal of Spacecraft and Rockets, vol. 22, p. 626, Nov.-Dec. 1985.

69. Cherrington, B.E., Gaseous Electronics and Gas Lasers, Pergamon Press, Oxford, 1979.

70. Elenbaas, W., Light Sources, Philips Technical Library, Crane, Russak & Company, New York, 1972.

71. Kapitza, P.L., "Free Plasma Filament in a High Frequency Field at High Pressure," Soviet Physics JETP, vol. 30, p. 973-1224, 1970.

72. Kapitza, P.L. and Filimonov, S.I., "Apparatus for the Production of a Free Plasma Filament. Determination of the Current and Resistance of the Filament," Soviet Physics. JETP, vol. 34, p. 542-553, 1972.

73. Dymshits, B.M. and Koretskii, Y.P., "Temperature of a Free Plasma Filament in a High Frequency Field at High Pressure," Opt. Spect., vol. 33, p. 17-18, 1972.

74. Arata, Y.,Miyake, S. and Kobayashi, A., "Research of a Stationary High Power High Power Microwave Plasma at Atmosphere Pressure," Journal of the Physical Society of Japan, vol. 40, p. 1456-1461, 1976.

75. Arata, Y., Miyake, S. and Kobayashi, A., "High Power Microwave Discharge in Atmospheric Hydrogen Gas Flow," Journal of the Physical Society of Japan, vol.44, p. 998-1003, 1978.

76. Rogers, J. and Asmussen, J., "Properties of Steady State, High Pressure Microwave Generated Arc Discharges in Argon Gas," 1982 IEEE International Conference on Plasma Science, Ottawa, Canada, May 17-19, 1982.

77. Hubert, J., Moisan, M. and Ricard, A., "A New Microwave Plasma at Atmospheric Pressure," Spectrochimica Acta, vol. 33B, p. 1-10, 1979.

78. Batenin, V.M., Zrodnikov, V.S., Roddatis V.K. and Chinnov, V.F., "Spectroscopic Investigation of a Microwave Discharge in Hydrogen," High Temperature, vol. 13, p. 250-257, 1975.

79. Batenin, V.M., Zrodnikov, V.S. and Chinnov, V.F., "Microwave Discharge in Helium," High Temperature, vol. 14, p. 186-188, 1976.

80. Bandel, H.W. and MacDonald, A.D., "Microwave Breakdown in Air Plus H_2O," Journal of Applied Physics, vol. 41, p. 2903-2904.

81. Mertz, S.F., Asmussen, J. and Hawley M.C., "An Experimental Study of Reactions of CO and H_2 in a Continuous Flow Microwave Discharge Reactor," IEEE Transactions on Plasma Science, vol. PS-2, p. 297-307, 1974.

82. Ward, M.A.V.,"Potential Uses of Microwave to Increase Internal Combustion Energy Efficiency and Reduce Exhaust Pollutants", Journal of Microwave Power, vol. 12(3), p. 187-198, 1977.

83. Ward, M.A.V., and Wu, T.T.,"A Theoretical Study of the Microwave Heating of a Cylindrical Shell, Flame-Front Electron Plasma in an Internal Combustion Engine", Combustion and Flame, vol. 32, p. 57-71, 1978.

84. Frimstrom, R.M. and Westenburg, A.A., Flame Structure, McGraw-Hill Book Company, 1965.

85. Gaydon, A.G. and Wolfhard, H.G., Flames, Their Structure, Radiation and Temperature, Barn and Noble Inc.,1970.

86. Glassman, I., Combustion, Academic Press, 1970.

87. Jaggers, H.C. and Von Engel, A.," The Effect of Electric Fields on the Burning Velocity of Various Flames", Combustion and Flame, vol. 16, p. 275-285, 1971.

88. Tewari, G.P., and Wilson J.R.," An Experimental Study of the Effects of High Frequency Electric Field on Laser Induced Flame Propagation", Combustion and Flame, vol. 24, p. 159-167, 1975.

89. MacLatchy, C.S., Clements, R.M., and Smy, P.R.,"An Experimental Investigation of the Effect of Microwave Radiation on a Propane-Air Flame", Combustion and Flames, vol. 45, p. 161-169, 1982.

90. Clements, R.M., Smith, R.D., and Smy, P.R., "Enhancement of Flame Speed by Intense Microwave Radiation," Combustion Science and Technology, vol. 26, p. 77-81, 1981.

91. Ward, M.A.V.,"Interaction of Propane-Air Laminar Flame Plasmas with the Microwave TM010 Mode Excited in a Cylindrical Combustion Bomb Cavity", Journal of Microwave Power, vol. 14(3), p. 241-259, 1979.

92. Ward, M.A.V.,"Microwave Stimulated Combustion", Journal of Microwave Power, vol. 15(3), p. 193-202, 1980.